ALMA MATER STUDIORUM
UNIVERSITÀ DI BOLOGNA

DOTTORATO DI RICERCA IN

BENI CULTURALI E AMBIENTALI

Ciclo 37

Gruppo Scientifico Disciplinare: 08/CEAR-04 – Geomatica

Settore Scientifico Disciplinare: CEAR-04/A – Geomatica

HIGH-DETAIL GEOMATIC 3D SURVEYING AND PROCESSING FOR SMALL-OBJECTS ROBUST DOCUMENTATION AND INVESTIGATION IN HERITAGE SCIENCE

Presentata da: Anna Forte

Coordinatore Dottorato

Donatella Restani

Supervisore

Gabriele Bitelli

Co-supervisore

Valentina Alena Girelli

Esame finale anno 2025

"The true woman who possesses infinite wisdom [...]

consults a lapis lazuli tablet,

dispenses advice to all the lands [...]

traces the boundaries of the heavens,

she lays ropes on the earth to measure it."

Excerpt from a hymn by Enḫeduanna, Mesopotamian poet, scientist and priestess, and the first attested writer in the history of humanity (XXIV century BC).

TABLE OF CONTENT

ABSTRACT & KEYWORDS

Heritage Science lies at the intersection of the humanities and sciences, embracing a multidisciplinary approach to studying and preserving cultural heritage. Integrating fields such as history, archaeology, philology, chemistry, biology, physics, and informatics provides a cohesive framework that deepens the understanding of cultural assets. This interdisciplinary collaboration not only enriches historical and archaeological perspectives but also addresses critical material challenges, advancing methods for the conservation and valorisation of heritage. In recent years, geomatic surveying, especially high-detail 3D surveying, has become essential in Heritage Science while also expanding its application to diverse fields such as medicine and industry. This widespread usage has led to inconsistencies in terminology, methodologies, and theoretical frameworks, which may risk positioning 3D surveying as merely a technical tool rather than as a scientific discipline with intrinsic value. This thesis addresses these challenges by providing a structured and comprehensive examination of the theoretical and practical foundations of high-detail 3D surveying within geomatics, particularly in its applications to cultural assets investigation. It opens with an extensive literature review highlighting terminological and conceptual inconsistencies, focusing on three main technologies: laser triangulators, structured-light projection scanning, and close-range digital photogrammetry. Building on this theoretical groundwork, the thesis details the methodologies employed in the experimental phase, particularly emphasising the comparative and integrative applications of structured-light projection scanning and digital photogrammetry. Real-world case studies are also presented to demonstrate the effectiveness of these technologies in the detailed 3D documentation and analysis of cultural assets. Finally, the thesis concludes by discussing the broader implications of its findings and proposing avenues for future research and innovation within the discipline.

Geomatics — High-detail 3D surveying — 3D data processing — Structured-light projection scanning — Close-range digital photogrammetry — Heritage Science — Cultural heritage

1. OVERVIEW

1.1 Thesis outline and context

The context of this PhD thesis is high-detail three-dimensional (3D) surveying for the investigation and robust digital documentation of small-size heritage assets. The geomatic technologies that serve this purpose have been employed in recent decades in the service of digitisation, study and valorisation of historical heritage, often proposing interesting and innovative solutions that have contributed substantially to Heritage Science and Studies. Beyond cultural heritage, these surveying tools are now widely used across various sectors—ranging from industry and medicine to geology and agriculture—and have become increasingly accessible due to technological advancements. This shift has gradually narrowed the gap between trained geomatics experts and non-professional users (Bitelli et al., 2017).

As a consequence, some may perceive 3D surveying techniques solely as "tools" rather than as a distinct discipline, overlooking the significance of the underlying theory and methodology that support them.

These issues – among many others – have led to a shortage of precise guidelines and, above all, to a lack of a solid delineation of high-detail 3D surveying theories and practices. Consequently, several ambiguities and uncertainties in terms of vocabulary and methodological approaches have been recently produced. At the same time, it is essential to emphasise further that geomatics has proven to be a precious support to a variety of disciplines and fields, perhaps also due to the capillary diffusion of geomatic instruments and the systematic introduction of surveying into new fields of study. These, as mentioned, include Cultural Heritage (CH), which is the application area for this PhD thesis, to which high-detail 3D surveying and processing have been tested. Yet, CH is a generic term for an enormously vast set of material and immaterial assets, as defined in the 1954 Hague Convention (UNESCO, 1954), and the identification of the area of application of this thesis to this generic ensemble does

not seem sufficient for the issues addressed and the purposes of the experiments performed.

To be more specific and circumscribed to a narrower domain, the application context of this thesis is not CH *per se,* but the study of it. Two main methodological approaches have emerged to address the countless issues related to historical heritage: Heritage Science and Heritage Studies. Before delving into the technical aspects – to avoid potential ambiguities – it is worth attempting to define and distinguish these two branches of knowledge.

Heritage Science (HS) is characterised by a multidisciplinary connotation, including the humanities such as archaeology, history, and philology, but also the so-called 'hard sciences' such as chemistry, physics, biology, computer science and geomatics. The definition of this cross-disciplinary discipline was proposed by the International Centre for the Study of the Preservation and Restoration of Cultural Property (ICCROM), stating on its official website that "Heritage science is the interdisciplinary research domain of the scientific study of cultural and natural heritage" (ICCROM, 2019). The concept of "scientific study" is also extended to social/humanistic disciplines involved in the comprehension of cultural and natural heritage properties. In other words, the integrated approach of Heritage Science is proposed for the study of cultural heritage in order to provide comprehensive knowledge from a historical-archaeological and philological point of view, but also from that of the constituent materials, chemical-biological degradation phenomena and physical integrity.

The second macro-discipline, "Heritage Studies", focuses more on CH's sociological, political and anthropological aspects. The discussion about the definition of "heritage" is a pivotal issue in this field of study, and several scholars proposed to include also the "intangible" assets (traditions, folklore, food…) as part of the human legacy to be studied and preserved (Bortolotto, 2007; Harrison, 2013). Also, the strategies for

properties' preservation and valorisation are included and investigated, but with a more humanistic and theoretical approach.

Both of these fields of knowledge have greatly benefited from geomatics in recent years. In the field of Heritage Studies, examples have been offered of preserving, documenting, and disseminating intangible heritage phenomena or folklore traditions through reconstructions in 3D, GIS (Geographic Information Systems), or virtual environments (Skublewska-Paszkowska, 2022).

Nonetheless, these approaches often encroach on digital technologies that are not strictly geomatic (non-reality-based digital reconstructions, extended reality...). Moreover, the domains of Heritage Studies and Sciences frequently intersect and overlap, and it is difficult to draw a precise boundary between the two. However, in the context of this thesis, the application area of the examples proposed in the literature review and case study section is more aptly ascribable to that of Heritage Science. Therefore – having clarified the two concepts – high detail 3D surveying will be proposed in its application to Heritage Science. To be even more specific, the study of cultural assets through geomatic techniques is proposed on small objects. This is due to the inherent nature of high-detail survey tools, which, as will be seen, are sensibly applicable only to limited areas.

1.2 Thesis objectives and structure

As mentioned earlier, high-detail 3D surveying technologies have undergone a rapid development, leading to their application in numerous sectors. Yet, the pace of theoretical research does not always proceed at the same rate as that of application, and this breadth of practice has led to a dispersion of terminology and a dilution of the theoretical basis. In this thesis, efforts will be made to compensate for this limitation. In Remondino & Menna (2008), mentioning the 1964 *International Charter for the Conservation and Restoration of Monuments and Sites*, the authors say that – despite the international recognition of the importance of preserving heritage properties – "the need for a clear, rationale, standardised terminology and

methodology, as well as an accepted professional principles and technique for interpretation, presentation, digital documentation and presentation is still evident".

Sixteen years later, these problems are still present in Geomatics, especially in the context of high-detail 3D surveying. The related terminology issues will be discussed in the opening chapter of the Literature Review, section 2.1, to provide a lexical framework for what will be subsequently discussed.

In addition, having defined the context of application of high-detail 3D surveying and processing to that of Heritage Science, the second main aim of this thesis is to propose the related technologies as valid tools in the investigation of heritage proprieties from a geometrical/morphological point of view (providing information about the state of preservation, the presence of engravings or superficial degradation phenomena…), but also from a historical or philological perspective (inscription interpretation, archaeological contextualisation…).

Hence, the purpose of this thesis is also to demonstrate the benefits that high-resolution 3D reconstruction could bring to the field of Heritage Studies in understanding the assets from diverse viewpoints. A selection of related examples from the literature will be proposed in section 2.2. In accordance with the aim of shedding light on the theory and practice behind high-detail 3D surveying, the subsequent sections of literature review 2.3.1, 2.3.2 and 2.3.3 will discuss the most employed technologies in this geomatics sector, investigating the theoretical principles behind them. Section 2.4 will instead present a set of scientific contributions in which the authors compare different types of surveying techniques.

In chapter 3, instead, a set of methodological strategies and procedures in high-detail 3D surveying are presented (section 3.2), starting with the technical description of the instruments available at the Geomatics and Topography research area of the Civil, Chemical, Environmental and Materials Engineering Department of Bologna University (section 3.1). These tools have been employed for the experimental part of this research and to obtain the 3D data that have been analysed and compared

according to the strategies described in section 3.3. In section 3.4, instead, a set of real case studies is presented, to which the described methodologies and procedures have been tested and evaluated, in accordance with the research questions: what are the possible outcomes obtainable with the tested geomatics instruments and which strategies can be more adequate for heritage investigation purposes? And, is it possible to consider high-detail 3D surveying and processing as a tool for heritage assets investigation?

Possible answers to these questions will be offered in Chapter 4 (discussion), in which the considerations that emerged during this research work (including the literature review and the experiments conducted), will be discussed. In addition, a more technical reflection on the advantages and disadvantages of the survey methods under consideration (Structured Light Projection Scanning and Digital Photogrammetry) will be proposed in section 4.2.

Finally, in Chapter 5, an attempt will be made to take stock of the situation, drawing conclusions on the theoretical/methodological issues discussed and on what emerged in the experimental phase. Open issues will also be outlined and further developments proposed to be explored in this area of geomatics.

In short, the sequence of sections in this thesis is structured to attempt to delve into the world of high-detail 3D surveying, from theoretical, methodological and finally applicative perspectives. The common thread is Heritage Science, which will be the background to be kept in mind during the more theoretical discussions on the techniques. This is because the technologies to be discussed have been approached with a focus on their application to the robust and detailed investigation of cultural heritage, to the exclusion of other areas such as digital documentation for heritage valorisation and dissemination purposes.

The broader motivation behind the conception of this thesis project is the fondness and interest for cultural heritage and the set of concepts, values and significance it embodies. Digital technologies can (and should) be used wisely to collaborate in

studying and preserving historical heritage. This seemingly trivial consideration takes on another meaning in the context of the current year, 2024, in which scenarios of conflicts and environmental catastrophes are everyday occurrences at various latitudes and longitudes. In the face of these frightening scenarios towards the future, cultural heritage stands as a *memorandum* of a population's roots, of all the road it has made over centuries or millennia of history and, therefore, of what constitutes the foundations of the present and the guidance to be taken in building the future.

The image presented in figure 1 is a photograph by the Italian artist Valerio Minato, who was awarded as the winner of NASA's "Astronomy Picture of the Day" contest on December 25th, 2023. This striking image serves as an artistic synthesis of this doctoral thesis, as well as a 'visual' inspiration for its genesis. It portrays a harmonious interplay between the mountain, symbolising natural and environmental heritage, and the cathedral, representing historical heritage. Both are captured in a symbiotic embrace by a technological medium that has transformed the world: photography. This seamless blend of art, nature, and technology is what led NASA to honour this image.

And the imperative to preserve—through various perspectives and with the tools at our disposal—the legacy of both our planet's natural environment and the cultural heritage created by humankind over generations, is a driving force behind the work of those who employ technology to document and study heritage, whether natural or cultural.

Figure 1. The winning picture of the NASA contest "Astronomy Picture of the Day" on December 25th, 2023: "Cathedral, Mountain, Moon". Image Credit & Copyright: Valerio Minato; available at: https://apod.nasa.gov/apod/ap231225.html

2. INTRODUCTION AND LITERATURE REVIEW

2.1 Terminological issues in high-detail 3D surveying

2.1.1 High-precision? -resolution? -detail?

Highly detailed 3D surveying techniques embrace a variety of technologies that constitute a distinct field in the geomatics domain. Yet, as is well known, geomatics has created a digital framework for disciplines such as topographic and 3D surveying, geodesy and remote sensing. This set of technologies is all part of the broad and varied "Geomatics container". For this thesis, the tools in topography, geodesy and remote sensing fields – despite being all employed in the CH context – will not be considered. The techniques considered here are exclusively pertinent to the field of three-dimensional surveying and refer to the set of instruments that allow to create 3D digital models (point clouds and meshes) that reproduce the geometry of objects in a highly detailed way, allowing to discriminate between the finest discontinuities of the surface morphology analysed.

Nevertheless, these types of techniques and the resulting output are referred interchangeably to by the terms "high-precision", "high-resolution", "high-accuracy", "high-detail" or "high fidelity". Hence, there is a variety of terms that gravitate around this world, although the terms listed refer to different concepts in the field of Geomatics and especially 3D surveying. For instance, in Zong et al. (2022), the authors present an example of detailed 3D reconstruction for industrial applications, referring to the technology used as "high-precision" 3D surveying; a similar example is presented by Zhang et al. (2024) in the geology field. In (Wycisk et al., 2009), instead, the article title includes the term "High-resolution" to describe the methodology employed, while the world "resolution" is also found in the description of the high quality of the obtained output, especially in terms of geometrical detail (Wang et al., 2021; Callieri et al., 2012).

"High-detail" 3D reconstruction/surveying/modelling is another way to refer to this kind of applications, as shown in (Bitelli et al., 2005; Fassi, 2007; Figueiredo et al., 2014), usually when describing procedures that resulted in high density of the 3D output (finely describing morphological characteristics).

The term "accuracy", instead, is mainly used when speaking about the output quality from the metrical correctness point of view, as in the case of Rinaudo et al. (2007). Sometimes also the expression "high-fidelity" is employed, to refer either to the "geometric fidelity" (Silvester & Hillson, 2019) or to reality-based texturing approaches (Dostal et al., 2018). However, the term "fidelity" is not a scientifically rigorous or objective descriptor when referring to geomatic survey methodologies or digital products, as it lacks a clear, universally accepted definition and quantifiable criteria.

Given the terminological discontinuity described for this type of technology, it seems appropriate to recall the meaning of each of the previously discussed terms in the context of geomatic surveying, namely 'precision', 'accuracy', 'resolution', and 'detail'. These concepts are pivotal in geomatics and have precise meanings that define different characteristics and properties of both the surveying instruments and the resulting outputs. For the reasons outlined above, the definition of "fidelity" will not be included in the following list.

Precision in surveying refers to the consistency or repeatability of measurements obtained under the same conditions. It is a measure of the random errors associated with measurement processes. In other words, high precision is indicated if multiple measurements cluster closely together (Fryer et al., 2007). Accuracy, instead, denotes the closeness of a measured value to its corresponding – so-called – 'true' value. In the context of surveying, this means how close the captured spatial coordinates are to the actual positions in the physical object/scene. Accuracy is affected by systematic errors, instrument calibration, environmental conditions, and the methodologies employed during data acquisition (Wolf & Ghilani, 2012).

While precision and accuracy are often discussed together, it is important to distinguish between them. A dataset can be precise without being accurate if a consistent bias or systematic error is skewing all measurements away from the “true” value. Conversely, measurements can be accurate on average but not precise if they are scattered around the true value due to random errors.

Resolution, instead, refers to the smallest discernible detail that can be distinguished by a surveying system (Campbell & Wynne, 2011). In Remote Sensing (RS) and Digital Photogrammetry (DP), the term “resolution” is associated to different concepts as “Image resolution” and “Spatial resolution” (the latter being equivalent in this context to Ground Sampling Distance – abbreviated as GSD – and Ground Resolution).

Table 1 hierarchically summarises the meaning of each considering the concept's complexity, starting with a mention of the meaning of Sensor Dimensions and Pixel Size (which are correlated with the subsequent concepts). Higher imagery resolution results in capturing more detail that potentially allows for more accurate and detailed reconstructions. However, as will be clarified in the section on photogrammetry, the initial image resolution and the GSD are not the only factors contributing to the quality of the geometric and metric output; instead, they describe the 'raw data' and indicate the potential quality of the final product.

The concept of “resolution” is also present in the context of active, range-based measuring systems. As defined by the International Vocabulary of Metrology, resolution is the “smallest measurable change that the device can detect” (Guidi & Remondino, 2012; Zanuttigh et al., 2016). In other words, in 3D data active acquisition, the resolution defines the level of geometric detail that can be captured, influenced by the instruments' characteristics. It comprises axial resolution, along the z-axis, and lateral resolution, on the xy-plane. While the instruments may specify their maximum resolution, the actual value may be determined by adjusting the sampling step. This concept of resolution in a 3D space, then, is used to describe the

capability of range-based sensing devices to distinguish between surface features while scanning (Luhmann et al., 2019).

Nevertheless, although this concept of (3D) resolution is not commonly used to describe quality characteristics of the output, such as polygonal models (meshes) and 3D point clouds, it can be found as an alternative to the concepts of point cloud and mesh "density" in the terminology of some 3D data processing software. For instance, CloudCompare allows to resample point clouds to a specified "resolution", which directly affects the number of points (CloudCompare, 2021). Similarly, Geomagic Design X uses the term "mesh resolution" when exporting meshes, where adjusting the resolution parameter controls the density and size of the mesh elements (Geomagic Design X, 2020). MeshLab also employs "resolution" in tools for remeshing and simplification, where the target resolution determines polygons count and size (Cignoni et al., 2008). The term (3D) resolution can therefore be found as an alternative to refer to “density” characteristics, as they determine the degree of detail of both meshes and point clouds.

Notably, the (3D) resolution of the digital outcomes can be modified in post-processing procedures, as clouds and mesh sub-sampling, cropping or remeshing. For this reason, when speaking in these terms, we should refer to the density characteristics of the original (“raw”) products, before any further procedure that may introduce any change.

To better clarify the concepts of “density”, in polygonal models it may refer both to the total number of polygons forming the mesh or to the average length of the polygons’ sides (Johnson & Hebert, 1998). Hence, it can describe the “granularity” of the model, indicating the size of the individual polygons. Similarly, in 3D point clouds it is associated with both the total points count or to describe the number of points per given unit area, expressed as points per square millimetre (points/mm^2).

Term			
In Digital Photogrammetry	**Definition**	**Expression**	**Method of Determination**
Sensor Dimensions (Sensor Pixel Count)	The total number of pixels in the width and height directions on the camera sensor *Clarification: This defines the raw capacity of the sensor to capture data, directly influencing pixel size and GSD	Pixel number in the width and height direction on the camera sensor (e.g., 5472 × 3648 pixels, as in a ~20 Megapixel camera)	Known by the camera manufacturer
Physical Pixel Dimensions (Pixel Size)	The size of individual pixels on the camera sensor, defined by dividing the sensor dimensions by the number of pixels in each direction	Pixel size (e.g., 6.54 μm/pixel)	Sensor Width & Height / Number of Pixels in the Width & Height direction (by manufacturer)
Image Resolution (Image Pixel Count)	Total number of pixels in the width and height directions of the captured image *Clarification: may differ from the sensor's pixel count if the image has been resampled, cropped, or due to crop factors or aspect ratio changes in the camera settings	Pixel number in the width and height direction in the final image (e.g., 4000 × 3000 pixels)	Known by the image properties
Spatial Resolution (GSD or Ground Resolution in RS and DP)	The smallest ground distance that is represented by a single pixel in the image, indicating the geometric sampling of ground features by each pixel *Clarification: In DP and RS it is often equated to the GSD	Ground distance per pixel (e.g., 1 mm/pixel)	Pixel size at the image scale: GSD= Pixel Size× Acquisition Distance/ Focal length
In Range-based surveying			
(3D) Resolution in active sensing devices (e.g. TLS or SLS)	Instrument property defined as the "smallest measurable change that the device can detect"	Distance units along the Z-axis (axial resolution) and on the XY plane (lateral resolution)	Known by instruments' manufacturer

3D products (point clouds and models)			
(3D) Resolution as an alternative to density	Total points count or points count per unit area (point clouds); Total polygons count or average polygon sides length (models) *Clarification: It is commonly reported as "density"	Tot. points count (e.g. 1 mln) or points per unit area (e.g., 100 points/mm^2); Tot. poly count (e.g. 1 mln) or length of the polygons' sides (e.g., 0.1 mm)	Computed by analysing the geometrical features of the models with 3D processing software

Table 1. Concepts associated with resolution in photogrammetry and range-based surveying (Schenk, 1999; Awange & Kiema 2019)

Also in scientific literature, the concept of resolution is used to describe quality characteristics of 3D models or point clouds ascribable to the concept of "density". Fang et al. (2015) discuss how point cloud "resolution" influences the level of detail in a 3D dataset. Similarly, Remondino et al. (2009) highlight the importance of high-resolution 3D scanning in capturing detailed point clouds for cultural heritage objects, where "resolution" refers to the density of points acquired. These examples confirm that a concept of "resolution" in the 3D domain is indeed used also to describe qualitative characteristics of final models and point clouds, not only to instruments' capabilities.

A similar concept to (3D) resolution – yet more generic – is that of detail, which pertains to the richness of information captured in spatial and/or geometrical data (Kraus, 2007). In 3D surveying, detail is influenced by the sensors' capabilities, the data processing techniques used and the noise level in the dataset. The term (high/medium/low-) detail can be also found in association with the output data, not only to the sensing devices. High-detail datasets are characterised by the capability to represent fine features, crucial for applications such as forensic analysis, precision engineering and, as in the case of this thesis, heritage investigation.

Importantly, a digital product can be highly detailed but not accurate, or vice versa. For instance, a 3D model generated from high-resolution images may exhibit a high

level of detail, capturing intricate features of a structure. However, if the control points used for positioning and scaling are inaccurate – or absent – the entire model can be shifted or scaled incorrectly, resulting in high detail but low metrical accuracy (Lerma & Muir, 2014; Barazzetti, 2017). Conversely, a model might be accurately positioned in space with correct dimensions (high accuracy) but lack fine details due to low-resolution data acquisition, resulting in poor detail.

This distinction is crucial because the level of detail does not inherently guarantee accuracy. Detail relates to the amount of information and the smallest features that can be represented, while accuracy relates to how correctly that information reflects the real world from a metrical point of view. In practice, achieving both high detail and high accuracy requires careful planning, appropriate equipment selection, and rigorous data processing methods (Barber & Mills, 2007).

Lastly, high detail is not necessarily equivalent to correctness and high-quality output. The level of detail can be also too high due to an oversampling of the raw data and/or to a forced creation of extremely high-density models. In these cases, the redundancy of the data may result in noise and aberrations in the digital reconstructions. Moreover, it is important to notice that a highly detailed visualisation of a surface in a digital format, can also be achieved through a high-resolution texture, to balance the lack of geometrical details with a highly refined visual representation.

In light of all these considerations, it is important to clarify that the survey methodologies considered in this thesis will be referred to as "high-detail". This terminology has been chosen because the level of detail in the geometric reconstruction has been prioritised for the proposed applications, which focus on capturing the finest and most complex surface characteristics of the objects under study.

Therefore, the term "high-detail 3D survey" will be preferred over "high precision" or "resolution". While the survey tools presented can indeed ensure high levels of

accuracy and resolution in the resulting outputs, the emphasis here will be on their ability to achieve a highly refined digital representation of the analysed geometry. This capability allows for an in-depth morphological analysis, serving various purposes aligned with the application field of Heritage Science.

2.1.2 Lexical issues in close-range photogrammetry

Another terminology issue to be addressed concerns the discipline of digital photogrammetry, more specifically the vocabulary related to the field of (very) close-range image-based detail reconstruction methodologies. First, the expression 'very close-range' is here proposed to define photogrammetry applications in which single objects or limited portions of larger surfaces are digitised but at a remarkably high level of detail (at least below one millimetre as spatial resolution and as final 3D resolution of point clouds and models). Some other scholars proposed the use of "very close-range" in the field of detailed 3D reconstructions, such as Yanagi & Chikatsu (2010) or Patrucco et al. (2023), to better distinguish between this type of applications to those of "close-range". This category is indeed quite broad and also refers to site- and architectural-level photogrammetric applications, in which the need for a very high level of detail is not always the main priority. In fact, the expression "close-range" photogrammetry was conceived to distinguish terrestrial applications of image-based 3D surveying from airborne ones (McGlone, 2004).

However, during the decades, the terrestrial usage of photogrammetry has expanded at many different levels, from the site to architectural to single-objects level. Yet, the practices of site and architectural 3D documentation are peculiar and different from many points of view from those implemented in single-object digitisation (De Paolis et al. 2020). Hence, it appears that including this wide range of applications under the same category may be a potential source of ambiguities and imprecisions. Some scholars, such as Luhmann et al. (2023), proposed to categorise photogrammetry according to the camera acquisition distance, distinguishing "close-range" photogrammetry from "macro"-photogrammetry: the first applies for images acquired

at a < ca. 300 m distance, while the second is referred to images with a > 1 scale. Moreover, the authors add a parenthesis to clarify the definition of macro-photogrammetry, writing "microscope imaging". Hence, the terms "macro" and "micro" appear to be used with a similar meaning.

In the photogrammetric context, in fact, the terms "micro-photogrammetry" and "macro-photogrammetry" are frequently used interchangeably for very similar types of applications and techniques. One study, for instance, mentions "micro-scale photogrammetry" to refer to surveying equipment consisting of a laser speckle projection system and a camera equipped with a macro lens (Sims Waterhouse et al., 2017). Similarly, Arriaza et al. (2017) report an application of "micro-photogrammetry" for the analysis of animals' tooth morphology, using a macro-lens mounted on a standard camera.

In a set of articles, instead, Antinozzi et al. (2021, 2022a, 2022b, & 2023) propose the terms "micro-surveying" and "micro-photogrammetry" to refer to 3D reconstructions based on images acquired with a digital microscope, presenting different applications and configurations for the data collection and processing. Similarly, Previti et al. (2024) utilise the term in the context of high-detail surface analysis, emphasising the level of detail achieved with microscopy-derived imagery. As observed, the term 'micro-photogrammetry' is used to refer to imagery data collection performed either with microscopic equipment or with a camera equipped with macro lenses.

In contrast, a study on damage assessment within cultural heritage contexts adopts "macro-photogrammetry" to describe the documentation – with macro lenses – of structural damages in larger heritage artefacts (Angheluță & Radvan 2019). Similarly, research investigating photogrammetric applications in archaeology employs "macro-photogrammetry" for the documentation of a very small object, photographed with extension tubes mounted on the cameras to further increase the magnification rates (Gajski et al., 2016; Vavulin et al., 2019). Marziali & Marziali (2019) propose the implementation of focus-stacking strategies for the reconstruction

of small-sized archaeological artefacts with “macro-photogrammetry”. In the mechanical field, instead, Rodríguez-Martín et al. (2016), discuss the employment of digital photogrammetry (using macro-lenses) for the measurement of the angle of misalignment in welding.

The examination of these articles reveals that despite the congruence in techniques and applications, the terminology remains inconsistent, underscoring the need for a unified lexical framework. Establishing uniform definitions and consistent terminology could enhance scholarly communication and collaborative efforts within the domain of digital photogrammetry. To accomplish this aim, it seems useful to recall the original – and well-established – meaning of “micro”, “macro” and “close-up” in the context of photography, which is strictly related to photogrammetry and from which these terms have been “borrowed”.

Micro-photography involves capturing images of subjects that are generally invisible or difficult to distinguish with the naked eye. This technique is typically employed for specimens of a few mm or even smaller than 1 mm. The term implies a magnification ratio starting from 10x and often exceeding 100x, depending on the resolution required. To achieve such high magnifications, a compound microscope with a digital camera attachment is typically used, as well as optical and stereomicroscopes in fields such as biology, crystallography, chemistry etc. (Murphy, 2012).

On the other hand, macro-photography is employed to capture subjects at a 1:1 or greater object-to-sensor reproduction ratio. This range is ideal for revealing fine details that are barely visible to the naked eye, requiring detailed imaging to showcase their intricate features. Unlike micro-photography, macro-photography does not rely on microscopes but instead uses dedicated macro lenses mounted on standard cameras. These lenses typically have a focal length between 50 mm and 200 mm, allowing photographers to achieve high magnification without the need to position the camera too close to the subject, while maintaining large object-to-sensor reproduction ratios (Thompson, 2017).

It is important to note that the 1:1 reproduction ratio refers to the size of the subject projected onto the camera sensor, regardless of the sensor type. For example, a 1 cm object will be reproduced as 1 cm on the sensor. However, the field of view differs depending on the sensor size. On a full-frame sensor, the captured area will appear wider, while on smaller sensors like APS-C, the same 1:1 ratio results in a narrower field of view, making the subject appear larger in the final image. This effect is due to the crop factor, not a change in the reproduction ratio itself (Allen & Triantaphillidou, 2010).

Close-up photography, instead, is less "extreme" compared to the other two techniques, with a typical reproduction ratio ranging from 1:10 to 1:1. Standard lenses with zoom capabilities are often sufficient for this type of technique. Hence, the magnification rate is not the main focus in close-up photography, since its aim is not to capture extremely fine details but to isolate the subjects in the captured scene (Davies, 2009).

While all three techniques may be used to capture fine details – also depending on the camera sensors' specifications – they differ significantly in terms of magnification range, equipment requirements, and application contexts. In other words, they have precise definitions and are well-distinguishable from one another. Within the field of geomatics, instead, the terms "micro" and "macro" have been adapted from their original photographic context but are applied in a less precise manner. This "semantic borrowing" from the photography world has resulted in conceptual ambiguities, as the terms do not consistently correspond to the original distinctions.

Some authors within the 3D surveying community have acknowledged this issue, advocating for a more precise and standardised application of terminology. Mancuso & Pasquali (2015), for instance, propose to make a distinction between close-up and micro/macro photogrammetry based on the magnification ratio: "macro and micro is therefore related to shots that capture the subject with a factor of at least 1:1, with the result that the subject captured by the camera sensor has got the same dimensions

that it really has". Here the authors equate the concepts of "micro" and "macro" because – in their opinion – the confusion between the two is due to inconsistencies in the related terminology among different camera brands: some, when referring to lenses with a 1:1 magnification ration, use the term "macro", while some other brands prefer "micro".

In Verdiani et al. (2018), instead, an example of macro-photogrammetry is offered, in which the authors compare the obtained 3D output with different lens configurations, macro and non-macro, but guaranteeing a reproduction ratio of at least 1:1. The authors also mention that macro photography could be applied to "all lenses that are able to focus very closely objects", because also "some compact cameras have the macro function and are able to return quality images". Hence, the authors extend the concept of "macro" photography – and photogrammetry – to those applications in which the camera-object distance is limited. This definition seems, instead, more adherent to that of "close-up photography", which is a more generic category for images acquired at short distances.

Nevertheless, despite the context of photogrammetry being different from that of photography from many points of view, aligning the terms "close-up", "macro" and "micro" with their original definitions may contribute to greater precision and consistency also in the photogrammetric field, in which several lexical misalignments are present. Therefore, in light of these observations, a proposal is made to attempt to clarify and standardise terminology in the context of close-range photogrammetry, with a sub-distinction into three main categories:

- Close-up photogrammetry: surveying with non-macro lenses (less than 50 mm nominal focal length) at close distances to objects allowing for sub-millimetre spatial resolutions. For example, this may be the case of a survey of a centimetres/meters-range object conducted with a 20 *Megapixel (*MP*)* camera equipped with a 24 mm focal length lens where, at an average shooting distance of 1.5 *metres*, a GSD of ~0.4 mm is obtained (figure 2).

- Macro-photogrammetry: a survey with macro lenses (greater than 50 mm nominal focal length) that, despite the fact that the object-sensor reproduction ratio is not necessarily ≥ 1:1 (it is quite unusual to digitise objects that entirely falls within the sensor's dimensions), still permits to obtain extremely detailed imagery sets with sub-mm GSDs. It may be the case of an object (in the range of some centimetres) photographed at an average distance of ~15.5 cm with a 100 mm focal length macro lens mounted on a 20 MP camera with a 6.2 microns pixel size (GSD ~0.010 mm, figure 3).
- Micro-photogrammetry: a survey using magnification devices to enable image acquisition at high zoom levels (≥ 10×). For instance, a specimen measuring a few millimetres can be captured with a digital microscope (1280 × 1024 pixels image resolution, ~5 cm acquisition distance, 4.89 mm focal length, 2.5 microns as pixel size on sensor), resulting in a 0.025 mm GSD – as in the image presented in figure 4.

Notably, the high magnification achieved in microscopy imaging does not necessarily correspond to long focal lengths, nor does it guarantee exceptionally high spatial resolution. In other words, greater magnification does not always result in a significantly reduced GSD. In fact, in the mentioned examples, the GSD obtained with the macro-lens equipped full-frame camera is 10 microns, while the one obtained with the digital microscope is 25 microns. This is because the GSD is inversely proportional to the focal length, which in magnification devices tends to be quite short.

Figure 2. A close-up image of the Neptune fountain in Bologna (photography by the author)

Figure 3. A macro image of a xylographic stamp in Bologna "Palazzo Poggi" collection (photography by the author)

Figure 4. A micro image of a scarabaeus-shaped gem in Bologna Archaeological Museum (photography by the author)

Magnification in optical systems is determined by a combination of factors, including the focal length, the object distance, and the sensor size. According to the lens equations presented in OpenStax College Physics book (2022, section 26.4: Microscopes), the magnification (M) of a lens is given by:

$$M = \frac{h_i}{h_o} = -\frac{d_i}{d_o}$$

Where:

- h_i and h_o are the image and object heights, respectively,
- d_i is the image distance (distance from the lens to the sensor),
- d_o is the object distance (distance from the object to the lens),
- The negative sign indicates image inversion.

The lens equation relates the focal length (f) to the object distance (d_o) and image distance (d_i) as:

$$\frac{1}{f} = \frac{1}{d_o} + \frac{1}{d_i}$$

These equations demonstrate that magnification depends on the ratio of the image distance to the object distance, not solely on the focal length. In digital microscopy, high magnification is achieved through short focal lengths and minimal object distances. By placing the specimen very close to the lens (small d_o), the image distance (d_i) increases to maintain focus according to the lens equation, resulting in higher magnification. Therefore, even with a short focal length, significant magnification is possible because the optical design focuses on close-up imaging rather than relying solely on focal length.

The sensor size (S) also plays a role in effective magnification. A smaller sensor captures a smaller portion of the image projected by the lens, effectively increasing

the perceived magnification when the image is displayed. The angular field of view (θ) is influenced by the sensor size – as well as by the focal length – and can be expressed as:

$$\theta = 2 \cdot \arctan\left(\frac{S}{2f}\right)$$

A smaller sensor size (S) results in a narrower angular field of view (θ), causing the subject to occupy a larger portion of the image. The focal length (f) also plays a role in determining the field of view: as f increases, the field of view narrows. This inverse relationship means that shorter focal lengths allow for a wider field of view, while longer focal lengths zoom in on a smaller portion of the scene, narrowing the field of view.

In high-magnification devices such as digital microscopes, the pixel size on the sensor is also very small (e.g., 2.5 microns in the case of our example), primarily because the sensors themselves are much smaller compared to those in standard cameras. In theory, a smaller pixel size leads to a smaller GSD, thus improving spatial resolution. However, despite the advantage of having smaller pixels, the GSD in digital microscopes remains relatively large due to the short focal lengths typically used in these devices. Hence, it is important to recognise that in microscopic imaging, the GSD is not necessarily extremely small because the focal length appears in the denominator of the GSD equation.

The GSD, describing the real-world distance represented by each pixel in the image (as anticipated in section 2.1.1), is defined by:

$$\text{GSD} = \frac{d_o \times \text{Pixel Size}}{f}$$

This formula illustrates that for a fixed object distance (d_o) and pixel size, a shorter focal length (f) leads to an increased GSD. Consequently, although high magnification is achieved through the use of short focal lengths and minimal object distances, the

spatial resolution in microscopic imagery may not be as fine as expected due to the inverse relationship between focal length and GSD, even if the pixel size is very small. This insight into the relationship between magnification and focal length and GSD seemed necessary to clarify the reasons why, as in the mentioned examples, a macro photograph with a standard 20 MP camera and a 100 mm macro lens can produce better results in terms of GSD than a microscope with high magnification ratios.

Thus, these considerations further underscore the importance of precise terminology in very close-range photogrammetry. The term "micro" is often used, perhaps misleadingly, to imply a qualitatively "better" result in terms of image resolution. However, as discussed, this is not necessarily the case. Based on the observations and arguments presented above, it is suggested that a clearer distinction be made between the three subcategories of very close-range photogrammetry, focusing solely on the optical devices employed (figure 5), rather than on the quality of the output. Moreover, the proposed differentiation aims to align more closely with established photographic terminology, providing a more structured approach to the vocabulary used in image-based, detailed 3D surveying. As will be further discussed in the following section, the applications of such methodologies in the study of cultural heritage are numerous and of significant interest.

Figure 5. From right to left: a zoom lens for close-up photography, a macro lens and a digital microscope

Nevertheless, a lack of consistent terminology persists in describing both the tools employed and the results obtained. This inconsistency, as previously highlighted, may be attributed to the use of high-detail 3D reconstructions across a wide range of disciplines beyond cultural heritage, including industry, medicine, and many others.

The broad applicability and diverse usage of geomatic techniques have encouraged many researchers to adopt them with a more investigative approach. This shift is evident as experts from a variety of fields have actively engaged in research involving geomatic topics, particularly 3D surveying. Additionally, as noted in section 1.1, the rapid advancement of accessible technologies, increasingly available to a broader audience in terms of usability and cost, has facilitated their widespread adoption. Solutions marketed as "user-friendly," combined with affordable devices like those integrated into smartphones, have fostered a perception of geomatics as a "service technology", accessible and usable also by users with limited expertise.

Traditionally, geomatics and surveying have functioned as support disciplines, providing critical assistance to a variety of research fields. However, with the increased accessibility and user-friendliness of geomatic technologies, researchers from various disciplines are now more directly involved in their application, often without specialised geomatic training. This development may be seen as a reflection of the so-called “democratisation” of technology, but at the same time, it also raises questions about the role of specialised expertise in this context.

This thesis does not seek to criticise this trend but rather aims to examine some of its implications. The intent is to foster reflection on these developments without attempting to provide a definitive answer to the broader ethical and theoretical question: is this shift beneficial or detrimental to the field?

2.2 High-detail 3D surveying in Heritage Science: examples from the literature

Human vision exhibits impressive resolution capabilities, allowing us to perceive fine details in our environment. Under optimal conditions, the human eye can resolve two points separated by as little as 0.1 millimetres when viewed at a distance of about 25 centimetres (Ogle, 1951). The capability of modern high-resolution digital models to represent objects' surfaces in an exceptionally refined manner, and in some cases even surpass the resolving power of the human eye, makes them a powerful tool in the field of heritage science. This possibility to digitise objects at a level of detail exceeding human vision is crucial not only for the detailed documentation of surface textures but also for enabling the virtual manipulation of these models in ways that are physically impractical or impossible.

The digital format of 3D models allows researchers to explore artefacts in their global geometry, to inspect them from different angles and at high magnification, or to examine them under various virtual lighting conditions that can reveal otherwise imperceptible features. These capabilities are particularly valuable for cultural heritage objects, which often cannot be physically accessed or manipulated due to their fragility or location. This flexibility, combined with the ability to capture data at both macroscopic and microscopic levels, positions high-detail 3D models as essential tools for the preservation and study of heritage.

Moreover, the possibility to integrate high-detail 3D surveying with other analytical and diagnostic techniques provides valuable opportunities to study and conserve cultural heritage objects in a comprehensive and non-invasive manner. Consequently, combining 3D surveying technologies – such as photogrammetry, laser scanning, and structured-light projection scanning – with other non-contact diagnostic methods like computed tomography (CT), multispectral and hyperspectral imaging (MSI and HSI), thermography, and endoscopy has become a cornerstone of modern heritage research. This integrated approach not only provides detailed surface and internal

data but also supports more accurate assessments of material properties and degradation phenomena.

The selection of research works analysed in this review highlights the diverse applications and advantages of using high-resolution 3D surveying for Cultural Heritage. These studies are grouped into five thematic categories, based on their primary focus: (1) robust digital documentation to support diagnostics and restoration, (2) philological analysis, (3) material and state of conservation characterisation, (4) archaeological and historical contextualisation, and (5) virtual restoration. Each category underscores the role of high-detailed 3D models – also used in combination with diagnostic technologies – in providing a more nuanced understanding of cultural heritage, enhancing both academic research and practical conservation efforts.

- *Robust Digital Documentation to Support Diagnostics and Restoration*

Robust digital documentation can form the basis for subsequent conservation, restoration, and research activities. High-detail 3D models, capable of capturing precisely the geometry and texture of heritage objects, are crucial for documenting their conditions. Several studies emphasise the role of 3D reconstructions in monitoring and documenting cultural heritage, making them invaluable for restoration planning and condition assessments.

For instance, Hodač et al. (2023) utilise close-range photogrammetry to assess changes in stone surface topography following restoration interventions on historical artefacts. The team documented stone surfaces before and after various treatments using photogrammetry, achieving geometric accuracy within single-tenths of a millimetre. This enabled the identification of even the subtlest changes to surface features and tool marks. The study illustrates how close-range photogrammetry can serve as a non-invasive method for evaluating the impact of different conservation strategies on stone artefacts, providing detailed data to guide future interventions.

A similar example is offered in Girelli et al. (2019), where the authors document the restoration of the Neptune fountain in Bologna using a hybrid approach combining laser scanning, structured-light projection scanning and photogrammetry. This integrated methodology addressed the specific requirements of documenting complex geometries and material textures at different levels, ensuring that both fine details and broader structural features are captured accurately (figure 6). This survey was instrumental in supporting restoration planning by allowing conservators to assess the monument's condition virtually and to map the results of their investigations and interventions in a spatially-referenced informative system.

The authors highlight, however, the challenges related to the high levels of expertise required and the operational constraints when integrating multiple scanning technologies, but adopting a multi-scaled approach can represent a solution for large and complex assets' documentation.

Figure 6. The Neptune Fountain (Bologna, Italy) 3D model (Girelli et al., 2019)

Trevisiol et al. (2022) present a valuable case study on the integration of high-detail 3D models with diagnostic data for material characterisation and structural monitoring. Their research on the Santa Croce Complex in Ravenna utilises a combination of laser scanning, photogrammetry, and multi-temporal thermography to document the condition of historical masonry structures. A notable aspect of this study is the use of both passive and active thermography to detect moisture-related damage and thermal anomalies. By incorporating these thermal datasets into the geometric 3D survey, the authors created a comprehensive tool for visualising moisture distribution patterns, mapping hidden structural weaknesses, and assessing the effectiveness of previous conservation treatments.

This multi-layered approach provided a more complete understanding of the masonry's condition, enabling dynamic monitoring of degradation patterns and structural integrity over time. However, the study also highlights the challenges of integrating thermal and geometric data. Despite these complexities, the methodology offers a framework for enhancing the long-term preservation and management of heritage structures.

Another significant study by Colizzi et al. (2008) demonstrates the use of reality-based Virtual Reality (VR) environments for heritage diagnostics. The research integrates photogrammetry, laser scanning, and thermography to create a VR-based diagnostic model of the S. Stefano Crypt in Vasto (Lecce, Italy). This virtual scenario allows users to explore different diagnostic layers and visualise the interaction of materials and environmental factors in real-time. The integration of thermal data, in particular, provides valuable insights into the material conditions and structural health of the basilica, enabling a comprehensive platform for testing and visualising different restoration scenarios, and supporting more informed decision-making.

In the same context of 3D data integration with diagnostics, interesting examples are offered by Zhan et al. (2021) and Kim et al. (2023). In the first research work, the authors introduced an integrated methodology of photogrammetry, CT, and

endoscopy to digitise a complex example of technological heritage, a 200-year-old gyroscope, which could not be fully captured by a single method. This multimodal approach allowed for the creation of comprehensive 3D models that detailed both external and internal structures, supporting its digital documentation and analysis. Analogously, Kim et al. (2023) adopted a similar workflow for a deer-shaped pottery horn cup excavated from archaeological tombs in Marisan Mountain (South Corea), by merging CT scanning and 3D scanning. The study developed a mesh-based convergence methodology that fused internal and external data, overcoming the limitations of individual scanning methods. The resulting models enabled a holistic view of both surface and internal features, which were used to evaluate the structural integrity and guide restoration decisions.

- *Philological Analysis*

High-resolution 3D models have proven to be particularly valuable in philological research, where the study of inscriptions and texts often relies on the accurate representation of surface geometries. Traditional methods of textual analysis, such as manual transcription and two-dimensional imaging, are often insufficient for capturing the nuances of worn or damaged inscriptions. Moreover, the integration of 3D data with imaging techniques like Polynomial Texture Mapping (PTM) and Reflection Transformation Imaging (RTI) can significantly improve the ability to analyse and interpret these materials.

More specifically, in RTI, a series of photographs is taken from a fixed camera position while the object is illuminated from different angles. By combining these images through computational methods, a composite image is generated that allows for interactive virtual re-lighting, highlighting subtle surface features that would be invisible or hardly visible under normal lighting conditions (Malzbender et al., 2006). Polynomial Texture Mapping (PTM), instead, is a specific type of RTI that uses polynomial functions to model the reflectance properties of a surface. The resulting PTM files encode how each pixel changes with different light directions, creating a highly detailed image that enhances surface features (Malzbender et al., 2001).

These methodologies have already been experimented for many years to enhance the readability and analysis of cuneiform texts and other inscriptions. Willems et al. (2005), for instance, employed photometric stereo, a technique that involves taking multiple images of an artefact under varying light directions, to create 2D+ models that can be dynamically re-illuminated to highlight specific surface features and read faint inscriptions. While 3D models capture the full volumetric geometry of an object, 2.5D models represent surface relief and texture with limited depth information, yet allowing for a superficial analysis from different view angles and at high resolutions.

Hameeuw and Willems (2011) provide a detailed exploration of how PTM and RTI can enhance the visibility of cuneiform inscriptions. These techniques, when combined with 2.5D and 3D models, enable researchers to interactively manipulate lighting conditions to reveal subtle surface features, making it possible to discern characters that are otherwise invisible in standard photographs. The authors emphasise that the success of this approach depends on the quality of the initial 3D data, as surface irregularities or noise can obscure critical details. Despite these challenges, combining PTM, RTI, and high-resolution 3D models represented a significant advancement in the study of ancient texts.

Later on, Fisseler et al. (2014) developed the *CuneiformAnalyser* software, a tool that integrates 3D scanning and digital visualisation to support the virtual reconstruction of cuneiform tablets. The software facilitates the joining of virtual fragments and the extraction of text features, enabling philological analysis of fragmented texts. These studies emphasise the potential of 3D technologies to contribute to the reconstruction and interpretation of ancient texts, making them accessible to a wider audience of scholars and enhancing the preservation of epigraphic heritage. Similarly, Samaan et al. (2016) present a photogrammetric approach for creating high-resolution 3D models of stone inscriptions from a Mongolian archaeological site. Using open-source Structure-from-Motion software, the authors generated depth maps that allowed for a thorough analysis of the inscriptions' morphology, supporting epigraphic research.

More recently, Cantó et al. (2022) applied a multi-light photogrammetry approach to the study of Palaeolithic rock art in the *Cova de les Meravelles* (Spain). By capturing images under different lighting conditions, the authors enhance the visibility of faint engravings and distinguish between overlapping motifs. Moreover, in this work, the implementation of image analysis strategies to further enhance the collected dataset, namely Principal Component Analysis (PCA), was also tested. In essence, PCA is a widely used statistical technique for dimensionality reduction and feature extraction; it transforms a set of correlated variables (such as RGB – Red, Green, Blue – pixel values in images) into a set of linearly uncorrelated components, known as principal components. These components capture the maximum variance in the data and are ranked by their significance (Kurita, 2020).

This method is effective, for instance, for highlighting faint or subtle features in complex datasets, such as rock art motifs, by isolating the most relevant patterns from background noise. In the mentioned paper by Cantó et al. (2022), the authors noted that the integration of this method with a high-resolution photogrammetric model can provide a comprehensive representation of the site, supporting a more nuanced interpretation of the chronological and stylistic relationships between the motifs (figure 7).

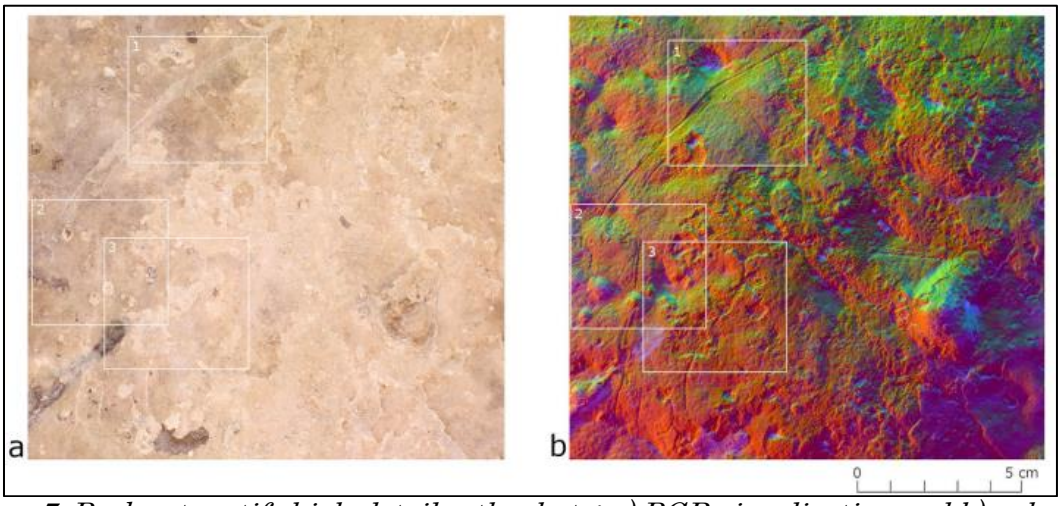

Figure 7. Rock art motifs high-detail orthophoto: a) RGB visualisation and b) enhanced visualisation with false-colour PCA-generated bands (Cantó et al., 2022)

- Material and State of Conservation Characterisation

As already mentioned, the detailed geometric data captured in high-resolution 3D models can be further enhanced by integrating diagnostic imaging techniques, providing a powerful tool for characterising the materials and assessing the state of conservation of cultural heritage objects. By mapping diagnostic data onto 3D models, researchers can visualise material properties and degradation patterns in a spatially accurate manner, supporting more informed conservation decisions.

Grifoni et al. (2020), for instance, employed a multi-modal approach combining 3D photogrammetry with X-ray Fluorescence (XRF) and Fourier-transform infrared (FT-IR) spectroscopy to analyse a collection of 19th-century poly-material artefacts. By overlaying the spectroscopic data onto the 3D models, the researchers were able to create a comprehensive map of material compositions and monitor changes over time. This dataset provides valuable information for conservators, offering a holistic view of the artefacts' condition. However, the study also emphasises the technical challenges of aligning spectroscopic data with 3D models, indicating that further research is needed.

Caballares et al. (2020) also explore the use of high-detail 3D surveying in material characterisation, focusing on the documentation of Palaeolithic engravings. Their study integrates macro-photogrammetry with image processing strategies. By generating high-resolution Digital Elevation Models (DEMs) and orthophoto-mosaic, layered with multispectral data and enhanced images with image-processing tools, the authors were able to identify pigment residues and surface alterations that are critical for interpreting the engravings' chronology and cultural context (figure 8). This combination of technologies enabled the differentiation between intentional engravings and natural weathering, highlighting the potential of integrated 3D and image analysis in characterising surface details.

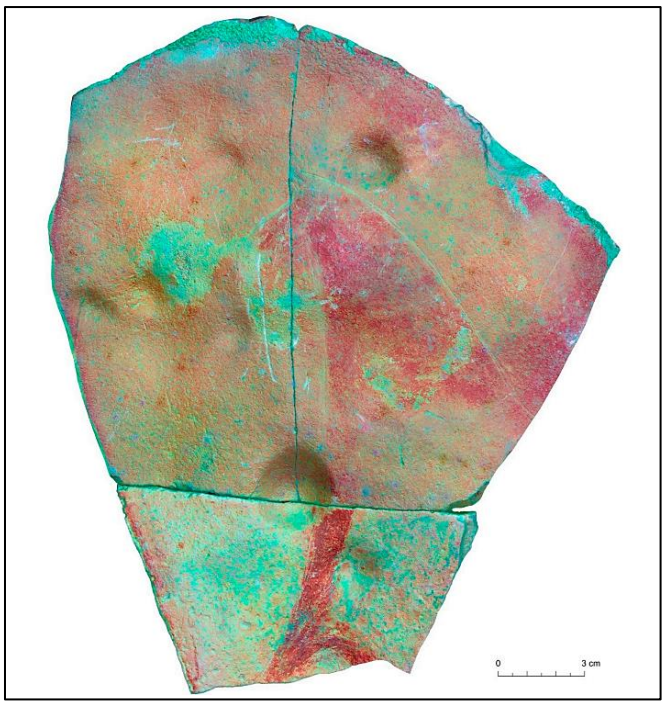

Figure 8. Rock art plaquette orthophoto-mosaic enhanced with image processing strategies (Caballares et al., 2020)

Palaeolithic engravings are the area of application of another research (Fonseca Moro & Perez Pavón, 2024). Here the authors propose a combination of low-cost and macro photogrammetry to achieve high-detail 3D models with exact measurements of engraved motifs, finely documenting Spanish Palaeolithic engravings. The resulting 3D models were used for both conservation and scholarly research, providing information that traditional methods could not capture.

The work by Rahrig et al. (2022) on urban graffiti takes a similar approach by combining MSI with photogrammetry to document complex urban surfaces. The use of MSI, which captures material-specific characteristics across multiple spectral bands, allows the authors to detect underlying paint layers, areas of loss, and other forms of degradation that are not visible in standard 3D models. By integrating this diagnostic data into a detailed photogrammetric model, the researchers produced a comprehensive digital representation of the graffiti, supporting a deeper understanding of its material composition and state of preservation. However, the authors point out that the integration of spectral data with 3D models requires careful

calibration and alignment, which can be challenging in uncontrolled outdoor environments.

The same research group, in Rahrig et al. (2023), took digital documentation a step further by integrating multiband photogrammetry and hybrid false-colour imaging techniques to study the wall paintings of Paolo de San Leocadio and Francesco Pagano in the Cathedral of Valencia. By combining data from the ultraviolet (UV), visible (VIS), and near-infrared (NIR) spectra, the researchers generated high-resolution orthophotos that revealed hidden details such as underdrawings, material differences, and areas of past interventions. This approach not only enhanced the visual documentation but also provided critical data for understanding the artist's techniques and the painting's condition.

In another example, Barbieri et al. (2023) investigate the integration of 3D data and thermographic surveys for the monitoring and management of a Rationalist architectural structure in Bologna, Italy. The study focuses on incorporating thermographic data into a Historic Building Information Model (HBIM), which represents both the geometry and material characteristics of the building. By integrating photogrammetry and terrestrial laser scanning, the researchers created a detailed 3D model of the building, which was then enriched with thermal data to map areas affected by water infiltration.

- *Archaeological and Historical Contextualisation*

High-resolution 3D models not only document the physical attributes of heritage objects but also support archaeological and historical contextualisation. By providing a robust digital representation of both fine details and broader spatial relationships of heritage assets, these models enable researchers to have insights into their environmental and historical contexts.

Schmidt et al. (2010), for instance, applied high-resolution 3D laser scanning and image processing to the documentation of Sutra inscriptions in China. These inscriptions, located in the Sichuan province, date back to the 8th to 12th centuries and

represent a significant cultural asset requiring meticulous documentation. The team employed hybrid scanning techniques, including structured-light projection scanning and PTM, to capture intricate surface details. The resulting digital models were then used for automated text recognition and historical analysis. This study exemplifies how 3D data can serve as a base for complex analytical tasks such as character recognition and stylistic analysis, enhancing the legibility of the inscriptions and providing new insights into their creation and use.

Likewise, Jalandoni and Kottermair (2018) employ Structure-from-Motion (SfM) photogrammetry and GIS tools to digitally trace and classify engraved motifs at a rock art site in the Philippines. The combination of 3D models with spatial analysis techniques enables the researchers to reconstruct the spatial relationships between motifs and explore their cultural significance. The digital models reveal patterns and groupings that would be difficult to discern *in situ*, providing new insights into the symbolic and ritual functions of the site. The authors highlight that while SfM photogrammetry is effective for capturing the geometry of large rock surfaces, its accuracy can be compromised by vegetation cover and uneven lighting conditions, suggesting that additional imaging methods may be needed for complex sites.

Similarly, Herzlinger et al. (2017) use 3D morphometric analysis to classify Acheulian handaxes based on their morphological characteristics. By generating high-resolution 3D models of the handaxes and applying geometric morphometric techniques, the authors were able to quantify shape variations and classify the artefacts according to different knapping techniques. This approach provides a framework for understanding the technological evolution of stone tool production, illustrating how 3D models can support archaeological research by enabling the accurate comparison of artefacts across different sites and periods. The study also emphasises the importance of capturing high-quality geometric data, as any errors in the 3D model can propagate through the morphometric analysis, potentially leading to inaccurate classifications.

Another relevant example in this context is the work of Bitelli et al. (2020). By integrating structured light scanning with historical research, the authors were able to reconstruct the original appearance of the Longobard basin inscriptions and propose new interpretations of their content. The high-resolution 3D models, combined with archival sources, reveal subtle stylistic differences that suggest the involvement of different craftsmen over time (figure 9).

This integration of digital documentation and historical research provides a more nuanced understanding of the inscriptions' production and use, especially for those "historically debated", highlighting the value of 3D models in reconstructing the historical context of heritage objects.

Figure 9. A portion of the unrolled 3D model of the Longobard basin from S. Stefano church in Bologna, enhanced with Radiance scaling shader (Bitelli et al., 2020)

- *Virtual Restoration*

Virtual restoration, which involves using high-detail 3D models to digitally reconstruct damaged or missing sections of heritage objects, has become a key application of 3D surveying technologies in CH. Virtual restoration offers a non-invasive alternative to physical restoration, allowing researchers to test different restoration scenarios and visualise potential outcomes before implementing physical interventions.

Examples of this kind are offered, for instance, in Arbace et. al (2012), where the researchers offered an interesting case of virtual restoration of a fragmented terracotta devotional statue, damaged during the 2009 earthquake in Abruzzo (Italy). They first digitised all the remaining fragments of the broken sculpture with a

triangulation-based laser scanner and then re-assembled them in a digital environment to recreate the original shape in its integrity. Moreover, they applied photo-texturing algorithms by aligning high-resolution images of the statue to the geometric model obtained, to offer a digital representation of the original polychrome decorations. Finally, in this work the authors also mention that all the phases of digital and physical restoration were also documented, providing an active record of the conservation operations.

In Higueras et al. (2021), instead, the authors presented an example of virtual restoration of a Hispano-Roman architectural ornament (Castulo, Spain). First, they conducted chemical and physical analysis on the sample to confirm the original materials and realisation techniques used for ornament fabrication in Roman times; these materials-related investigations served as guidance to ensure correctness during both virtual and physical restoration procedures. Finally, by creating a high-resolution digital model through close-range photogrammetry of the original structure, the researchers were able to design an accurate 3D-printed mould for the reintegration of lost fragments.

In a similar context, Tucci et al. (2017) use 3D models to simulate different restoration scenarios for the frieze of the *Ospedale del Ceppo* in Pistoia (Italy). The digital models allow the researchers to test various restoration procedures in a virtual environment, minimising the risk of damage to the physical artefact. This capability is particularly valuable for fragile architectural decorations, as it allows conservators to visualise the effects of different treatments and select the most appropriate intervention strategy.

Moreover, the authors proposed an example of virtual reconstruction of a broken portion of the decoration, depicting a female figure. They constructed a 3D model for the missing part of the figure's face (based on iconological hypotheses), aligned it to the photogrammetric model of the frieze and finally 3D printed it, proposing the physical replica as a potential re-integration material (figure 10).

Figure 10. Virtual restoration stages for the reconstruction of a female figure

The research works presented in this review illustrated the potential of integrating high-resolution 3D surveying with diagnostic, philological, and conservation methodologies in cultural heritage research. By providing detailed geometrical reconstructions, these technologies enable a more nuanced analysis of both the physical and historical dimensions of heritage objects, supporting investigations at different levels, from material characterisation to virtual restoration and more.

However, significant challenges remain in terms of the computational demands, costs, and technical expertise required to implement these technologies effectively, especially when combining tools of different domains such as 3D surveying and diagnostics. Addressing these issues will be crucial for maximising the impact of these integrated approaches in heritage science.

As anticipated at the end of the previous section about terminological issues, and as seen from the collection of articles here proposed, there is a variety of disciplines employing geomatic high-detail 3D surveying for heritage science purposes. From engineering (mainly civil but also computer and mechanical engineering) to history to conservation science, many scholars have been exploring the potential of high-detail 3D models for different kinds of investigations of heritage assets.

This variety is a sign that geomatics is having a major impact in this sector, but as mentioned previously, the heterogeneity of disciplines implementing technological

solutions of this kind can lead not only to terminological ambiguities (as seen in the previous section on this issue) but also to a dispersion of theoretical and methodological bases on the techniques employed. This sometimes results in the misuse of technologies or in difficulties in achieving the desired results due to a lack of communication with experts in the field.

This consideration applies in both senses: even surveying and geomatics experts, when applying their tools to the study of cultural heritage, should dialogue with humanities experts who can properly guide the technological applications. A more interdisciplinary dialogue would be beneficial in both directions, especially in the delicate field of cultural heritage. The specific issues related to this field, however, will be discussed in a dedicated section, i.e. section 2.6. First, the most commonly used geomatics instruments in detailed 3D surveying will be described, to provide an overview of the techniques from a theoretical and functioning point of view.

2.3 Main geomatic technologies for high-detail 3D surveying

The variety of geomatic instruments employed to generate high-detail digital outputs, such as those utilised in the case studies discussed earlier, differ across several dimensions. These instruments vary not only in their underlying operational principles but also in terms of precision, accuracy, resolution, portability, limitations, cost/time effectiveness and more.

Broadly speaking and in a more generic context beyond high-detail geometrical reconstructions, 3D surveying instruments in the field of geomatics are categorised into two main groups: passive and active systems. Passive systems depend on external energy sources, such as ambient light, to capture data, whereas active systems generate energy—typically in the form of lasers or structured light patterns—to illuminate objects and subsequently acquire geometric data.

An additional distinction arises from the methodologies used to capture the three-dimensional coordinates of an object's geometry. This leads to a division between

range-based and image-based systems (figure 11). Range-based systems, such as laser-based scanners, are capable of directly measuring distances (i.e., instrument-to-object range) using methodologies such as triangulation, time-of-flight, or phase-shift. Conversely, image-based systems, such as photogrammetry, rely on the acquisition of multiple images from various viewpoints to reconstruct the 3D geometry of an object. These systems are founded on geometrical principles and, in currently available digital-based technologies, also on Computer Vision algorithms (Guidi & Remondino, 2012).

Nevertheless, the boundary between range-based and image-based systems is not always straightforward. Advances in technology have resulted in the development of hybrid systems that integrate stereoscopy and high-resolution imaging with direct distance measurements. These hybrid approaches incorporate the strengths of both methodologies, thereby improving the accuracy and resolution of 3D reconstructions.

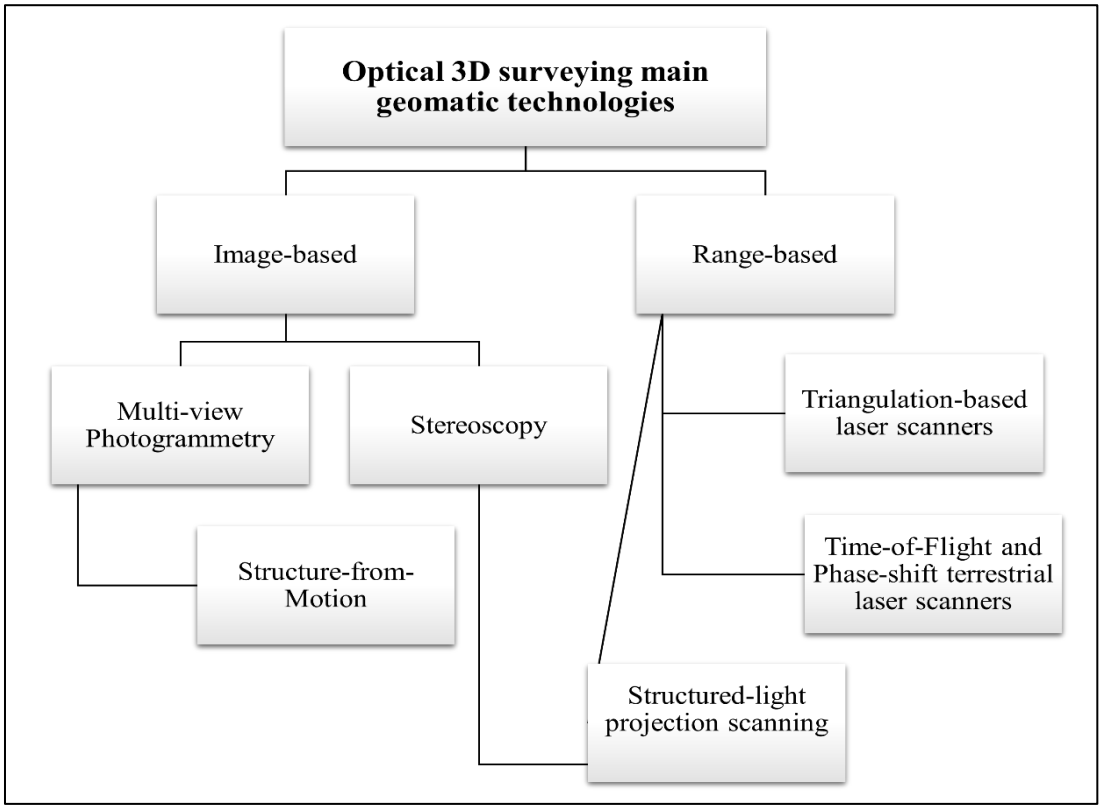

Figure 11. Geomatic 3D surveying main techniques and simplified classification

In this context, for instance, mobile scanning technologies as SLAM (Simultaneous Localisation and Mapping) systems, represent significant advancements. These systems combine direct distance measurements, typically acquired through laser sensors, with image-based 3D reconstruction techniques based on stereoscopy and computer vision algorithms, both actively contributing to the 3D reconstruction process.

As Remondino and Rizzi (2010) and others have noted, selecting the appropriate geomatic instruments for a survey requires a multifaceted evaluation. The decision-making process should consider factors such as the complexity of the object being surveyed in terms of materials and geometry, the desired level of detail, environmental conditions, accessibility of the survey site, and budgetary and time constraints. These considerations play a pivotal role in determining the optimal technology – or combination of technologies – for specific surveying applications, ensuring that the chosen instruments meet the technical and operational requirements of the project.

In high-detail surveying, the choice of surveying instrument(s), and consequently the upstream planning of the work, is an even more delicate matter. This is because, in addition to the mentioned more generic factors to be considered, further challenges arise in this specific branch of geomatics: the trade-off between metric accuracy and geometric detail, balancing the completeness and complexity of the data with its manageability, combining multi-layered information to reconstruct objects both in their entirety, but also in great detail for certain parts of interest... Other challenges, related to the specific context of cultural heritage, will be described in a dedicated section of this thesis (2.6).

From a technical perspective, the most employed geomatic tools in high-detail 3D surveying are laser triangulators and structured light-projection scanners (among the range-based instruments) and digital very close-range photogrammetry (image-based). These three techniques present their unicity, from a theoretical, functional

and operative point of view. Before understanding which could be the benefits and the limitations of them all, several aspects related to these technologies will be analysed further in the next technical sections to provide a theoretical framework which is, indeed, very much connected to the operative issues.

The first technology discussed is a range-based active sensing technology, namely that implemented with Laser Triangulators. It is important to note that other scanning systems exploiting laser sources, such as terrestrial laser scanners, are also used extensively in the documentation of cultural heritage. However, the latter will be excluded from this discussion because such technologies are implemented for architectural or site-level 3D reconstructions, and therefore do not belong to the category of high detail-surveying. Laser triangulators, on the other hand, were developed precisely for this purpose and are mainly applied to small-sized objects.

2.3.1 Laser Triangulators (LT)

Laser triangulation (LT) systems have been employed in 3D scanning and metrology since the 1970s, calculating distances to points on an object's surface using geometric triangulation. LT systems are highly effective in surface profiling and 3D reconstruction, particularly in industrial inspection and automated quality control (Keferstein & Marxer, 1998). The versatility and non-contact nature of these systems have led to widespread use in various fields, including manufacturing and industrial metrology. Additionally, LT systems are often used as an alternative to Coordinate-Measuring Machines (CMMs) for specific applications, offering greater flexibility and speed, particularly when dealing with complex geometries or requiring rapid, non-contact measurements.

Despite their benefits, LT systems are costly – some instruments of this type can reach hundreds of thousands of euros – which has limited their use in cultural heritage documentation compared to more affordable techniques such as structured-light projection scanning or photogrammetry. The high costs are driven by the precision of the spatial coordinate retrieval and the sophisticated physical

components required to generate the laser source. Nonetheless, LT systems have been successfully employed also in CH, especially in contexts that demand extreme accuracy and level of detail, as in the reconstruction of complex morphology and small-dimension objects (Boehler & Marbs, 2001; Guarnieri et al., 2010; Hess, 2017).

- *Historical overview of LT*

As mentioned, the history of LT technology dates back to the late 1970s, when scientists explored using LASER technology (Light Amplification by Stimulated Emission of Radiation) for metrological purposes (Agin & Binford, 1973). Early developments were driven by the laser's unique properties—coherence, small divergency, high intensity, and monochromaticity—which enabled unprecedented precision in distance measurements (Giacomo, 1976).

The characteristic coherence of laser light, referring to the phase relationship between emitted waves, ensures that the light waves remain in phase over long distances, making the laser beam tightly focused and minimising diffraction. Coherence is crucial in LT because it allows the beam to maintain its precision across varying distances (Saleh & Teich, 2019). An important characteristic of laser light is its remarkable intensity, which allows for detection from far away or on surfaces with low reflectivity. This intensity helps minimise the signal-to-noise ratio in LT systems, making accurate distance measurements more feasible. The monochromaticity of laser light, i.e. the emission of a single wavelength, ensures uniform wave behaviour, reducing chromatic aberrations (Svelto, 2010).

Early LT systems were simple (figure 12), projecting a laser spot onto objects and observing it with a camera from a known angle (Penney & Thomas, 1989). With the advent of position-sensitive detectors (PSDs) and charge-coupled devices (CCDs), the resolution and speed of these systems increased significantly, enabling real-time measurements.

By the 1990s, these improvements in the optical components and the integration of galvanometric mirrors allowed for more sophisticated systems that addressed

problems like speckle noise and edge effects, further improving accuracy (França et al., 2005). In parallel, laser triangulation systems were soon integrated into CMMs, where they replaced traditional mechanical probes. Laser line scanners projected a line of laser light across an object's surface and captured the deformed reflection using a camera, which allowed CMMs to measure complex surfaces without physical contact (Smith & Zheng, 1998).

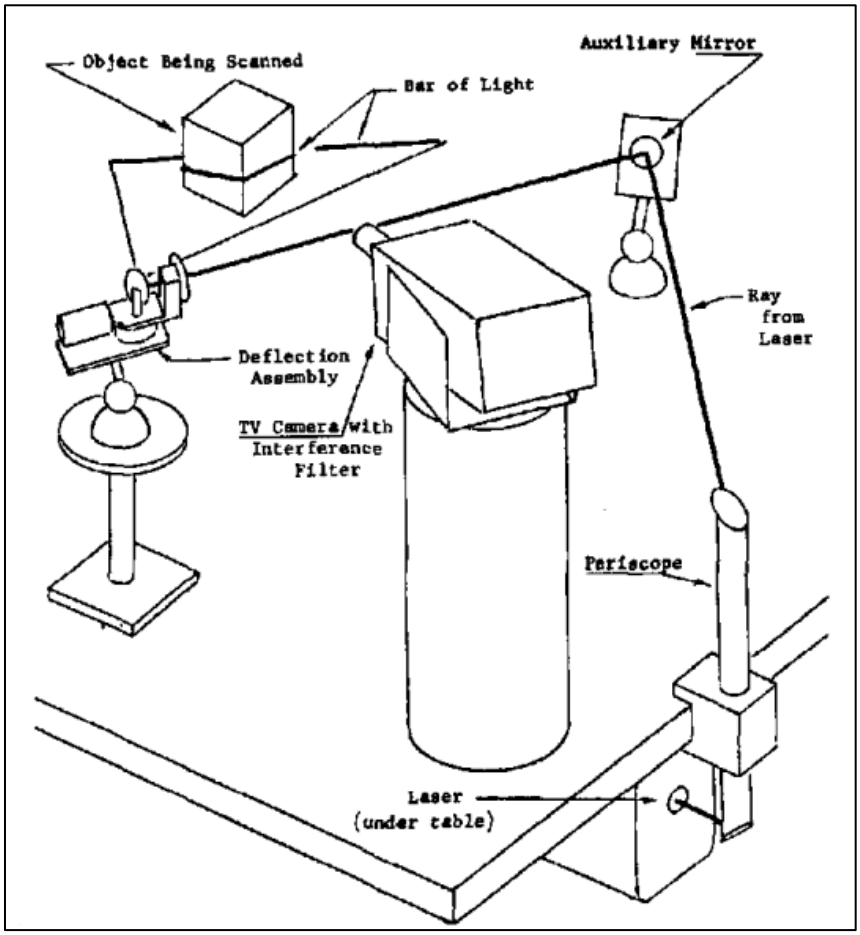

Figure 12. Schematic principle of an early LT system (Agin & Binford, 1973)

Subsequent advancements in laser triangulation systems have significantly enhanced the precision and resolution of surface reconstruction, also integrating high-resolution image processing strategies. Systems like the one developed by Marani et al. (2013) employ advanced 3D vision technology to achieve high-resolution surface measurements. Recent innovations in LT systems have focused on improving accuracy, speed, and adaptability also in low-cost systems (Zhao et al., 2020). For

example, AI-driven algorithms are now being used for real-time error correction and automated calibration, allowing for more robust systems capable of operating in dynamic environments (Liu et al., 2020).

- *Theoretical basis and working principles*

Laser triangulation operates on the geometric principle of triangulation, where the position of a laser spot or line is used to calculate the 3D coordinates (X, Y, Z) of a target surface. In a standard LT setup, a tightly focused laser beam is initially directed at the object being measured, either in pulses or continuously, creating a visible spot or line (point P). The reflected beam is then captured and recorded by a receiver, typically a CCD or CMOS camera.

The light source, the projection centre on the sensor, and the point P form the vertices of a triangle with a known baseline distance (L) between the laser and the sensor (figure 13). According to the principles of triangulation, determining the coordinates of point P requires knowledge of specific angles. The laser projection angle θ is a known parameter determined by the current orientation of the laser emitter relative to a fixed reference point in the system. It is measured directly based on the design and alignment of the laser source.

The sensor detection angle ϕ is obtained by analysing the position of the reflected laser spot on the sensor array. As the object surface varies in distance, the laser spot shifts across the sensor. By knowing the exact position of the spot on the sensor's pixel grid and using the sensor's intrinsic parameters (such as pixel size and focal length), ϕ can be calculated using geometric relationships inherent in the system's configuration.

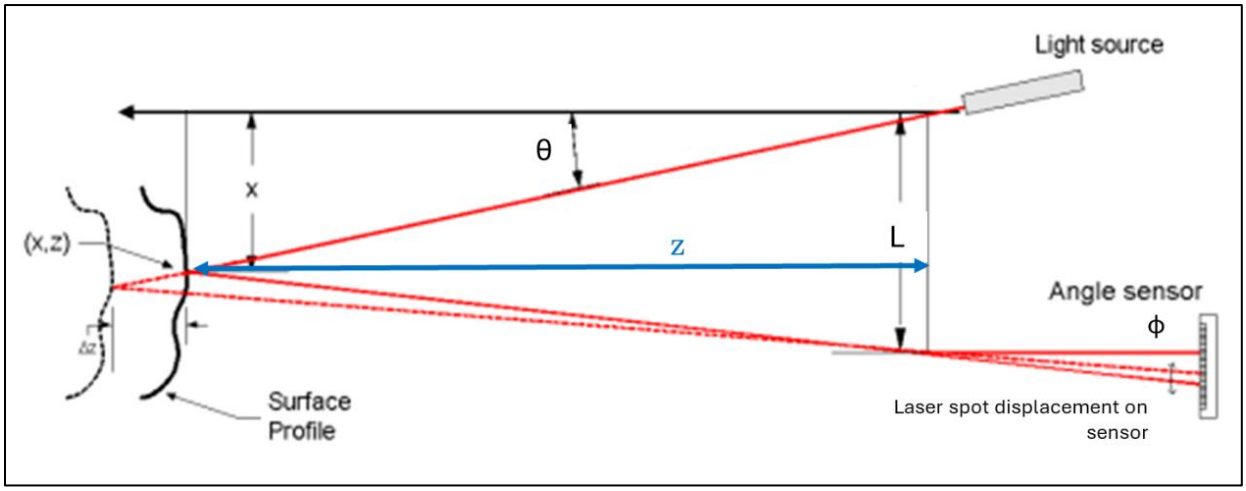

Figure 13. Laser triangulation schematic working principle (modified from Beraldin et al., 2000)

By utilising these angles along with the known baseline, the distance Z between the camera and point P on the objects can be calculated as follows (Azlan et al., 2020):

$$Z = \frac{L}{\tan(\theta) + \tan(\phi)}$$

Where:

- Z is the distance to the object,
- L is the baseline distance between the laser emitter and the sensor,
- θ is the laser beam angle,
- ϕ is the sensor angle.

As well as determining the depth (Z) of the laser spot on the object's surface through triangulation, another key issue is the retrieval of the X and Y coordinates to complete the 3D reconstruction of the scanned surface. This is done through the use of well-established trigonometric principles that depend on the emission angle of the laser (θ), the sensor, and the distance between them (L).

For the horizontal position calculation (the X coordinate of the points), Francolini (2021) and Guidi & Remondino (2012) describe similar approaches. To derive the

horizontal coordinate X, consider the triangle formed by the angle θ, the baseline distance L, and the horizontal displacement X, which is the distance between the vertical projection of the laser source and the point where the laser hits the surface of the object, along the X-axis.

Using the tangent function, which relates the opposite side to the adjacent side in a right-angled triangle

$$\tan(\theta) = X / L$$

Solving for X is given by:

$$X = L \cdot \tan(\theta)$$

This equation shows that the horizontal position X of point P on the object's surface is directly proportional to the tangent of the laser emission angle θ and the known baseline distance L. By measuring θ and knowing L, the horizontal displacement X of each point on the object can be calculated. This displacement is crucial for reconstructing the 3D geometry of the surface.

The coordinate Y can be retrieved in different ways, depending on the type of sensor and the mechanical setup of the system. In simpler LT systems that utilise a single array of photosensitive elements (1D sensor), this coordinate is often not directly measured optically. Instead, it is controlled mechanically through a predetermined displacement, allowing the vertical position to be fixed relative to the known origin.

In such systems, the position along the Y-axis is predetermined by mounting the optical measurement system on a micrometric mechanical device, which provides precise control over the vertical positioning of the system. This method eliminates the need for vertical optical measurement and simplifies the system, as only the horizontal displacement is captured by the sensor.

In more advanced LT systems, especially those employing a 2D sensor array (such as CCD or CMOS sensors), the retrieval of both horizontal and vertical coordinates is performed optically. These systems are capable of measuring horizontal and vertical parallaxes, allowing for the full retrieval of the X and Y coordinates of points along the laser profile. The vertical parallax refers to the vertical displacement of the laser spot on the sensor's pixel grid as the object surface varies in height. By analysing this shift and using the sensor's intrinsic parameters (such as pixel size and focal length), the system calculates both the horizontal and vertical angles of the detected laser points. Using these angles, along with the baseline distance L, the 3D coordinates of each point can be computed This process involves applying trigonometric principles to the captured displacement, enabling full 3D reconstruction of the surface (Beraldin et al., 2000).

In systems that utilise a laser sheet or slit scanner, as described by both Francolini (2021) and Guidi & Remondino (2012), a line of laser light is projected onto the object's surface, capturing a full profile of points in a single scan. The deformation of the laser line provides critical information about the surface geometry, as this deformation directly corresponds to changes in the object's distance from the scanner. These slit scanners are particularly efficient in capturing multiple points simultaneously, which significantly accelerates the scanning process. As explained by Guidi & Remondino (2012), the system can displace the light plane along its normal direction (the Y-axis), scanning the surface strip by strip to generate a full 3D model of the object.

To summarise, the retrieval of X and Y coordinates in laser triangulation systems leverages well-established trigonometric relationships. The horizontal coordinate X is calculated using the baseline distance and the laser angle, while the vertical coordinate Y can either be controlled mechanically or measured optically, depending on the system configuration. In simpler systems, mechanical displacement simplifies the setup, while in more advanced systems, vertical parallax allows for full 3D coordinate retrieval.

Therefore, the capture of the laser point or line projected onto the target surface is one of the most critical aspects of LT systems, since the position of this point or line on the sensor provides the data necessary for triangulation and subsequent X and Y coordinates retrieval. This is done, as mentioned, by optical systems, typically consisting of a CCD or CMOS sensor. To enhance the detection of these points, several techniques have been developed, including sub-pixel interpolation, Gaussian fitting, and edge detection-based methods. Sub-pixel interpolation enhances the resolution beyond the sensor's pixel grid by analysing the intensity profile across multiple pixels and determining the spot's position with sub-pixel precision. This method is often improved through Gaussian fitting, where a Gaussian curve is fitted to the intensity profile of the laser spot, allowing for accurate determination of the spot's centre and reducing noise in challenging environments (Selami et al., 2018).

In edge detection-based methods, algorithms track the position where the intensity of reflected laser light changes sharply, indicating the edges of the projected line. For example, the method proposed by Xiu-Feng (2007) involves detecting the local maximum intensity within a mask moving along the laser line (or light ring) and using this intensity variation to identify the edge points. These points are then fitted using the least square method to improve accuracy. Each of these techniques plays a critical role in improving the reliability of laser triangulation systems, ensuring accurate data retrieval from the projected laser spots or lines on target surfaces.

As mentioned previously, laser triangulation has broad applications in both industrial and cultural contexts. In industrial inspection, LT systems are used for high-precision quality control and part inspection. For example, the FARO Scan Arm CMM and Hexagon Romer Absolute Arm are equipped with laser line scanners that allow for real-time, micrometre-level measurements. Some of these instruments, in ideal conditions, can reach up to 10-15 microns accuracies (Amir & Thörnberg, 2017).

LT systems, as anticipated, have proven to be fundamental tools also in the high-detail digitisation of historical artefacts. A pioneering example in this field is the

Digital Michelangelo Project by Levoy et al. (2000). In this ambitious project, the team digitised several of Michelangelo's masterpieces, including the iconic David, achieving sub-millimetre accuracy with an innovative laser triangulation scanner specifically designed to handle large, fragile objects under non-laboratory conditions. The survey enabled the identification of minute details such as chisel marks with a resolution of 0.29 mm and depth accuracy of up to 50 microns.

Another relevant example is offered in Bitelli et al. (2007), where LT was employed to develop a high-accuracy 3D model of an archaeological stela, demonstrating the robustness of laser triangulation in documenting complex geometries in archaeological contexts. The system allowed for robust documentation, ensuring both the conservation of the asset and the availability of data for further research.

More recently, Patrucco et al. (2023) utilised a coordinate measuring machine system equipped with a laser line triangulator, achieving an impressive accuracy of 15 microns (figure 14). This advanced system was successfully applied to the 3D scanning of complex museum artefacts, handling challenges related to intricate geometries and varying material properties.

Figure 14. Laser triangulator for museum properties 3D scanning (Patrucco et al., 2023)

As discussed in these articles, LT systems can offer remarkable accuracies and level of detail in capturing the surface morphology of complex geometry heritage objects; nevertheless, the very high costs and logistical issues that may arise from the instrument transportation *in situ* remain a critical impediment in a massive employment of this type of surveying technique in CH. For this reason, in this context, it is more frequent to find examples of digitisation based on more cost-effective technologies, such as photogrammetry or structured-light projection scanning, described in the following sections.

2.3.2 Structured-light projection scanning (SLS)

One of the most employed geomatic tools in high-detail 3D surveying is Structured-light projection scanning (SLS). Very briefly, it is an active scanning technique relying on the projection of a structured-light pattern onto objects' surface to retrieve their geometry. To begin delving into it, it may be useful to analyse the meaning of each term included in the definition of SLS.

The word "Structured" emphasises that the active light source in SLS is not random but organised in a specific, known pattern, made of dots, stripes, grids or waves. The term "light" refers to the non-coherent, diffused form of radiation (unlike lasers), emitted to create the pattern by Light-Emitting Diodes (LEDs), semiconductor devices that emit electromagnetic radiation through electroluminescence. The wavelength ranges used are usually in the visible (400-700 nm) or near-infrared (700-1000 nm) spectrum (Rieke-Zapp & Royo, 2017). The word "projection" in SLS refers to the fact that LEDs actively project the luminous pattern on the objects' surface. Finally, the term "scanning" refers to the process in which, thanks to the pattern's deviation analysis and geometrical principles, a set of 3D coordinates is retrieved. Each phase of this process will be described in detail.

Commercially, several devices based on SLS are available and the costs may vary from a few thousand to tenths of thousands of euros. This depends on how sophisticated the implemented technology is, both from the hardware and the

software/algorithms side. The geometrical accuracies range from around 10 microns (0.01 mm) to around 1 mm. The SLS scanners available nowadays usually never exceed the millimetric accuracy, but this also depends on several factors like operational errors both in the data acquisition and processing phase, objects' materials, environmental conditions and more (as will be discussed later).

Since these scanners are usually very accurate in calculating three-dimensional coordinates and guarantee a high density of the data collected (hence, a high level of detail) they are suitable for areas of limited size (from few mm to some meters). They are in fact widely used in fields such as industry, mechanics, medicine, and, of course, in the digitisation of small-sized heritage assets.

Beyond this practical information, scanning techniques based on structured light projection constitute a fascinating field of geomatics. The basic idea of exploiting diffuse and non-coherent light, and the way it interacts with shapes to derive their geometry, has been revolutionary in the field of surveying. However, it is a rather complex technique to define since it relies on different and combined types of operating principles and, above all, because of the great development brought to this technology by private companies. The latter have started to develop very sophisticated SLS equipment for commercial purposes, thus, the functioning principles of most of the systems on the market are not known for industrial confidentiality reasons.

Before arriving at the state-of-the-art SLS systems of the present day, this scanning methodology has seen decades of theoretical formulations and practical experimentation. In the next sub-section, an attempt will be made to trace the threads of structured light history, from its first 'flashes' to the present day.

- *Historical overview of SLS*

The development of SLS has followed a series of alternating phases, moving between technological innovation and the practical application of established techniques. Since its introduction, SLS has gradually evolved, with early works in optical triangulation and pattern projection providing the foundation for future advancements.

The groundwork for SLS was laid during the late 1970s, with initial experiments defining the basis for using non-coherent light projection to capture depth information. Few traces of these first steps are found in the literature, and many of them are experimental Master's or PhD theses (Conati, 1977).

During the 1980s, more consistent experiments were carried out, and the first simple hardware for SLS was developed (figure 15). Besl (1988) and Yang & Aggarwal (1988) present comprehensive reviews of the available optical range imaging sensors at that time, discussing the implementations of linear and point-based projection methods, Coded Binary Patterns, random texture, and colour-coded stripes. They mention, for instance, the work by Boyer and Kak (1987), who introduced colour-encoded sequences, an innovative method for structured light patterns that allowed to obtain range maps of objects from a single projection.

These early innovations were primarily theoretical and technological, laying the foundation for further advancements in the field.

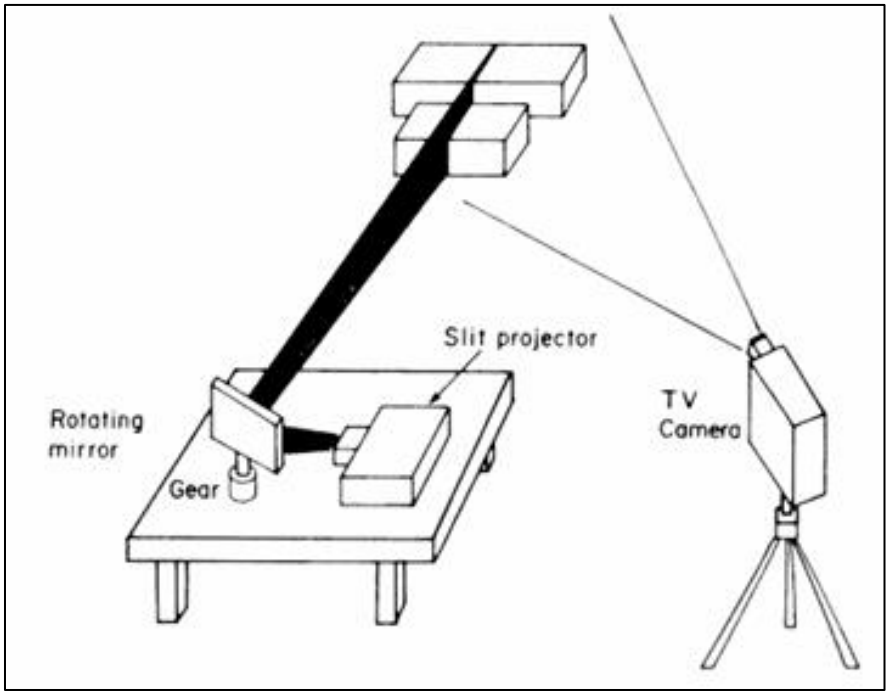

Figure 15. Schematic principle of an early SLS system (Boyer & Kak, 1987)

With advancements in computational power and digital projection technology, the late 1990s and 2000s saw major innovations in SLS. Rocchini et al. (2001) developed new algorithms for handling complex geometries, such as those found in cultural artefacts, further improving the precision of 3D reconstructions. This period also introduced improvements in system calibration and object alignment, making SLS systems easier to use and more versatile. Peng (2006), for instance, contributed to increasing the depth resolution of SLS systems by integrating phase-shifting techniques, a method that reduced errors in depth measurement and allowed for more and time-effective detailed scans (described in detail in the next sub-section). At this time, SLS systems were increasingly applied in high-precision fields such as aerospace and medical imaging, where detailed 3D models were required.

The early 2010s saw SLS systems becoming more accessible and widely adopted across industries. Salvi et al. (2010) and Geng (2011), provided comprehensive reviews of the main coding strategies present at that time, helping consolidate SLS knowledge and guiding for further improvements. This period saw the expansion of SLS into dynamic applications, such as robotics and human-computer interaction, thanks to the work of researchers as Zhang and Yau (2006) who developed real-time scanning methods. CH too largely benefited from the advantages of newly developed SLS systems for the high-accuracy and high-detail digitisation of heritage properties, as highlighted in the related case studies section 2.2.

Moreover, during those years, new solutions were implemented to enhance the capabilities of SLS, also considering the most problematic issues for this technique. Gupta and Nayar (2012), for instance, introduced the concept of sinusoidal micro-phase shifting, which improved the quality of scans in complex lighting environments, further broadening SLS's applicability. Similarly, Kazo (2012) developed turntable-based SLS systems that offered fully automated 360-degree scans, making SLS easier to integrate into automated production lines. Zhang et al. (2016), instead, combined Gray code and phase shifting techniques to enable better handling of specular and reflective surfaces, which had historically posed challenges for SLS. These

advancements allowed SLS systems to operate more efficiently in critical and challenging environments.

The next significant wave of innovation came with the recent integration of Artificial Intelligence (AI) and Machine Learning (ML). Song et al. (2017), for instance, proposed a new method for identifying patterns in binary shape-coded structured light systems, using a grid design with geometric shapes at key points, and a symmetry-based detector helps isolate these shapes. They tested, then, a deep learning-based method to accurately identify the pattern elements, supported by a large training dataset.

Similarly, Zhang et al. (2021), developed AI-driven SLS systems that used deep learning algorithms to optimise the structured light patterns in real-time, improving accuracy in challenging environments. This marked a significant leap in how SLS systems could adapt to complex, real-world scanning scenarios. Pham et al. (2023), instead, introduced a GAN-based (Generative Adversarial Network) edge detection method for colour stripe patterns in structured light, which significantly improved the accuracy of feature detection in dynamic and noisy environments. Zhao et al. (2024) offered a comprehensive review of techniques for scanning highly reflective surfaces, such as metal parts, a challenge that had persisted since the early days of SLS. They highlighted the potential of using deep learning-based methods for improving the accuracy of scans in these difficult conditions; however, as they point out, the quality of the outcomes is strongly dependent on the algorithm's training, which requires a high quantity of data and significant computational efforts. Therefore, there is room for improvement in this new frontier for SLS.

To sum up, the progression of Structured Light Projection Scanning (SLS) has been marked by alternating phases of technological innovation and practical applications. From its theoretical foundations in the 1980s to its integration with AI in the 2020s, SLS has evolved into a critical tool for 3D scanning across a wide range of fields, including cultural heritage digitisation.

- *Theoretical basis and working principles*

In essence, Structured Light Scanning (SLS) aims to reconstruct the 3D shape of an object by projecting a sequence of structured light patterns onto its surface. These patterns—whether stripes, grids, or more complex waveforms—deform when they hit the object, depending on its geometry. A camera (or more cameras), positioned at a known distance from the projector, captures these deformations.

The fundamental challenge is to determine which part of the projected pattern is being reflected from the object's surface and observed by the camera. Each part of the pattern corresponds to a specific location in the projector's coordinate system, which defines the direction of the emitted light rays. The camera, on the other hand, captures the reflected light but only records a 2D image of the deformed pattern.

This is where pattern decoding algorithms become crucial. They establish correspondences between the camera's captured image and the light rays from the projector. Specifically, for every pixel in the camera's image, we need to identify which part of the projector's light (or which light ray) is illuminating the corresponding point on the object. Pattern decoding defines this relationship between the camera's pixel grid and the projector's coordinate system.

Different decoding algorithms—such as Gray codes, De Bruijn sequences, or phase-shift techniques—uniquely label each part of the pattern, ensuring that the camera's pixels to the projector's space are mapped. Once the pattern is decoded and the correspondences between the camera and the projector are established, the next step is to use triangulation to compute the 3D coordinates of the surface points.

The following sub-sections will detail the most common types of patterns used in SLS, the strategies for decoding them, and how this decoding process directly supports the triangulation-based calculations, which are the metrical foundation of this scanning technique.

- *A. Main structured-light pattern's types and strategies for their decoding*

The first step in SLS is the projection of a known pattern of light onto objects, as already anticipated. The deformed pattern is then captured by optical systems and decoded in different manners according to the implemented technology in the system. As anticipated in the historical review of SLS, one of the earliest and most widely used structured-light patterns is the binary pattern, commonly implemented using Gray codes (figure 16).

Gray codes are a binary sequence where consecutive values differ by only one bit, minimising the likelihood of decoding errors due to noise or small distortions. Binary patterns work by projecting sequences of black and white stripes onto an object, with each stripe uniquely identified by its binary sequence. For each pixel in the camera image, the decoded binary sequence corresponds to a specific position on the projector along a single axis, typically horizontal or vertical. To determine the full 2D position on the projector, an additional set of patterns with stripes oriented perpendicularly is projected, encoding the position along the other axis.

For example, if a camera pixel receives the sequence [0011], it is mapped to the corresponding position on the projector along the encoded axis (Salvi et al., 2004). Gray codes ensure that even if small errors occur, the pixel is likely to be decoded correctly due to the one-bit difference between consecutive patterns. Once the projector coordinates of a pixel are known, triangulation is used to retrieve the 3D coordinates of that point, as will be explained in the following sub-section.

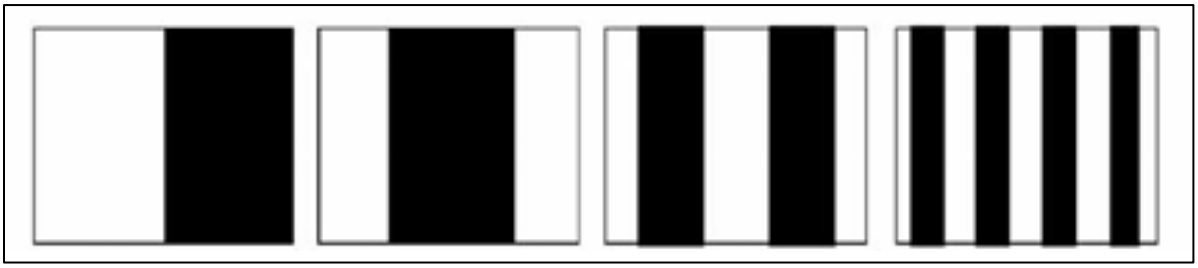

Figure 16. Schematisation of binary patterns in SLS (Salvi et al., 2004)

Although binary patterns are robust and highly accurate in static scenes, they struggle in dynamic environments where multiple images must be projected and captured sequentially. Nonetheless, due to their simplicity and precision, binary patterns remain a key method in many controlled applications where unambiguous surface reconstruction is required.

Colour-coded structured-light systems (figure 17) improve upon binary patterns by using multiple colours to encode information, allowing dense 3D data to be acquired in a single shot. In these systems, each pixel of the projector emits a specific colour or combination of colours (e.g., red, green, and blue), (Zhang et al., 2002). When the camera captures the scene, the RGB values of each pixel are extracted and compared to the projected colour pattern to determine the corresponding projector coordinates. After mapping the camera pixel to its projector position, triangulation is again used to calculate the 3D position (Yang et al., 2014). However, as explained by Zhang & Yau (2006), in colour-coded patterns the accuracy of shape acquisition is compromised when scanning objects with varying colours, as the pattern's colour coding interacts with the surface properties, leading to potential distortions in the captured data.

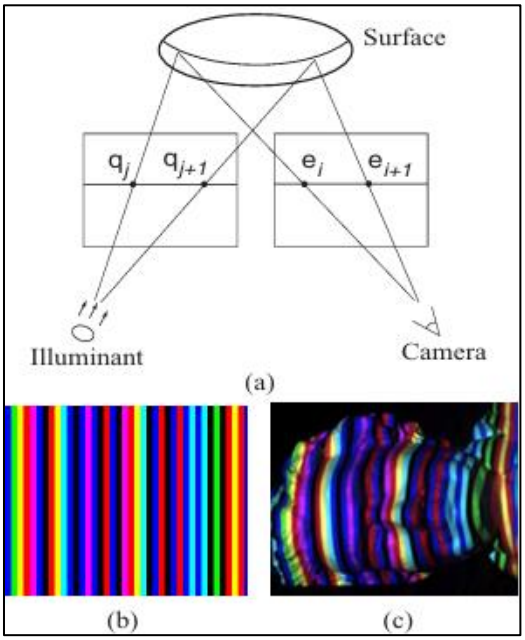

Figure 17. Scheme of colour-coded SLS, as seen in Zhang et al., 2002: a) system configuration; b) the projected colour stripes pattern; c) an image captured by the camera

Among the most advanced and effective types of patterns in SLS are those based on sinusoidal fringe projection, particularly when combined with phase-shifting techniques. Unlike patterns with sharp transitions between light and dark regions or colour variations, sinusoidal patterns involve gradual intensity variations (figure 18). This method excels at achieving sub-pixel accuracy and is particularly well-suited for capturing complex surface geometries.

The core concept of this technology lies in projecting sinusoidal fringe patterns with phase shifts onto an object and capturing the resulting deformed fringes. The projected intensities at each point on the object are typically measured in multiple steps, each with a shifted phase. Considering a three-step phase-shifting algorithm, as explained for instance in (Zhang & Yau, 2006; Lin et al. 2016; Zuo et al. 2018), the intensities (I) at each pixel on the projection coordinates (x, y) can be described as follows:

$$I_1(x,y) = I'(x,y) + I''(x,y)\cos\left[\Phi(x,y) - \frac{2\pi}{3}\right]$$

$$I_2(x,y) = I'(x,y) + I''(x,y)\cos\left[\Phi(x,y)\right]$$

$$I_3(x,y) = I'(x,y) + I''(x,y)\cos\left[\Phi(x,y) + \frac{2\pi}{3}\right]$$

From these equations, the phase ϕ(x,y) at each projected pixel can be calculated as:

$$\phi(x,y) = \tan^{-1}\left(\frac{\sqrt{3}(I_1 - I_3)}{2I_2 - I_1 - I_3}\right)$$

This phase information is wrapped within the interval [0, 2π], and it represents the relative phase between different points on the object surface. This phase must undergo a process called "unwrapping" to eliminate discontinuities and retrieve the true continuous phase value at each point. More specifically, phase unwrapping is the step resolving the inherent ambiguities in the wrapped phase, where, as mentioned,

the phase cycles between 0 and 2π. The continuous phase can then be mapped to the 3D coordinates of the object through a calibration process finding correspondences between projector and camera coordinates.

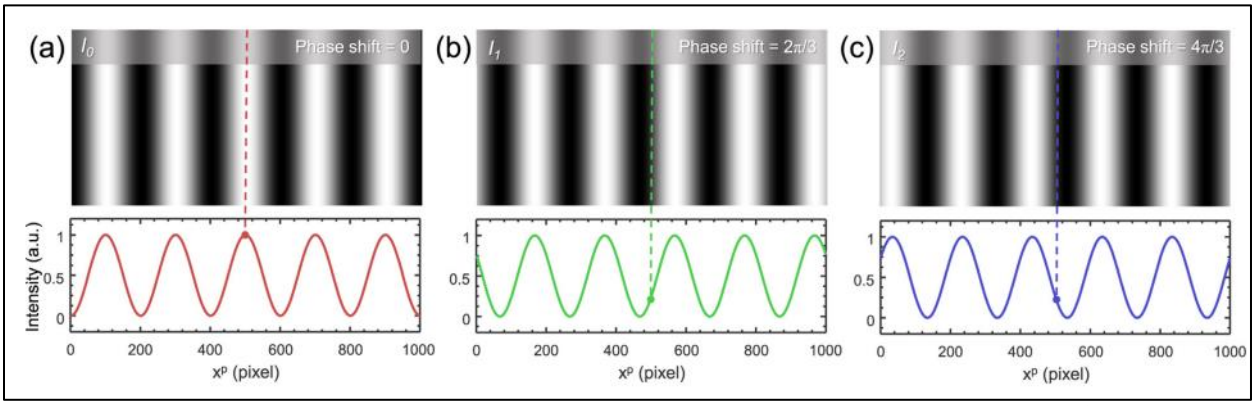

Figure 18. Sinusoidal fringe pattern projection in a three-step phase-shifting (a: 1st phase shift, b: 2nd shift, c: 3rd shift); Below the corresponding cross-sections. (Zuo et al., 2018)

However, the challenge arises when the phase difference between adjacent pixels exceeds 2π, as occurs in areas with sharp discontinuities or with "isolated" objects in the scanned scene. These situations introduce difficulties in determining the correct phase continuity, as no adjacent reference points are available. In other words, for each jump in phase greater than 2π, the unwrapping algorithm must correctly interpret the number of 2π cycles to produce a continuous phase map. So, in objects with isolated regions – as noted for example by Chen et al. (2000) and in Garcia & Zakhor (2012) – the unwrapping process becomes problematic because there are insufficient neighbouring points to guide the algorithm.

The wavelength of the sinusoidal fringe pattern is another critical factor in the performance of phase-shifting systems. Fringe wavelength determines the spatial frequency of the projected pattern, and shorter wavelengths generally yield higher spatial resolution. In addition, shorter wavelengths allow the projection of fringe patterns with higher spatial frequencies, increasing the number of phase cycles on the object's surface and improving depth resolution. This allows not only to capture finer details but also to reduce phase ambiguities in the unwrapping process because

phase changes are faster and more easily distinguishable, minimising errors in the determination of absolute phase (Norouzi & Mehdi, 2021).

However, shorter wavelengths also increase the sensitivity of the system to noise and can complicate the unwrapping process, particularly in areas with steep gradients or reflective surfaces. Longer wavelengths, on the other hand, are less sensitive to noise but reduce the system's ability to capture fine details, making them less suitable for high-detail applications. Therefore, choosing an appropriate wavelength is a trade-off between resolution and robustness in phase unwrapping.

As anticipated, compared to other types of patterns such as Gray code or colour-coded patterns, phase shifting offers several advantages. First, phase-shifting methods provide higher accuracy and resolution by utilising the full-field surface measurement approach, which captures continuous phase data across the entire surface. Additionally, phase-shifting techniques require fewer images to be captured than Gray code methods, which rely on a sequence of binary patterns.

Nonetheless, phase-shifting techniques present limitations. One significant drawback is the sensitivity to ambient lighting conditions and surface reflectivity. Surfaces with highly variable reflectivity – as in any SLS scanning system – can cause phase measurement errors, as the projected fringes may not be captured accurately (Norouzi & Mehdi, 2021). Moreover, phase-shifting methods rely heavily on a precise calibration of the system, and any inaccuracies in the calibration can propagate throughout the 3D reconstruction.

Additionally, one of the major challenges in phase-shifting techniques is the phase unwrapping process, especially in scenarios involving isolated objects or surfaces with sharp discontinuities. As mentioned, Chen et al. (2000) and Garcia & Zakhor (2012) – among others – highlighted this issue, where the absence of adjacent points with known phase values complicates the unwrapping algorithm. In such cases, without clear references, the algorithm may fail to correctly unwrap the phase, leading to errors in the 3D reconstruction.

De Bruijn sequences (figure 19) represent another important approach in structured-light scanning, wherein every local sequence of pattern elements is unique. De Bruijn sequences are typically implemented as pseudo-random binary or colour patterns, with each subsequence being distinguishable from its neighbours (Keerativittayanun et al. 2011; Barone et al., 2013). When the camera captures the pattern, a small window of adjacent light elements is extracted for each pixel, forming a unique sequence of values (e.g., binary or colour codes). This sequence is then matched to the corresponding location on the projector. The uniqueness of each subsequence ensures accurate pixel identification, even in complex environments. Once the projector coordinates are determined, triangulation is performed, as will be explained in the next sub-section (Hsieh, 2001).

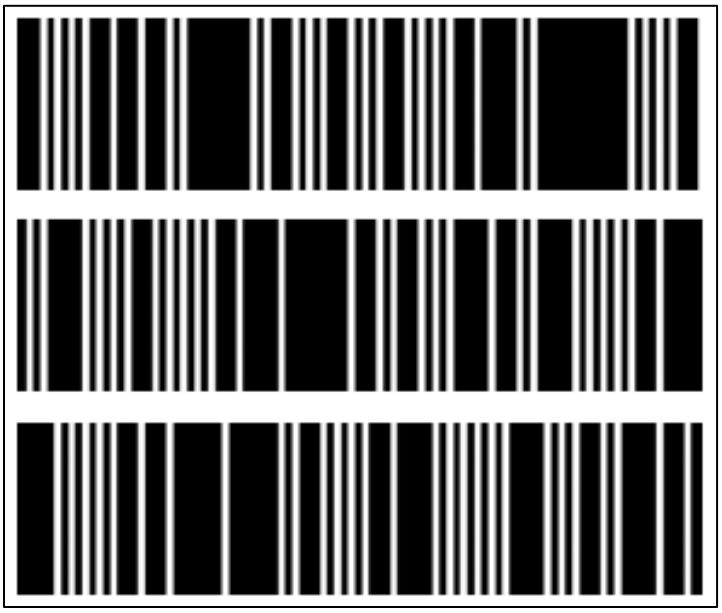

Figure 19. Binary sequences in a De Bruijn pattern (Barone et al., 2013)

It is important to note that other pattern types exist beyond those discussed here. Examples include random patterns or shape-coded patterns, which consist of more complex geometrical elements, such as triangles or hexagons. Additionally, hybrid patterns, combining techniques like Gray codes and phase shifting, or Fourier-based and Hadamard patterns, have been explored in some research. However, the patterns covered here (Gray codes, colour-coded systems, sinusoidal phase shifting, and De Bruijn sequences) are the most commonly employed in SLS due to their advantages.

Numerous studies focus on these methods, often exploring novel systems or combinations to improve accuracy and robustness.

As anticipated, each of these structured light patterns above described serves the purpose of decoding the correspondence between the points on the projector's light and the camera's image. The process of decoding involves analysing the deformed patterns captured by the camera to determine which part of the projector's light was reflected from each point on the surface. This step is crucial for establishing the pixel correspondence between the camera's image plane and the projector's space. Without accurate pattern decoding, it would be impossible to determine which specific light ray from the projector hit each object point.

While pattern decoding is essential for identifying correspondence, it does not, by itself, provide the 3D coordinates of the object points. This is where triangulation comes into play.

- *Triangulation in SLS for X, Y and Z coordinates calculation*

Once correspondences between the camera's captured images and the projector's emitted light patterns are established via pattern decoding, triangulation can then be applied to calculate the 3D coordinates—X, Y, and Z—of the object's surface.

In this process, a triangle is formed between the projector, the camera, and a point on the object's surface. The known parameters in this setup include the baseline distance (L), between the camera and the projector, and, from the pattern decoding, the specific projector rays that illuminate points on the object. Simultaneously, the camera's pixels corresponding to those points provide the directions from which the camera observes the same surface points (Albarelli et al., 2014).

Essentially, triangulation involves tracing the paths of the light rays from both the projector and the camera and determining where these rays intersect in space. With the available information—the projector's projection angles (θ_p), the camera's viewing angles (θ_c), and the known baseline (L)— geometric principles can be applied to

compute the 3D coordinates (figure 20). Considering the triangle formed by the projector (*p*), the camera (*c*), and the surface point (*s*), the Law of Sines relates the sides and angles of the triangle:

$$\frac{L}{\sin(\theta_s)} = \frac{D_p}{\sin(\theta_c)} = \frac{D_c}{\sin(\theta_p)}$$

where:

- L is the known baseline distance between the projector and the camera.
- θ_p is the projection angle.
- θ_c is the viewing angle.
- θ_s is the angle at the surface point, calculated by: $\theta_s = \pi - \theta_p - \theta_c$
- D_p is the distance from the projector to the surface point.
- D_c is the distance from the camera to the surface point.

From this relationship, one can solve for D_c, the distance from the camera to the surface point:

$$D_c = L\frac{\sin(\theta_p)}{\sin(\theta_s)}$$

With D_c known, providing the depth (Z coordinate) relative to the camera, we can determine the X and Y coordinates using the camera's geometry and the angles involved by utilising the established correspondences and calibration parameters. Consequently, the accuracy of the 3D coordinates computation depends on the precision of the measurement of angles θ_p and θ_c, which is strongly affected by the strategies used in pattern decoding, as they determine the exact correspondences between the projected and captured patterns, thus retrieving these angles (Geng, 2011).

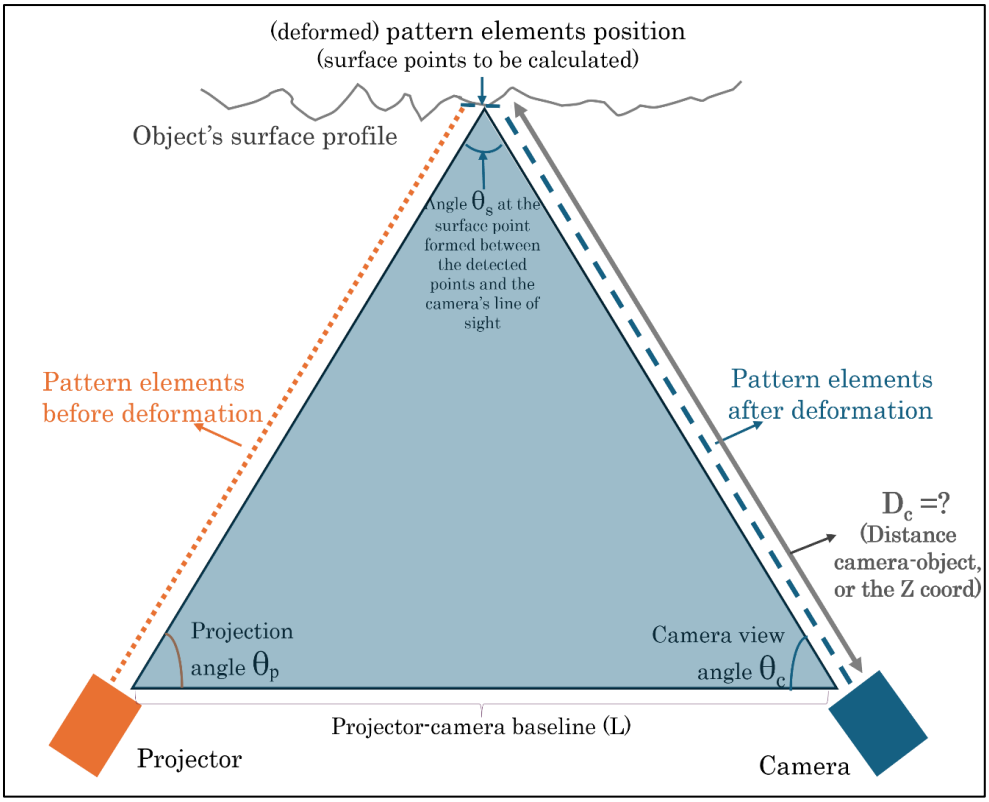

Figure 20. SLS single-camera configuration working principle scheme

Camera calibration, as mentioned, is also crucial in this process. It involves determining intrinsic parameters such as focal length, principal point coordinates, and lens distortion coefficients of the camera's optical components in the SLS system. This calibration maps pixel coordinates to rays in the camera's coordinate system. Similarly, projector calibration, which treats the projector as an inverse camera, establishes the relationship between the projector's pixel coordinates and projection angles. Extrinsic calibration defines the spatial relationship (rotation and translation) between the projector and the camera, ensuring that the coordinate systems are aligned (Georgopoulos et al., 2010).

By combining the intrinsic and extrinsic calibration data with the established correspondences, the triangulation process computes the intersection point of the camera's viewing ray and the projector's projection ray in 3D space. This intersection yields the X, Y, and Z coordinates of each surface point. In practical terms, the computation involves transforming the pixel coordinates into rays in the camera's

coordinate system using the intrinsic parameters. The direction of each ray is determined by the pixel position and the camera's optical characteristics.

The triangulation equations, which are derived from the geometric relationships between the camera and the projector, are then solved to find the point of intersection in 3D space (Geng, 2011).

However, it is important to point out that in sinusoidal fringe projection systems utilising phase shifting, the calculation of the Z coordinate relies heavily on the process of phase unwrapping, while the X and Y coordinates are determined using the camera's geometry and calibration parameters, similar to traditional SLS systems. In this approach, sinusoidal fringe patterns are projected onto the object's surface, and the resulting deformations of the fringes provide crucial phase information related to surface depth.

As already mentioned, by capturing multiple images of the fringe pattern at different phase shifts, it becomes possible to determine the unwrapped phase value for each point on the surface. This unwrapped phase is directly correlated with the depth (Z coordinate) along the projection axis. The relationship between the measured phase and the depth is established through system calibration (Zuo et al., 2018). The X and Y coordinates are derived from the pixel positions in the camera's image sensor. Using the camera's intrinsic parameters—such as focal length, principal point coordinates, and lens distortion coefficients—the pixel coordinates are mapped into the camera's coordinate system. By combining these with the calculated depth from the phase information, the X, Y, and Z coordinates of each point are determined through triangulation.

In more advanced systems of this kind, researchers have improved this method by adding a secondary camera to provide extra constraints for accurately identifying fringe order and resolving phase ambiguities. One of the first examples of this approach was proposed by Weise et al. (2007), who combined sinusoidal fringes SLS

with stereo-vision to address phase discontinuities and improve the reconstruction of complex and dynamic scenes.

This idea was further developed by Garcia and Zakhor (2012), who introduced methods for phase unwrapping in stereo structured light systems. By verifying correspondences from both cameras or using stereo vision algorithms to initialise fringe order, these methods reduce absolute phase errors caused by occlusions and improve calibration results. Hence, these hybrid methods integrate the advantages of stereo triangulation with the precision and speed of sinusoidal fringe phase-shifting SLS. The implementation of combined SLS with stereoscopy, besides phase-shifting systems, will be described more generically in the next section.

- *Multi-Camera Structured Light Systems*

As discussed, SLS systems were initially constituted of a projector – emitting the light pattern – and one camera to collect and analyse the induced deformation. In recent developments, however, multi-camera configurations have become common in SLS. The key advantage lies in its use of stereoscopy and multi-view, where two or more cameras observe the object from different angles. Each camera captures a unique perspective of the deformed structured light pattern, allowing the system to triangulate the position of each point on the object's surface. This setup enables the system to resolve areas of the object that may be occluded or hidden from the view of one camera, while also improving the overall accuracy of the depth calculations (Aliaga & Xu, 2008; Wang et al., 2021).

A critical aspect of multi-camera SLS systems is the calibration of both the cameras and the projector. Calibration is essential for ensuring that the system can accurately compute the depth of each point on the object's surface, as it defines the intrinsic and extrinsic parameters of the system. The intrinsic parameters of each camera include characteristics such as focal length, lens distortion, and the internal geometry of the sensor. These parameters are necessary for mapping the 2D coordinates captured by the camera into a 3D space. Extrinsic calibration, on the other hand, refers to the

positions and orientations of the cameras and the projector relative to each other and to the object being scanned. This step ensures that the system knows the exact location and orientation of each camera and the projector, which is critical for accurate triangulation (Zhan et al., 2015; Deetjen & Lentink, 2018).

Once the system is fully calibrated, the reconstruction process begins. The projector casts a structured light pattern onto the object, and the cameras capture images of the deformed pattern (figure 21). The system then compares the captured images with the original, undistorted pattern to establish correspondences between the camera's captured image and the projector's emitted light (as explained earlier). The 3D coordinates of each point on the object's surface are calculated by triangulation using the baseline distances between the cameras, and the angles formed between the cameras' lines of sight and the light pattern projected onto the object (as discussed for the single-camera SLS).

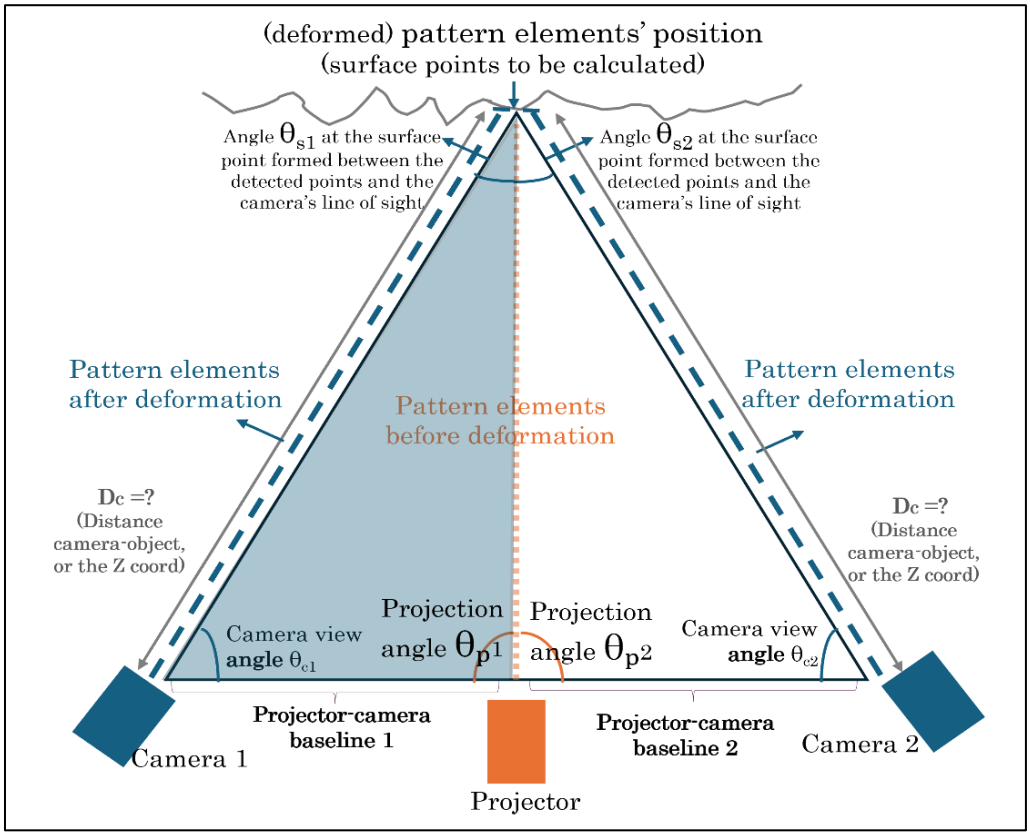

Figure 21.SLS multi-camera configuration working principle scheme

Therefore, in a multi-camera SLS system, the geometry calculation is performed using the perspectives of multiple cameras, with each camera providing a slightly different view of the deformed pattern. In other words, the system uses these multiple perspectives to perform stereo-triangulation, which allows to resolve occlusions (due to the multiplicity of camera viewpoints of the deformed pattern) and to improve the overall accuracy of the depth measurement (Chen et al., 1997; Cristina et al., 2011).

Furthermore, it is important to point out that SLS systems utilising multiple cameras fundamentally enhance the capabilities of traditional stereoscopy by incorporating known geometric parameters to derive metric depth information. In conventional stereoscopic techniques, depth perception is achieved through the analysis of the relative positions of corresponding points in images captured from different angles. However, in the absence of a known distance value in the surveyed scene, this approach provides only relative depth information without a reference scale.

In contrast, multi-camera SLS systems leverage the principles of stereo-triangulation while integrating the known baseline distances between the cameras and the projector, hence integrating a distance value – and consequently a metrical information – to the survey.

In addition, compared to traditional stereoscopic 3D imaging systems which rely solely on the natural surface features of the object to find corresponding points between images, SLS offers several significant advantages. The structured light pattern provides the system with artificial, high-contrast features that can be used to match corresponding points with greater accuracy, even on surfaces that lack texture or exhibit complex shapes. This controlled feature set allows for more reliable depth calculations, as the system can use the known positions of the pattern elements to precisely determine the shape of the object's surface. Moreover, the use of structured light helps resolve issues associated with reflective or textureless surfaces, where traditional stereoscopic methods might struggle (Bell & Zhang, 2016).

Given the strong reliance on stereoscopy in multi-camera SLS systems, combined with the use of an active light projection (structured light), SLS can be considered a hybrid system that combines both range-based and image-based 3D surveying techniques. On the one hand, SLS functions as a range-based system because it actively projects a light pattern onto the object and uses the deformation of that pattern to calculate depth.

On the other hand, the system also incorporates image-based principles through the use of multiple cameras and stereo-triangulation, where the depth is calculated based on the views of the cameras. This hybrid nature gives SLS systems significant advantages over purely image-based or purely range-based systems. By combining the strengths of both approaches, multi-camera SLS systems allow to resolve occlusions, to handle complex surfaces, and to improve depth calculations, proving effective in a variety of applications that require detailed 3D surface reconstruction.

- *Practical limitations in SLS*

Despite the discussed advantages in the SLS in terms of reliability and obtainable accuracies and resolutions, the performances of this technique can be limited by a range of challenges. Having clarified the theoretical and functioning principles behind SLS, this section outlines the main challenges of these instruments in practical applications, mentioning the materials and environmental lights-related interactions, the operative issues caused by the limited scanning coverage and working distance, and more.

As discussed, SLS relies fundamentally on the interaction between the projected light and the surface of an object. However, the reliability of the reconstruction process hinges on how the projected light interacts with the object's surface. Surfaces that are either too reflective, absorbent, translucent, or vitreous (glass-like) introduce complexities that often result in inaccurate or incomplete data. For this reason, this type of materials is often referred to as "non-cooperative" toward the scanning procedure.

To understand why these materials pose a challenge, it is crucial to first delve into the basic physical principles of how light interacts with matter. When light strikes a surface, it can undergo different types of interactions, based on the optical properties of both the emitted radiation and the objects' materials (Angheluţă & Radvan, 2020):

- Reflection: Light bounces back from the surface, maintaining its wavelength and speed. Reflection can be categorised as specular (when light reflects in a single, predictable direction, like on a mirror) or diffuse (when light scatters in multiple directions, as in rough surfaces).
- Refraction: Light changes its direction as it passes from one medium into another with a different refractive index. This bending of light is dependent on the angle of incidence and the properties of both media.
- Absorption: The surface material absorbs the light, converting it into other forms of energy, such as heat, reducing the amount of light that is reflected back.
- Transmission: Some surfaces allow light to pass through them (partially or fully). This is particularly relevant in transparent or translucent materials, where part of the light may pass through while some is refracted or reflected at different angles.

Each of these interactions plays a role in how the projected structured light in SLS behaves when it hits a material, and each can introduce specific challenges to the scanning process.

Highly reflective materials, such as polished metals or glossy finishes, exhibit specular reflection. In specular reflection, light reflects off the surface in a concentrated, directional manner, rather than scattering diffusely. For SLS systems, which rely on diffuse reflection to capture the deformation of the projected pattern, this specular reflection is problematic because the reflected light does not return to the sensor from all parts of the surface uniformly. Instead, strong reflections

(highlights or glares) appear in the camera image, disrupting the structured pattern and leading to incorrect depth calculations (Zhao et al, 2024).

Highly absorbent surfaces, such as dark or matte materials, pose a different challenge. These surfaces absorb a significant portion of the incoming light, reducing the intensity of the reflected light that returns to the camera. The light that does return is often too weak to be detected by the system with sufficient accuracy. This results in low signal-to-noise ratios, where the amount of useful signal (reflected light) is overshadowed by random noise from the environment or the system itself (Lin et al., 2016).

Translucent materials and those that exhibit glass-like properties are particularly problematic for SLS. For this type of objects, a phenomenon called subsurface scattering usually takes place, in which light penetrates the surface, scatters within the material, and then exits at various angles. Subsurface scattering is prominent in materials like marble, skin, or plastics. For the SLS system, this means that the light returning to the sensor no longer corresponds to the actual surface geometry, but rather to an average or smoothed representation influenced by the material's internal structure (Chen et al., 2007).

The second critical limitation concerns the influence of ambient light on the scanning process. Bright or varying light sources in the environment can interfere with the structured light pattern, leading to an incorrect detection of its deformation. This can introduce errors into the model, such as missing data points or incorrect geometry. It is crucial then to operate SLS in environments where the light conditions are stable, typically indoors. Scanning in outdoor environments poses a significant challenge, as natural light, especially direct sunlight, can overpower the projected light and render the system almost unusable without extensive shielding (Gupta & Nayar, 2012).

Another notable limitation is the restricted field of view and working distance of most SLS devices. These systems are designed for close-range, high-accuracy and high-detail scanning, which makes them ideal for small to medium-sized objects. Therefore,

they typically have a restricted scanning area, necessitating multiple scans from different angles to cover the entire surface to be surveyed. This introduces challenges especially in environments where access to all sides of an object is limited, or in cases – as often occurs in heritage properties – in which the assets cannot be moved from their original locations (Balzani et al., 2023).

Other more generic factors may constitute a practical limitation in SLS. For instance, the high sensitivity of these systems to environmental factors such as dust, humidity, or temperature variations can compromise the accuracy of the scans. Humidity can cause issues with the optical components of the scanner, affecting both the projection and capture of light. In environments with temperature fluctuations, the calibration of the system may shift, necessitating frequent recalibration to maintain accuracy (Adamczyk et al., 2014).

Finally, the cost of high-end SLS systems remains prohibitive for many institutions or researchers, particularly those involved in cultural heritage preservation or small-scale scientific research. While technology is advancing, and more affordable systems are becoming available, there is often a trade-off between cost and the reliability of the instruments.

In conclusion, while Structured Light Scanning offers great accuracy and resolution for close-range 3D digitisation, it is essential to recognise its practical limitations. Non-cooperative materials, interference from ambient lighting, restricted scanning coverage and working distance, and other environmental factors pose significant challenges in various applications.

Despite these drawbacks, SLS remains one of the most employed and most effective techniques in high-detail 3D surveying, also of heritage assets. Future research will focus on further advancing these systems, improving aspects as accuracy, reliability, adaptability and costs of the equipment.

2.3.3 (Very) close-range Digital Photogrammetry (DP)

Photogrammetry is one of the most intriguing and versatile techniques in Geomatics. In brief, it is a discipline that combines mathematical models, projective geometry principles and – in modern applications – advanced algorithms, to convert 2D images into 3D representations. Terminological aspects related to this technique have been discussed in section 2.1.2, where the reasons for referring to it as "very close-range" DP in this context are also explained. For conciseness, it will be abbreviated as DP in this section.

The origins of photogrammetry can be traced back to the mid-19th century, initially for topographic and cartographic applications. Early photogrammetric methods relied on stereoscopy and analogue instruments to interpret image pairs. The introduction of digital imaging in the late 20th century transformed the field, offering new possibilities for automation, precision, and flexibility. Today, digital photogrammetry is a fundamental technique in Geomatics, with applications that go beyond traditional surveying to include fields like forensic science, industrial metrology, and detailed heritage documentation (Wolf et al., 2014).

This technique is widely used in various sectors due to its versatility and its ability to produce high-resolution digital outputs. Key advantages include non-invasive data acquisition, flexibility in handling a variety of scenarios (from territorial survey to the microscopic level), and cost-effectiveness when compared to other 3D scanning technologies, such as laser-based or structured-light projection scanning. In its very close-range configuration, photogrammetry enables the creation of highly detailed 3D models, allowing for robust inspection of the surveyed objects.

As anticipated, the theoretical foundations of photogrammetry are firmly rooted in projective geometry, blending principles from mathematics and optics to transform two-dimensional image data into three-dimensional spatial information. Before delving into detailed explanations, it is important to establish a premise: photogrammetry, as a discipline, dates back to the 19th century, standing as one of

the most enduring techniques in geomatics. Therefore, over time, the theory underlying photogrammetry has been thoroughly consolidated and is now well understood by experts in geomatics, who continue to study and apply it extensively.

This contrasts with more recent techniques, such as laser triangulation (LT) and structured light scanning (SLS), which were developed only a few decades ago. And, as previously mentioned, these range-based methods have been incorporated into commercial systems, rendering them more user-friendly but simultaneously reducing the understanding of their theoretical foundations. Consequently, for this PhD thesis, an in-depth discussion of LT and SLS theory was prioritised, while the theoretical treatment of photogrammetry will be more concise; hence, the focus will be on key concepts and aspects pertinent to high-detail surveying through this image-based technique.

This section will therefore begin with a brief overview of photogrammetry's theoretical foundations, followed by a discussion of operational aspects in very close-range photogrammetry. It will also introduce the importance of digital signal sampling theory in determining the images' GSD, a critical factor, especially in the context of high-detail close-range photogrammetry, where the spatial resolution of images used to generate models is of paramount importance.

- *Theoretical basis and working principles*

In photogrammetry, multiple images of the same object from varying viewpoints are essential to reconstructing accurate 3D coordinates. A single image cannot provide depth information, as each 2D point on the image corresponds to an entire line of possible 3D locations along a ray extending from the camera's projection centre. By capturing images from different angles, the lines of sight (or rays) from each viewpoint intersect, allowing for triangulation. This process is the metric foundation of photogrammetry, as it provides the geometric basis for calculating 3D coordinates through the intersection of lines of sight from multiple views. To achieve this, photogrammetry relies on mathematical models and principles of projective geometry

(specifically, the pinhole camera model and the collinearity equations) that allow for the projection of 3D points onto a 2D image plane. Through a sequence of calibrated transformations, these models enable the retrieval of 3D spatial coordinates.

First, the pinhole camera model serves as the idealised framework for understanding how a camera captures a 3D scene onto a 2D plane (figure 22). In this model, light rays from the scene pass through a single point—called the camera's projection centre—and project onto the image plane, forming an inverted image of the scene. This simplified model describes the geometric path of light from the 3D world onto a 2D image, establishing the foundational relationship between 3D points and their 2D projections (Horn, 1986; Hartley & Zisserman, 2004). Mathematically, this relationship is represented as follows:

$$x=PX$$

Where:

- $x=(u,v,1)^T$ is the image point in homogeneous coordinates,
- P is the camera projection matrix,
- $X=(X,Y,Z,1)^T$ is the 3D point in homogeneous coordinates.

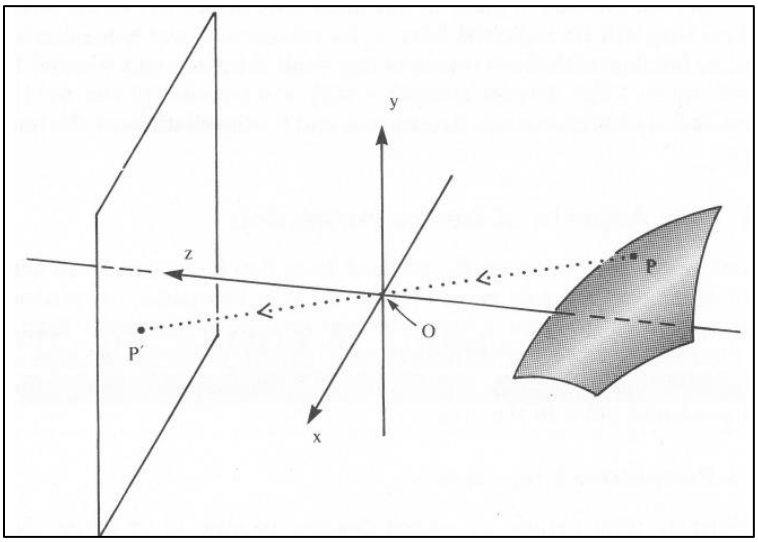

Figure 22. A schematic representation of the pinhole camera model, where P represents a point in the object space, P' is the corresponding projection on the image plane, and O is the origin of the coordinate system and the camera's projection centre (Horn, 1986).

The camera projection matrix P encapsulates both the camera's intrinsic and extrinsic parameters in practical applications, as it defines how points in 3D space map onto the image plane through the geometry of the camera. This matrix is often decomposed into:

$$P = K[\,R \mid -RC\,]$$

Where:

- K is the calibration matrix, containing intrinsic camera parameters,
- R is the rotation matrix, indicating the camera's orientation,
- C is the camera centre in world coordinates, with $-RC$ representing the translation vector from the world coordinates to the camera frame.

The calibration matrix K has the following structure:

$$K = \begin{bmatrix} \alpha_x & s & u_0 \\ 0 & \alpha_y & v_0 \\ 0 & 0 & 1 \end{bmatrix}$$

In this matrix:

- α_x and α_y are the scale factors in the x- and y- directions, related to the focal length and pixel dimensions,
- s is the skew parameter, which compensates for any non-orthogonality between the x- and y- axes in the image sensor,
- $(u0,v0)$ are the coordinates of the principal point in the image plane.

In synthesis, the pinhole model provides the fundamental relationship needed to project 3D points onto a 2D plane, but for 3D reconstruction from multiple images, an additional geometric condition is required, namely the collinearity condition (figure 23).

This condition asserts that the camera's projection centre, any object point in space, and its corresponding image point must all lie on a single straight line. This alignment is crucial for triangulation because it ensures that rays extending from the camera projection centres intersect in 3D space, enabling the calculation of spatial coordinates (Khalil, 2011).

The collinearity condition is expressed mathematically as:

$$x = x_0 - c \cdot \frac{r_{11}(X - X_0) + r_{12}(Y - Y_0) + r_{13}(Z - Z_0)}{r_{31}(X - X_0) + r_{32}(Y - Y_0) + r_{33}(Z - Z_0)}$$

$$y = y_0 - c \cdot \frac{r_{21}(X - X_0) + r_{22}(Y - Y_0) + r_{23}(Z - Z_0)}{r_{31}(X - X_0) + r_{32}(Y - Y_0) + r_{33}(Z - Z_0)}$$

where:

- (x,y) are the image coordinates (after correction for lens distortion)
- (X,Y,Z) are the coordinates of the object point
- (X_0,Y_0,Z_0) represent the coordinates of the camera's projection centre, which is the point where all rays converge in the camera
- c is the principal distance, or the distance from the camera's projection centre to the image plane along the optical axis
- (x_0,y_0) are the coordinates of the principal point in the image coordinate system; this is where the principal axis intersects the image plane
- r_{ij} are elements of the rotation matrix

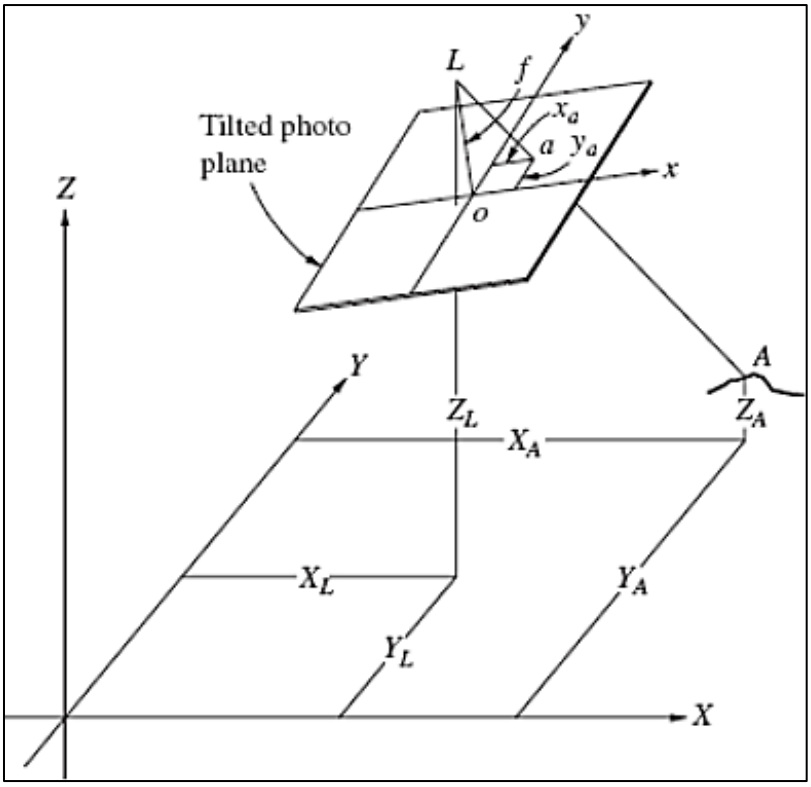

Figure 23. A graphical representation of the collinearity conditions; in this scheme, "L" represents the coordinates of the camera's projection centre (X0,Y0,Z0), and "f" represents the principal distance, referred to as "c" in the text
(Wolf et al., 2014 - and others)

These equations incorporate both the interior orientation (intrinsic parameters like principal point coordinates and the principal distance) and the exterior orientation (extrinsic parameters including translation and rotation) of the camera, which are necessary for transforming 3D points into 2D image points. The exterior orientation comprises six parameters: three translation coordinates (X_L,Y_L,Z_L), which define the position of the camera centre in object space, and three rotation angles—often represented as Omega, Phi, and Kappa—that define the camera's orientation in 3D space. This orientation information, encoded in the rotation matrix elements r_{ij}, ensures that each 3D object point is projected onto its 2D location on the image plane (Kraus, 2007).

In photogrammetry, the principal distance c is often used in the collinearity equations as the distance from the camera's projection centre to the image plane along the optical axis. While focal length f refers to an optical property of the lens itself,

describing the distance where light rays converge when focusing at infinity, principal distance c is a calibrated measurement that incorporates both the focal length and the camera's internal configuration. In practical terms, c is used in place of f in photogrammetric applications because it reflects the actual distance within the camera system.

In the applied implementation of photogrammetry, these intrinsic and extrinsic parameters are determined through camera calibration, a process that refines measurements for parameters like principal distance, principal point, and distortion coefficients, all of which play critical roles in the 3D reconstruction. To achieve this, these primary approaches are commonly used:

- Calibration with known geometric patterns: typically conducted in controlled conditions, this method uses a known target (e.g., a checkerboard) to determine the camera's intrinsic parameters, estimating the calibration matrix K.
- Self-calibration: when predefined calibration targets are not feasible, self-calibration methods are used, commonly relying on bundle adjustment. This method enables the estimation of both intrinsic and extrinsic parameters directly from image sequences, making it suitable for unstructured scenes in field environments (Remondino & Fraser, 2006).

More specifically, bundle adjustment is a nonlinear optimisation process that minimises the reprojection error—the difference between observed image points and the projected 3D points— based on the current camera model and orientation (Triggs et al. 1999; Hartley & Zisserman, 2004).

Mathematically, bundle adjustment aims to solve:

$$\min_{\{P_i, X_j\}} \sum_{i,j} |x_{ij} - \pi(P_i, X_j)|^2$$

Where:

- P_i represents the parameters of camera i
- X_j represents the 3D coordinates of object point j
- x_{ij} are the observed image coordinates of point j in image i
- $\pi(P_i,X_j)$ denotes the projection of X_j into image i using camera parameters P_i

This optimisation not only enhances the accuracy of the 3D reconstruction but also corrects for any inconsistencies in camera orientation and positioning. So, while triangulation provides the initial 3D structure by calculating spatial points from multiple images, bundle adjustment further refines this structure.

Moreover, in real scenarios, the pinhole model alone does not account for lens optical distortions, which are critical to correct for accurate photogrammetric reconstruction. Remondino and Fraser (2006) categorise these lens distortion corrections as Additional Parameters (APs), with the most common set being the 8-term "physical" model introduced by Brown (1971).

This Brown-Conrady model includes parameters for the principal distance and principal point offset (x_p,y_p), along with three coefficients for radial distortion and two for decentring distortion. It then describes the relationship between distorted coordinates (x_d,y_d) and undistorted coordinates (x_u,y_u) as follows:

$$x_u = x_d + (x_d - x_0)[k_1r^2 + k_2r^4 + k_3r^6] + [2p_1(x_d - x_0)(y_d - y_0) + p_2(r^2 + 2(x_d - x_0)^2)]$$

$$y_u = y_d + (y_d - y_0)[k_1r^2 + k_2r^4 + k_3r^6] + [p_1(r^2 + 2(y_d - y_0)^2) + 2p_2(x_d - x_0)(y_d - y_0)]$$

where:

- (x_d,y_d) are the distorted (observed) image coordinates,
- (x_u,y_u) are the undistorted (corrected) image coordinates,
- k_1,k_2,k_3 are radial distortion coefficients,
- p_1 *and* p_2 are tangential distortion coefficients,

- r is the radial distance from the principal point: $r = \sqrt{(x_d - x_0)^2 + (y_d - y_0)^2}$
- (x_0, y_0) are the coordinates of the principal point.

The integration of these APs into the calibration process is essential for refining the projection model, minimising distortions, and achieving more correct results in photogrammetric reconstructions.

In conclusion, the theoretical framework of photogrammetry is built on a sequence of geometric models and mathematical formulations that translate 2D images into accurate 3D spatial representations. The pinhole camera model provides the fundamental projection mechanism, while the collinearity equations expand this framework by incorporating camera orientation and position. Camera calibration ensures that both intrinsic and extrinsic parameters are accurately determined, accounting for lens distortions that could compromise measurement precision. Bundle adjustment refines all parameters by minimising reprojection errors, leading to more accurate reconstructions.

Together, these models and techniques form a robust foundation for modern photogrammetric applications across various fields, including industry, architecture, and cultural heritage high-detail documentation.

- *Structure from Motion (SfM) photogrammetry*

In modern digital photogrammetry, Structure from Motion (SfM) is an advanced technique for reconstructing 3D models from 2D images. It builds upon the principles of the pinhole camera model and collinearity equations, integrating semi-automated workflows powered by advanced image analysis and computer vision (CV) algorithms. The term "motion" in SfM refers to the shift in viewpoint between images, enabling the system to infer depth and structure by capturing multiple perspectives of a scene.

By analyzing these viewpoint variations, SfM estimates depth information to generate 3D representations. Unlike traditional photogrammetric methods that require prior camera calibration, SfM simultaneously determines both intrinsic

parameters (such as focal length and lens distortion) and extrinsic parameters (position and orientation) by detecting and matching common features across images. A key advantage of SfM over conventional analytical photogrammetry is its automated feature extraction and matching, reducing the manual effort once required for identifying corresponding points (Snavely et al., 2007; Abdel-Wahab et al., 2012).

The reconstruction process typically begins with two highly overlapping images to establish an initial 3D structure. Additional images are incrementally incorporated, refining the model with each new addition. For large-scale datasets, global or hierarchical SfM approaches improve efficiency—either by computing all camera positions in a single global solution or by merging intermediate reconstructions. These methods are particularly beneficial for complex geometries and extensive image sets (Shen, 2013; Westoby et al., 2012).

The accuracy of SfM reconstructions depends on image resolution, overlap, and clarity. Distinct, well-defined features enhance keypoint detection, which is often performed using algorithms such as SIFT (Scale-Invariant Feature Transform), SURF (Speeded-Up Robust Features), and ORB (Oriented FAST and Rotated BRIEF). While SIFT offers high reliability at a greater computational cost, SURF and ORB provide faster processing, making them suitable for handling large image collections (Cao et al., 2018).

After initial feature correspondences are established, outlier removal is conducted using RANSAC (Random Sample Consensus) to filter inconsistent matches, thereby refining camera orientation estimates. This step enhances the stability of the initial 3D model, and the resulting exterior orientation parameters are further optimized through bundle adjustment. By minimizing reprojection errors across all images, bundle adjustment fine-tunes both camera parameters and 3D point coordinates, ensuring an accurate and coherent reconstruction (Francolini, 2021).

SfM's ability to estimate camera parameters without prior calibration, combined with its capacity to handle large image datasets, has made it an invaluable tool in

applications requiring dense scene reconstruction. It is widely used for detailed documentation of heritage sites and other complex environments, integrating photogrammetric principles with computer vision techniques to generate accurate 3D models.

In summary, SfM is a sophisticated method that fuses traditional photogrammetry with advanced computer vision and image analysis techniques to generate three-dimensional models from digital images. Robust algorithms such as RANSAC ensure reliable feature matching, while bundle adjustment refines reconstruction accuracy. This semi-automated, incremental workflow significantly accelerates image-based modelling compared to traditional analytical approaches, allowing for the efficient processing of large datasets and the handling of complex scenarios. As a result, SfM has become a powerful tool for diverse surveying applications, including high-detail 3D reconstructions of heritage assets.

- *Considerations on digital sampling theory, spatial resolution and acquisition geometry*

As previously mentioned, the successful generation of high-resolution and high-accuracy photogrammetric models is strictly related to the images' spatial resolution (the GSD in this context, refer to section 2.1.1). This is even more evident in the above-described SfM-based approach, where feature extraction and matching — and the subsequent creation of 3D point clouds — are directly influenced by the images resolution: higher pixel counts (assuming that the high density in the pixel is not a result of further pixels interpolation) correspond to more samples for computer vision algorithms to analyse, facilitating feature extraction for image orientation and subsequent point cloud generation.

The GSD, then, serves as a critical metric, providing insight into the potential final quality of a 3D model produced through image-based techniques. This is because, as discussed, the achievable level of detail in reconstruction is directly influenced by the spatial resolution of the initial images.

However, GSD is not the sole factor affecting output quality: as previously noted, images undergo a calibrated orientation process, refined through successive steps like bundle adjustment. In this process, various errors—such as the previously mentioned reprojection error—inevitably influence the final quality of photogrammetric outputs. Nonetheless, GSD remains an essential indicator, offering a qualitative measure of image quality and, consequently, of achievable results from a geometrical resolution perspective.

Despite its importance, spatial resolution is a theoretical metric that does not account for other influencing factors, such as noise, uneven lighting, or improper focus. When considering geometric resolution aspects alone, and excluding other factors that impact image quality, GSD must still be appropriately selected to accurately represent the surface characteristics intended for objects' digitalisation, especially when the level of detail in the final outputs represents a priority. In determining the correct GSD for the intended resolution to be obtained in the final models, some aspects of signal theory could be considered.

First, the digital imaging process involves transforming a continuous 3D scene into a 2D digital signal by capturing reflected light as intensity values on a sensor. Gonzalez and Woods (2008) explain that a digital image results from projecting a 3D object onto a 2D plane; the camera sensor captures the intensity of light reflected from each point on the object's surface and translates this information into discrete pixels on the sensor's 2D plane. This process treats the scene as a continuous 2D function, $f(x,y)$, of light intensities, simplifying the 3D spatial configuration into two spatial coordinates (x and y) of intensity distributions.

In the context of image spatial resolution, the GSD can be seen as the sampling rate at which this continuous signal — the intensity of light reflected from the object's surface — is converted into a digital format. The selection of this rate is then critical because an incorrect sampling rate can lead to aliasing, a phenomenon where high-frequency information in the scene is misrepresented in the sampled image. This issue

commonly affects high-frequency regions, such as sharp edges or fine textures, and can result in unwanted artefacts in the final digital image (Ficker & Martišek, 2015). Aliasing, then, occurs when the sampling rate (in this context, the image spatial resolution) is insufficient to capture the highest frequency components present in the continuous signal.

This brings us to the Nyquist-Shannon sampling theorem, a foundational principle in signal processing. According to this theorem, the sampling rate must be at least twice the maximum frequency of the signal to reconstruct it without loss of information. In this context, the "frequency" can be understood as the minimum spatial detail necessary to represent the continuous signal of light intensity in the digital images, while the sampling rate is represented by the GSD.

Originally formulated for one-dimensional (1D) signals, as discussed in (Shannon, 1949), the Nyquist-Shannon theorem establishes that a continuous 1D signal can be accurately reconstructed from its samples if it is sampled at a rate of at least twice its highest frequency component. For a 1D signal with maximum frequency R, this requirement is resolved by adhering to the ideal Nyquist sampling interval:

$$\Delta \leq \frac{1}{2R}$$

Where Δ is the sampling interval and R is the maximum frequency to be sampled. So, if the maximum frequency is 1, the sampling interval must be 0.5. However, some scholars propose to adapt this 1D criterion to account for the frequency distribution in two-dimensional signals, such as digital images.

Almroth (1985), for instance, explored a possible extension of the theorem, proposing that, in 2D, the radially distributed nature of spatial frequencies in an image unit (i.e., a square pixel) must be taken into account:

$$\Delta \leq \frac{1}{2\sqrt{2}R}$$

The addition of $\sqrt{2}$ to the formula may represent mathematically the contribution of the diagonal axis along which the frequency is distributed in the square pixel, to be considered in addition to the X and Y axis directions. To give a practical example, assuming a maximum spatial frequency of 1 cycle per mm in the image, Almroth's adapted formula suggests an approximate sampling interval of $\Delta \approx 0.35$ mm, resulting in a finer sampling rate compared to the 1D criterion's (which, in the case of this example, would imply a sampling interval of 0.5 mm). This adjustment can be feasible because, in 2D images, the multiplicity of directions in which the frequency is distributed in the pixel is considered.

In contrast, Gonzalez and Woods (2008) among others take a more conventional route by treating each spatial dimension independently, as in 1D sampling. They apply the classic Nyquist criterion, ensuring that each axis (X and Y) is sampled at least at $\Delta T_x \leq 1/2\mu_{max}$ and $\Delta T_y \leq 1/2\upsilon_{max}$, where ΔT_x and ΔT_x are the sampling interval along the X and Y axes, respectively, and μ_{max} and υ_{max} are the maximum spatial frequencies along X and Y axes. By treating the two axes independently, this approach applies the Nyquist-Shannon theorem in its original form, which states that, to avoid aliasing, the sampling frequency must be at least twice the highest frequency component.

That said, there are no examples of empirical validations of the two-dimensional sampling theory for photogrammetric purposes. In practical applications, using the Nyquist-Shannon theorem for a photogrammetric survey means choosing a GSD that is at least half—or, as Almroth (1985) suggests, even finer if we consider the radial distribution of the 2D frequency—of the maximum frequency to be sampled (i.e., the smallest spatial detail that one aims to represent in the images).

In conclusion, both approaches may provide a theoretical groundwork for selecting GSD, considering the images as a 2D continuous signal to be digitally sampled. In practical terms, if we need to obtain a final 3D model with a resolution (or, a point density) of 1 mm, the GSD (our sampling interval) must be at least 0.5 mm to guarantee that the digital image is not affected by aliasing or loss of information.

Nonetheless, as pointed out, there are very few literature examples in which the authors try to verify the practical applicability of the Nyquist-Shannon sampling theorem for photogrammetric approaches. This theorem is, indeed, scarcely considered in the field of photogrammetry. Yet, in the context of very high-detail and resolution image-based reconstruction, it may represent a significant theoretical groundwork, because in this specific branch of DP, the resolution and the need to represent very fine details is pivotal.

This leads to another consideration: achieving accurate 3D models also requires optimising the photogrammetric setup to represent depth accurately and, up to now, the image was considered as a continuous bidimensional function, $f(x,y)$. However, accurately capturing depth information (Z-axis) is vital since the surface discontinuities along the Z direction (or the depth variation) must be accurately represented in the final 3D model. To do that, a robust images acquisition configuration in photogrammetric practice becomes pivotal: appropriate baseline distance and overlap between images, and multiple tilts and angles for raking photos are needed to ensure that the depth variations are captured and occlusions are avoided.

These issues about the importance of a controlled image acquisition configuration were addressed by several papers and books in the field of photogrammetry. Nonetheless, as noted by Guidi et al. (2020), this topic is usually discussed in the field of aerial or architectural photogrammetry, with few critical literature papers investigating the appropriate image acquisition configuration in close-range DP.

Moreover, in their study, Guidi et al. (2020) explore how specific acquisition geometry settings can improve very close-range photogrammetry outcomes, where conventional guidelines (typically requiring 80-90% overlap but originally formulated for architectural photogrammetry) may add redundant data and processing demands. The authors address this issue by comparing general guidelines with other, more precise approaches that emphasise tighter control over the baseline-to-distance ratio,

which is critical for depth accuracy. Lower overlaps, paired with optimised baseline management, are shown to maintain model quality without adding unnecessary data, improving processing efficiency. In their paper, they also conducted controlled experiments imaging rock samples at varied overlap levels, from the highest values down to approximately 60%. The results demonstrate that for very close-range photogrammetry, overlaps significantly lower than 80% can still yield accurate models if baseline distance is well-managed.

The study also addresses the challenges posed by Structure from Motion (SfM) photogrammetry, where feature detection and matching across images are essential for 3D reconstruction. While increasing baseline distance theoretically reduces depth error, it complicates the matching of features in SfM, especially when capturing small objects. In such cases, even minor inconsistencies in feature alignment can propagate significant errors through the model. Thus, Guidi et al. (2020) underscore that, although a larger baseline may reduce depth error, it risks degrading feature consistency and model integrity, particularly in applications with high-detail demands.

In conclusion, in photogrammetry, especially in the high-detail close-range configuration, integrating optimised GSD selection with an effective imaging geometry is essential. Considering signal theory basic concepts — and accurate survey planning to ensure a correct acquisition scheme — can contribute to successfully achieving 3D models that accurately and finely represent both the surface and depth characteristics of the original scene.

Nevertheless, as already mentioned, spatial resolution is not the only metric to be considered in photogrammetric procedures. Many factors can contribute to the successful creation of accurate and detailed outcomes, especially in this field of very close-range DP for small objects. The next sub-section will investigate more of these factors to be considered when approaching this challenging sector.

- *Other practical challenges in very close-range photogrammetry*

As mentioned, close-range photogrammetry has become essential in applications requiring high-detail 3D models, including the reconstructions of heritage assets. However, this specific field presents several technical issues that significantly impact model accuracy, resolution, and usability. In this section, some of the major challenges in this context will be discussed.

In very close-range photography, especially when using macro lenses, the depth of field (DoF) becomes extremely shallow, meaning only a limited portion of the object is sharply in focus. Studies like Sapirstein (2018) and Gallo et al. (2014) point out that this shallow DoF is detrimental to photogrammetry, as 3D reconstruction software requires sharply focused images for reliable feature-point matching and accurate model construction. The limited DoF is especially problematic for objects with irregular or highly detailed surfaces that require high magnification rates, such as very small or intricate artefacts.

To address this, methods like multifocal image stacking have been explored. This involves taking multiple images at different focal planes and combining them to produce a single image with an extended depth of field (figure 24). While effective, focus stacking presents further challenges: it increases the number of required images, introduces a significant processing load, and may produce alignment errors during stacking. Advanced image fusion algorithms have shown promise, but Gallo et al. (2014) emphasise that even with these algorithms, the stacking process remains a resource-intensive workaround rather than a definitive solution.

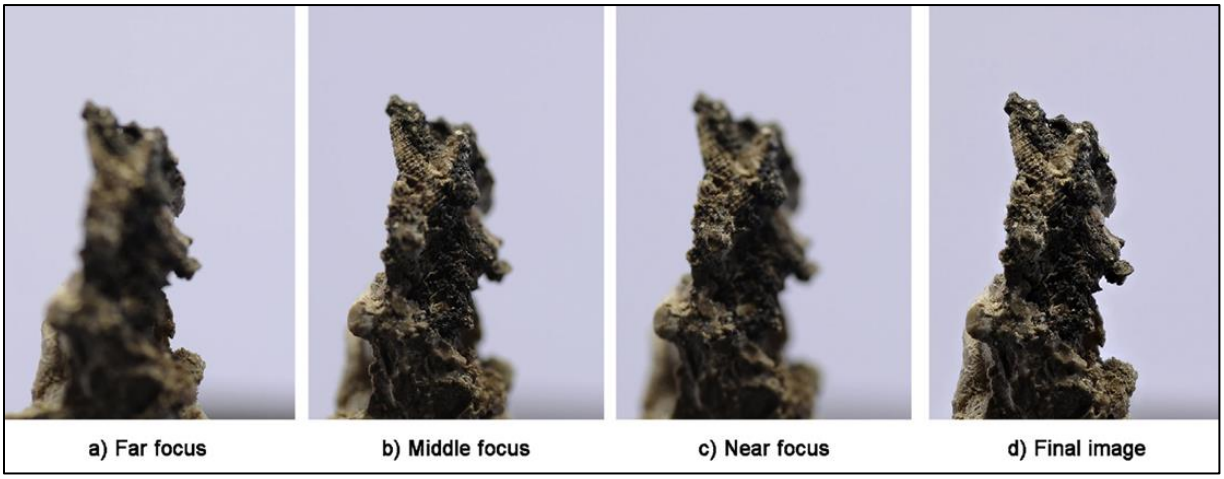

Figure 24. a, b and c are the three images captured at different focus planes; d is the resulting image from focus-stacking (Gallo et al., 2014)

Camera calibration is another critical component that directly impacts model accuracy in close-range photogrammetry. For small objects, the high magnification and narrow field of view required in macro-photogrammetry increase lens distortions and calibration instability. Galantucci et al. (2018), for instance, discuss how traditional camera calibration methods often struggle to deliver the required accuracy at these scales. Calibration instability, often caused by using zoom or macro lenses, results in distortions that can misrepresent the objects' geometry, especially when DoF limitations further complicate clear imaging.

There are also promising advancements in calibration software that incorporate self-calibration routines to enhance accuracy. For small objects with complex geometry, establishing precise, repeatable calibration standards remains essential, and further research into alternative calibration models and sensor technologies may provide more stable solutions.

Lighting is a third major challenge in high-detail photogrammetry for small objects. Effective photogrammetry requires uniform lighting to avoid shadows and reflections that can obscure details and create inconsistencies in the feature extraction process. Studies such as De Paolis et al. (2020) and Galantucci et al. (2018) indicate that lighting issues are particularly challenging with small, reflective objects, where even minor changes in lighting angle can significantly alter how features are captured on

the object's surface. Diffuse lighting is generally recommended to reduce harsh shadows and prevent specular highlights, which can confuse feature detection algorithms. Polarised filters are also commonly used to minimise reflections, though De Paolis et al. (2020) point out that the practical application of these methods is often inconsistent, as objects with highly varied surface properties may require individualised lighting setups.

To capture the full 3D geometry of small objects, many photogrammeters use a turntable setup, rotating the object while keeping the camera stationary (figure 25). While convenient, this approach presents new challenges, as the turntable may obscure parts of the object, particularly its base. Sapirstein (2018) highlights the risk of incomplete 3D models due to portions of the object remaining out of view, which compromises the accuracy of the reconstruction. Additionally, when background features are visible, the software can misinterpret the scene, aligning cameras to the background rather than the object. Some studies suggest capturing separate images of the top and bottom of the object and then merging these partial views in post-processing. However, this method requires precise alignment of the two halves, which is prone to error and time-consuming.

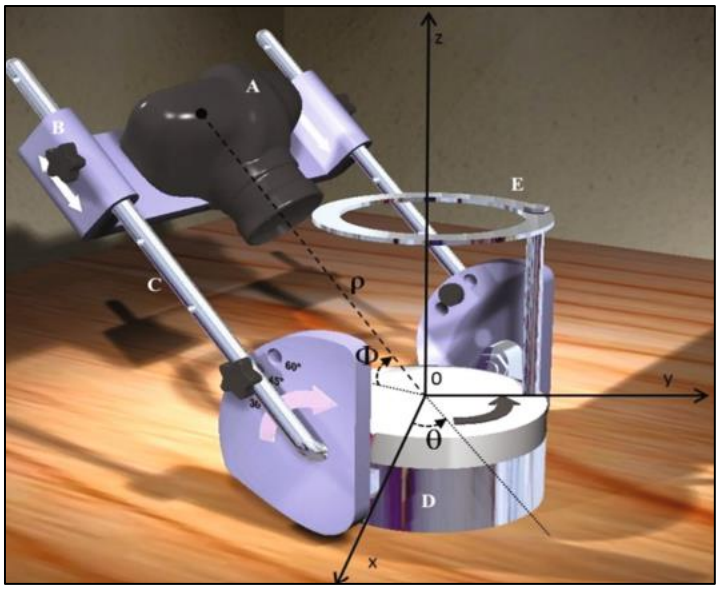

Figure 25. An example of an automatic rotating platform for close-range imaging (Galantucci et al., 2018)

Metrical accuracy in small-object detailed reconstruction remains a contentious issue, as photogrammetry software, while effective for larger structures, often struggles to deliver the precision required for minute details. The above-mentioned study by Sapirstein (2018) – among others – report that photogrammetry usually yields less accurate results compared to more costly techniques like laser-based or SLS scanning. A key reason for this discrepancy is that small deviations in camera calibration, lighting, and DoF alignment, which are often negligible at larger scales, become significant at micro and sub-millimetre scales.

Standardised accuracy assessments are generally conducted by comparing photogrammetric models to "ground-truth" measurements from high-precision scanning methodologies. While this provides a baseline, Galantucci (2018) argues that such comparisons do not account for real-world variances and can be overly optimistic.

Gallo et al. (2014) suggests that introducing coded targets during image acquisition may improve accuracy by providing reliable reference points for alignment, though this approach is often impractical in non-laboratory settings and in some scenarios – especially in CH small artefact – the application of targets in the scene is impracticable or prohibited. Ultimately, accuracy remains a challenge that requires a combination of software improvements, procedural rigour, and possibly more standardised benchmarks specific to very close-range photogrammetry.

In conclusion, significant technical challenges persist in high-detail image-based reconstructions. Issues related to depth of field, camera calibration, lighting, setup-related logistical problems, and metrical accuracy are inherent to the practice, and each requires specialised solutions. As photogrammetry technology advances, a combination of software innovations, refined procedural standards, and potential hardware adaptations will be essential to overcoming these limitations.

To sum up, digital close-range photogrammetry is a fascinating and promising – yet complex and challenging – geomatic technique. Behind the technical limitations highlighted in the previous paragraphs, this methodology can represent a valuable

tool in high-detail 3D reconstructions, as highlighted also in the related case studies section 2.2. Scholars and practitioners are now exploring the use of DP as an alternative to costly technologies as range-based ones, achieving promising results. This technique is indeed powerful and potentially – with high levels of expertise and practice – it can lead to even better results compared to range-based methodologies.

As new tools and methodologies emerge, the ability to document and analyse objects at very high levels of detail and accuracy will continue to grow, bringing new insights into several fields, including heritage science.

2.4 Examples from the literature of techniques comparisons

After outlining some theoretical and functional aspects of the main geomatic techniques used to obtain high-detail 3D models, this section will present examples from the scientific literature where the mentioned technologies have been compared. It is important to note that not all of the comparisons are directly related to the field of cultural heritage, as the focus here is on the technical and operational comparison of the tools themselves.

Many scholars, across various disciplines, have not only tested the different outputs of surveys conducted with different instruments, but have also made practical considerations from an operational standpoint. These include factors such as the time required for the survey, the cost of the equipment, and the practical challenges surveyors face in the field.

- *Structured Light Scanning vs. Digital Photogrammetry*

Several studies are present in the literature in which scholars try to investigate the advantages and disadvantages of SLS and DP. As pointed out in the instrument section, SLS is a powerful technique, but the equipment is expensive and its efficacy can be limited by different constraints, especially in terms of objects' materials. On the other hand, photogrammetry requires more expertise – both theoretical and

technical – and the data acquisition and processing phases can be much slower when compared to SLS.

In Freeman et al. (2021), for instance, the authors propose a comparison between SLS and DP in the context of physical prototype digitisation, where rapid iteration and accuracy are essential. The study systematically evaluates both techniques by digitising artefacts and comparing the results against a master model. The experimental setup emphasises practical applicability, with SLS emerging as the more reliable and user-friendly system for the context-specific requirements of the experiments conducted.

The main conclusion in this paper is that SLS delivers better model quality and faster digitisation, making it a preferable choice for rapid prototyping. On the contrary, photogrammetry, while capable of achieving similar geometric accuracy (within 0.1 mm), requires significantly higher manual intervention and expertise. The time-consuming nature of DP diminishes its practicality in high-speed design environments, particularly when compared to the faster, more automated SLS.

Guendulain-Garcia et al. (2023) extend the discussion of SLS vs. DP to the study of coral reefs, where structural complexity is a key ecological indicator. In this study, the authors highlight the limitations of DP in capturing highly complex, organic shapes, such as coral formations (figure 26). Although DP provides sufficient results for simpler morphological traits like area and volume, SLS outperforms DP in capturing traits that depend on surface complexity, such as fractal dimension and sphericity. Another critical point raised by the authors is the scalability of the two technologies. For large coral reef sections, DP's ability to reconstruct vast areas from numerous overlapping images presents an advantage over SLS, which is typically limited by its smaller scanning volumes and range.

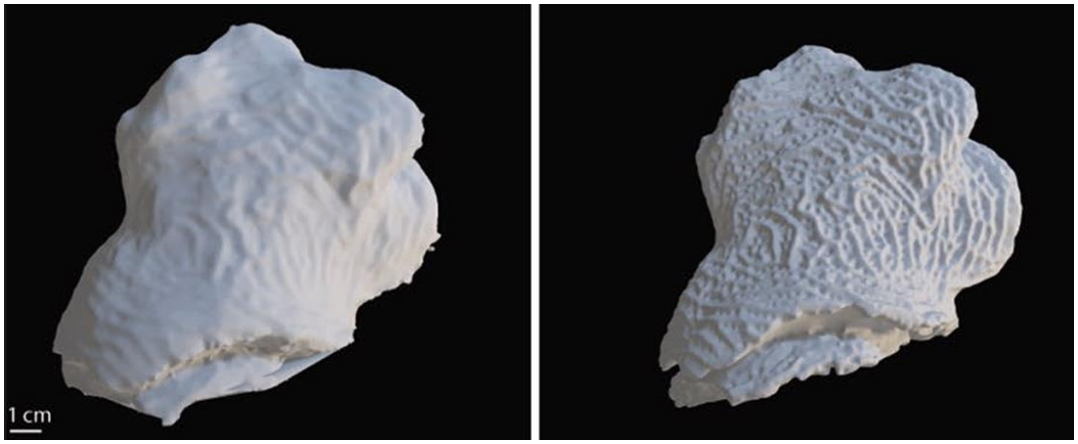

Figure 26. Comparison of corals 3D models obtained with DP (left) and SLS (right); (Guendulain-Garcia et al., 2023)

When examining both Freeman et al. (2021) and Guendulain-Garcia et al. (2023), a more profound comparative analysis of SLS and DP emerges. While both methods are effective for detailed geometric reconstruction, the intended application and requirements play significant roles in determining the appropriate method. SLS proved superior when fine-detail capture was critical, but it presented some hardware and logistical limitations (such as cost and size of the scanned area). In contrast, DP, offered greater flexibility, especially for larger-scale projects and in the presence of economic constraints.

- *Laser Triangulators vs. Structured Light Scanning*

Jecik et al. (2003) explore the use of SLS and LT in capturing complex free-form surfaces, providing an industrial perspective by focusing on the automotive industry. Their research highlights several technical aspects, such as measurement accuracy, speed, and the influence of object material and reflectance. The study concludes that laser scanning offers higher accuracy due to its coherent light source, which reduces errors associated with surface texture and reflectance. They also point out, however, that SLS offers comparable accuracy for certain applications but at a lower cost and with greater portability. This makes SLS a valuable alternative for industries where accuracy needs are moderate but speed and cost represent a priority.

They emphasise that SLS systems are often over-engineered for applications that do not require extreme precision, which makes SLS more suitable for many industrial applications, particularly in prototyping and design. The comparison between SLS and LT in this study also touches on the practical limitations of laser scanning, such as slower acquisition times and higher data processing requirements. Laser scanning excels in environments where extreme accuracy is needed, such as the aerospace or medical fields, but for everyday industrial use, SLS often provides sufficient accuracy at a fraction of the cost.

Pruitt et al. (2017) take the discussion into the field of palaeontology, focusing on the use of LT and SLS for fossils. This paper is especially relevant as it highlights the different workflows associated with each scanning method. LT, with its coherent laser beams, is capable of capturing subtle superficial details, particularly in fossils where micro-morphological observations are critical to understanding biological processes. A significant contribution of Pruitt's study is the workflow comparison—where LT, while accurate, requires more post-processing and editing, SLS offers a faster and more intuitive workflow.

In this study too, the context-specific nature of the choice between LT and SLS is discussed, suggesting that LT should be reserved for research-grade reconstructions, while SLS can be deployed for more general morphological studies.

- *Laser Triangulators vs. Digital Photogrammetry*

The 2019 study by Lastilla et al. offers a comprehensive comparison between LT and DP for the 3D reconstruction of archaeological inscribed objects. The researchers identify the geometric accuracy of laser scanning, particularly in capturing intricate features as inscriptions, as a critical factor in heritage preservation. From a geometrical detail point of view, the authors highlighted that LT ensured better outcomes when compared to DP (figure 27). However, photogrammetry provides an invaluable complement, as it captured surface textures that the LT equipment used could not reproduce.

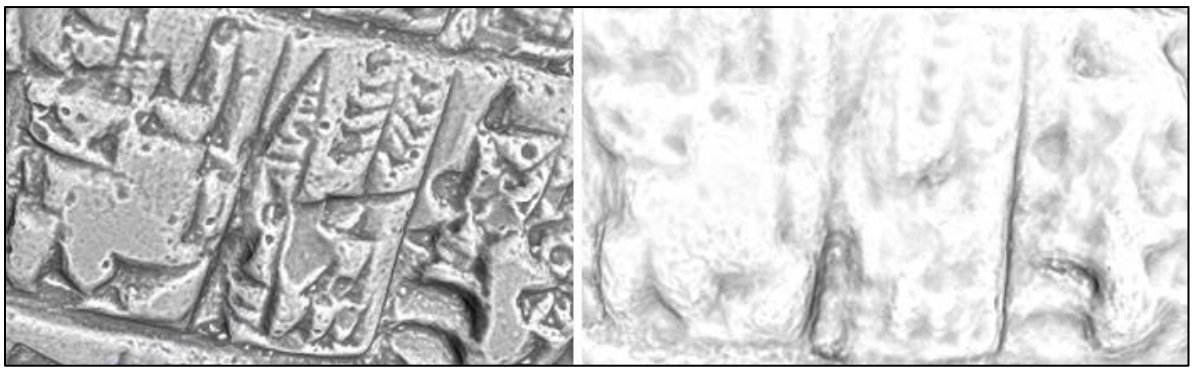

Figure 27. The same detail of an inscribed tablet 3D model, obtained with LT (left) vs DP (right); (Lastilla et al., 2019)

The study also provides practical solutions, suggesting that combining LT and DP techniques yields the best results. In the case of their experiments, while LT excelled in geometric details capture, DP's ability to integrate textures into the 3D model resulted in a more comprehensive digital representation. A combined approach is especially important in archaeology, where both geometric resolution and visual inspection are essential.

Re et al.'s (2011) study further explores the role of LT and DP in cultural heritage documentation, focusing on small to medium-sized museum artefacts. The authors emphasise that while LT provides superior metric accuracy, DP is a more cost-effective solution for objects that do not require micrometre-level precision. In addition, they also mentioned that photogrammetry is limited by environmental factors, such as lighting and object texture, which can introduce significant noise into the final model. However, the flexibility and accessibility of DP—particularly its ability to capture larger areas quickly—make it indispensable in resource-constrained environments like museums or archaeological sites. In this study too, the potential of combining both techniques for more comprehensive documentation is evidenced.

Another interesting example in the context of LT and DP comparison is offered by Adami et al. (2015). The paper explores this technique comparison for heritage high-detail documentation, testing both a range-based and image-based methodology to a terracotta bust conserved at the City Museum of Mantua, Italy. The sculpture presented a complex surface with intricate details, ideal for testing the capabilities of

LT and DP in capturing fine geometric elements. For the range-based survey, the authors employed two laser triangulators presenting a remarkable micrometre-level accuracy but limited colour reproduction. Conversely, the image-based method — employing a digital full-frame camera — offered detailed texturing and higher flexibility in data acquisition.

A detailed comparison of the obtained models revealed minimal discrepancies between the two techniques, with a mean error of only 0.0319 mm in the mesh-to-mesh distances (figure 28). Following this result, the authors concluded that close-range photogrammetry—when applied with methodological rigour—can serve as a viable alternative to the significantly costlier laser technology, even in terms of geometric detail. Furthermore, the image-based technique enables high-resolution texturing of the models, which is essential for the visualisation and inspection of heritage assets.

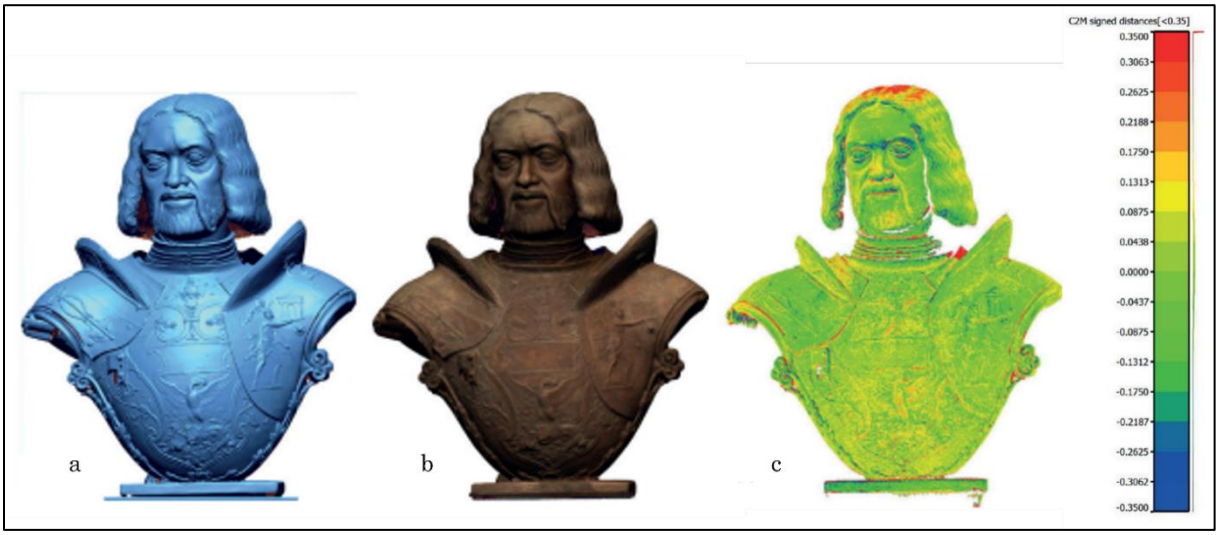

Figure 28. 3D model of the terracotta bust obtained with LT (a) and with DP (b); the results of the mesh-to-mesh distance comparison are shown in (c), with a colour visualisation highlighting the extracted distance values (Adami et al., 2015).

- *An integrated and context-specific approach can be the solution*

The comparisons between the tools in this section aimed to show that selecting geomatic instruments for a highly detailed survey depends on multiple factors. Researchers conducting these comparative analyses consistently observed that the

optimal tool was the one best suited to the specific conditions of each experiment. Including these technical discussions is useful to begin outlying the operational advantages and limitations of DP, SLS, and LT for high-detail surveys, while underscoring the importance of contextualising each tool's use according to the particular requirements of each case.

As a consequence, as already anticipated, the selection of instruments is a crucial issue in surveying, and planning should never be overlooked. Proper preliminary planning allows for careful theoretical and operational considerations, also considering the specific characteristics of the objects/environment and the goals to be achieved.

Furthermore, it is good practice in Geomatics—as in other disciplines—not to rely on the potential of a single tool or methodology, because each case presents its own complexities, each survey has unique requirements to be met, and each instrument presents its own advantages and disadvantages with respect to this variety of situations. Thus, the 'multi-modal' approach—combining different strategies to offset each technique's limitations while leveraging their respective strengths—is well established in this field.

Remondino et al. (2005), for instance, present a nuanced perspective on the debate between different 3D surveying techniques, proposing that a hybrid approach is often the most effective. Their study demonstrates that for objects with complex geometries, combining the geometric accuracy of laser scanning with the texturing capabilities of photogrammetry produces the most accurate and visually realistic models. In this paper the authors also highlight the scalability of this approach, which can be applied to objects ranging from small archaeological finds to large architectural structures, making it a versatile methodology for 3D surveying across various fields.

Therefore, the choice between SLS, LT, and DP should be dictated by the specific requirements of the project—whether it be precision, speed, scalability, costs and other case-specific challenges and constraints. The reviewed papers collectively

suggest that there is no one-size-fits-all solution, but rather a suite of tools that, when used in combination, provide the best outcomes for high-detail 3D surveying.

2.5 Surveying output: 3D point clouds and 3D polygonal models

After clarifying some theoretical aspects of the most commonly used techniques in high-detail 3D surveying and reviewing relevant comparative examples from the literature, it seems useful to provide an overview of the primary three-dimensional outputs achievable with these methods: 3D point clouds and polygonal models (meshes). This is because, in the context of high-detail surveying, the aspects related to the visualisation and use of geometric survey results are of paramount importance. The investigation of the surface geometry of the surveyed objects cannot disregard the quality of the digital reconstruction, whether in the form of a point cloud or mesh. It therefore seemed useful to offer a brief insight into these two formats for managing three-dimensional data and some related concepts.

Point clouds are a core output of several 3D surveying systems. In this form, a large number of discrete data points are generated, each represented by three-dimensional coordinates (x, y, z), providing the spatial information of the objects. In high-detail heritage digitisation, the density of point clouds (see section 2.1.1 for density definition) plays a critical role in ensuring that fine features are accurately represented.

Moreover, the spatial 3D coordinates can be optionally associated with colour information, represented by RGB coordinates values connected to each point. For heritage assets, colour and texture are often as important as geometry, especially for artefacts where surface colouration is critical to their interpretation. This colour data can be retrieved both in a direct way when processing imagery data in photogrammetric pipelines, or indirectly by aligning images to the geometry data (as occurs in laser-based surveying systems).

Point clouds generated by active surveying systems as laser triangulators can also include additional information, such as the intensity at which the emitted signal is detected from the system. Depending on the instrument used, point clouds can carry additional metadata such as timestamps, classification codes (to differentiate between types of objects or surfaces), and more. This information is usually stored in point clouds as a scalar field, which can represent any kind of numerical information associated with the 3D points.

One of the main issues with point clouds is their unstructured nature (figure 29a). This lack of inherent connectivity between points means that additional processing is required to create a cohesive surface digital representation. Noise and redundancy in point clouds, often due to the scanning process or environmental/material factors, can complicate this task. Heritage assets can present several challenges (see section 2.6 for further details), making it essential to process and clean the point cloud data before further analysis or before converting it into polygonal models through surface reconstruction algorithms (Kolluri et al., 2004).

A polygonal model, or mesh, provides a structured representation of the object's surface by connecting the points into a network of polygons, typically triangles. This serves as a continuous approximation of the asset's surface, facilitating operations such as surface inspection and analysis, virtual interaction/simulation, and even 3D printing for physical replicas. Hence, the mesh format represents a continuous and structured form which is more suitable for detailed surface visualisation (figure 29d).

However, the quality of the mesh is influenced by several factors, such as incorrect surface reconstruction strategies that can produce anomalies or inconsistencies in the topology. The main reason for this is the poor smoothness of the original point cloud which, as mentioned, can be affected by noise and outliers. So, as anticipated, the initial set of points must be processed accordingly before surface reconstruction. Several algorithms are used to convert point clouds into polygonal meshes.

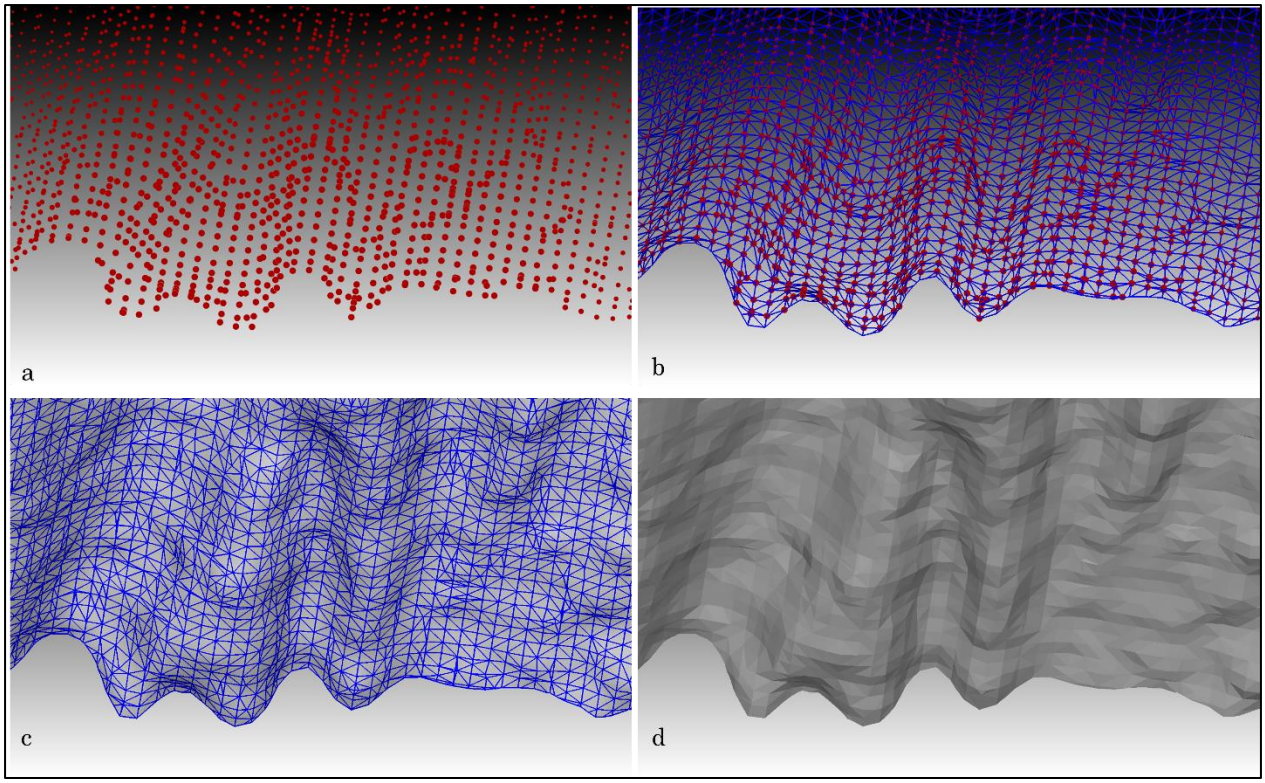

Figure 29. a) 3D points in a cloud; b) 3D points as vertexes in a mesh wireframe; c) Mesh wireframe visualisation over the reconstructed surface; d) Mesh reconstructed surface

Delaunay triangulation, for instance, is effective for creating well-proportioned triangles that ensure a consistent topology. Poisson surface reconstruction is another widely used technique that produces smooth, watertight surfaces. Marching Cubes and alpha shapes are also frequently employed in 3D surface reconstructions. The Marching Cubes algorithm, which is highly suited for volumetric data, is ideal for objects with intricate internal structures or where volumetric data needs to be analysed. Alpha shapes, on the other hand, are highly adaptable to different point cloud densities and noise levels, making them useful in situations where initial point clouds are uneven or contain imperfections (Salman et al., 2010).

The informatic formats used to store point clouds and polygonal meshes allow the data to be processed and shared across different software platforms, which is crucial to ensure interoperability, especially in interdisciplinary projects. Widely used formats such as PLY and OBJ support both point cloud and mesh data, allowing for flexibility in how the data is manipulated and visualised. As anticipated, point clouds

are formed by a set of points containing the spatial coordinates acquired and additional information such as colours, intensity values and other scalar fields. These details can also be contained in a .txt file or ASCII format (ASCII: American Standard Code for Information Interchange).

Mesh formats, such as the previously mentioned OBJ, or others like STL (abbreviation for stereolithography) and FBX (Filmbox), also contain additional information to enable software to correctly interpret the file as a polygonal model. These include—in addition to the vertex spatial coordinates—the topology of the mesh arrangement, providing information on the connections between vertices. Furthermore, information on the normal vector is embedded within these formats, typically as per-vertex or per-face normal vectors (figure 30a). Similar to point clouds, this data is represented by the X, Y, and Z components of a normalised (unit) vector that defines the orientation of the surface at a specific point or vertex. Each component indicates the extent to which the normal vector aligns along the three axes, thereby describing the directional tilt of the surface in 3D space.

In addition, 3D models can also be associated with vertex colours (similar to RGB values in point clouds) or with a texture map, typically a raster image (figure 30b), and a material library. A texture map provides detailed visual information by assigning 2D image coordinates (often called "UV" coordinates) to each vertex or face on the 3D model, ensuring that the texture aligns correctly with the geometry.

The material library (often stored in an MTL file when using OBJ format) is a set of material properties associated with a 3D model. It defines characteristics like diffuse, specular, and ambient colours, reflectivity and shininess. Combined, texture maps and material libraries enable photorealistic rendering by simulating how different materials interact with light and by adding fine surface details, especially if the texturing procedure is performed using high-resolution imagery.

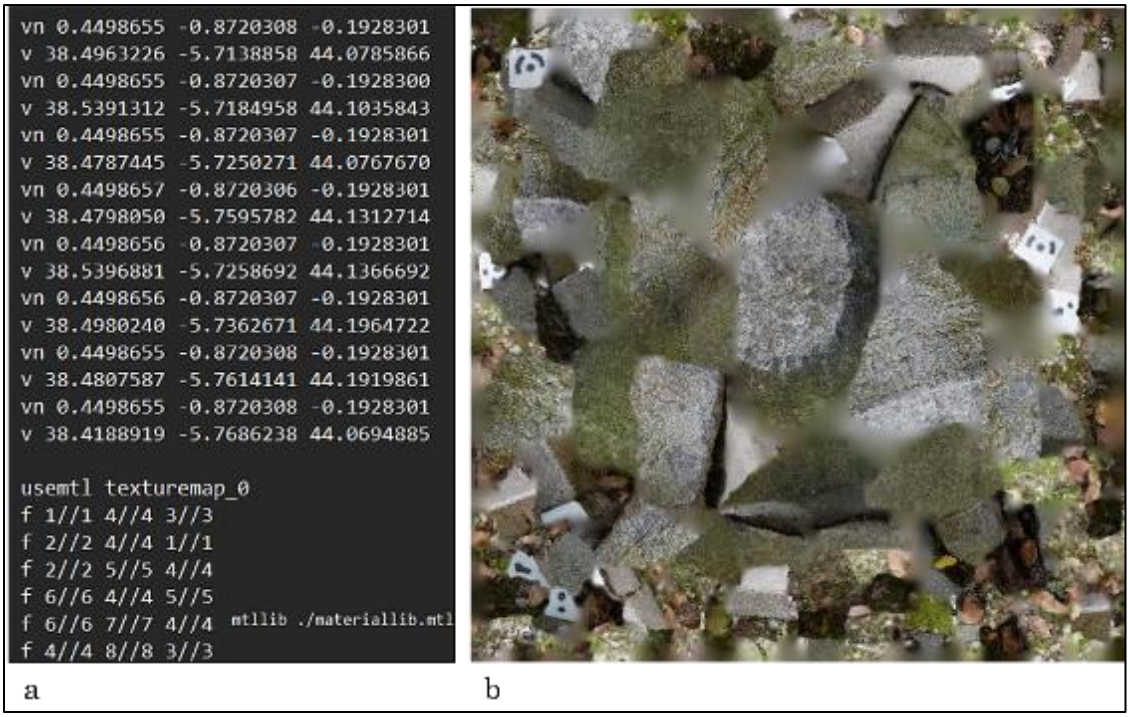

Figure 30. a) Example of OBJ file structure: 3D coordinates of vertices (v), vertex normals (vn), face configuration providing the topology (f), and references to the material library (mtllib) and texture map (usemtl) files; b) Example of a texture map raster

If 3D data from multiple scans is collected, it is often necessary to align and merge the various point clouds into a common coordinates system, a process known as registration. Iterative Closest Point (ICP) is one of the most widely used methods for aligning two point clouds, refining the alignment by minimising the distance between corresponding points. This process ensures that different portions of the reconstructed object, acquired from multiple angles or under different conditions, are combined into a single, cohesive point cloud or model.

Feature-based matching is also useful when distinctive features of the object, such as edges or surface markings, are used to guide the alignment. In challenging environments, such as scenes with uneven surfaces or significant wear, the RANSAC algorithm (mentioned in section 2.3.3 when discussing SfM photogrammetry) can help by identifying and aligning key points despite the presence of noise and outliers in the data (Gomes et al., 2014; Mejia-Parra et al., 2019; Cui et al., 2021).

2.5.1 3D output quality metrics and comparison strategies

The previous section discussed the main output of 3D surveying, namely point clouds and meshes, from their definition to related concepts such as surface generation and data alignment. Typically, when these types of outcomes are obtained, strategies are also undertaken to assess their quality, both from a metrical and a topological point of view.

As discussed in section 2.3, structured light projection scanners and laser triangulators are metrical instruments that directly calculate distance values relative to the objects being surveyed. This capability allows for the creation of scaled 3D point clouds and models, accurately representing the dimensions of the surveyed objects within the instrumental error ranges. Conversely, digital photogrammetry is not inherently a metrical technology; it does not provide dimensional information in the 3D output without the integration of metric data. Considering the specific context of close-range DP, this lack is addressed by incorporating metric information into the image set through two primary methods:

- Incorporating known distance measurements: known distances are introduced into the scene using objects of precisely measured length, such as rulers, callipers, or dedicated scale bars. These are placed within the scene during image acquisition and are visible across multiple images. Photogrammetric software allows the definition of these known distances by manually selecting pairs of points corresponding to the ends of the scale bars in the images and then uses these distances to add metrical information to the 3D model. The metric residual error on these scale bars is calculated by comparing the known physical length of the scale bar with the length measured in the reconstructed 3D model. The overall scaling accuracy can be assessed by considering the collective residuals of all scale bars used.
- Control points with measured coordinates: a common practice in close-range DP is to associate 3D coordinates obtained from high-accuracy measurement

techniques, such as laser triangulators or SLS systems, to specific points in the captured scene. These control points are identifiable features or markers that are clearly visible in the images. In photogrammetric software, these control points are manually marked in the images, and their known coordinates are input into the model. The software uses these points to scale and align the photogrammetric model within the local coordinate system of the metrical instrument used to survey them, enhancing both the scale accuracy and the spatial positioning of the model. The metric error is calculated by comparing the known, measured coordinates of the control points with the coordinates estimated by the photogrammetry software.

This last step involves computing the Root Mean Square Error (RMSE). As defined by the *Positional Accuracy Standards for Digital Geospatial Data* (2023) from the American Society for Photogrammetry and Remote Sensing, RMSE is "the square root of the average of the set of squared differences between dataset coordinate values and coordinate values from an independent source of higher accuracy for identical points", and it is calculated as follows, either for each individual axis or by considering the combination of X, Y, and Z coordinates integrally:

$$\mathrm{RMSE}_X = \sqrt{\frac{1}{n}\sum_{i=1}^{n}\left(x_i(\text{estimated}) - x_i(\text{measured})\right)^2}$$

$$\mathrm{RMSE}_Y = \sqrt{\frac{1}{n}\sum_{i=1}^{n}\left(y_i(\text{estimated}) - y_i(\text{measured})\right)^2}$$

$$\mathrm{RMSE}_Z = \sqrt{\frac{1}{n}\sum_{i=1}^{n}\left(z_i(\text{estimated}) - z_i(\text{measured})\right)^2}$$

$$\mathrm{RMSE}_{3D_1} = \sqrt{\mathrm{RMSE}_X^2 + \mathrm{RMSE}_Y^2 + \mathrm{RMSE}_Z^2}$$

Where:

- $X_{estimated}$, $Y_{estimated}$, $Z_{estimated}$, are the coordinates of the points in the 3D model as estimated by the software,
- $X_{measured}$, $Y_{measured}$, $Z_{measured}$ are the coordinates of the measured points,
- n is the number of control points used.

Lower RMSE values indicate higher accuracy, and minimising this error ensures that the model closely matches the known coordinates, enhancing the reliability of the model's scaling procedure.

In very close-range photogrammetry for high-detail objects, it is often unnecessary to georeference the model within a global reference system. Therefore, Ground Control Points (GCPs) with global coordinates are typically not used in these applications. Moreover, metric control points from standard geodetic and topographic surveys are generally not employed. This is because, while metric accuracy is important, the level of surface detail in the reconstruction is often a higher priority (as discussed in section 2.1.1). Consequently, the most common practices in close-range photogrammetry include, as mentioned, the integration of manual measurements or the incorporation of control points extracted from 3D models of the same object acquired with high-precision and accuracy metrical survey systems.

The configuration of control points—both in terms of quantity and spatial distribution—substantially influences survey accuracy. In drone-based photogrammetry, studies by Ferrer-González et al. (2020) and Agüera-Vega et al. (2016) highlight the importance of strategically positioned Ground Control Points (GCPs) to optimise accuracy. Conversely, in terrestrial photogrammetry—and especially in very close-range photogrammetry—the approach differs. This is due both to logistical factors, such as the extent and accessibility of the scene or the presence of occlusions, and to the previously mentioned need to prioritise geometrical detail.

In this context, the configuration of control points is often determined more pragmatically. While fewer points may be used, their strategic placement remains critical for controlling accuracy across the varying depths and features of the object. A carefully targeted layout of control points or scale bars can enhance the accuracy of the resulting models, addressing the specific challenges of close-range imagery acquisition (Yogender et al., 2020). Additionally, distributing control points across the scene provides a more robust metric support network for the survey, including in close-range photogrammetry.

In the context of SfM, another important metric is the already mentioned reprojection error (section 2.3.3), which measures how well the 3D points, once projected back onto the 2D image plane, align with the original image points. Reprojection error provides an internal measure of the model's consistency and can indicate potential alignment or calibration issues.

As for Luhmann et al. (2023), this error is related to the *a posteriori* standard deviation of unit weight (σ_0), which serves as an approximate measure of accuracy within bundle adjustment. σ_0 represents the mean reprojection error in the absence of systematic errors and outliers and should ideally match the expected precision of image measurements. While a low reprojection error (and correspondingly, a low σ_0) suggests a good fit between the 2D images and the 3D model, it is crucial to complement this internal consistency measure with external validation using scale bars, control points, and checkpoints. This combination helps identify and mitigate internal model biases, ensuring the overall accuracy and reliability of the photogrammetric model.

Modern SfM software, such as the well-known and largely employed Agisoft Metashape, also generates confidence maps, which visually represent the reliability of different regions in the 3D model based on factors like image overlap, point density, and reprojection error. These maps represent a useful tool for identifying areas that may require additional data acquisition or refinement (Agisoft LLC, 2024).

All quality metrics described here are typically applied to the initial output of the 3D survey, namely the point clouds. However, as discussed in section 2.5, point cloud generation may be followed by the creation of a continuous polygonal surface, or mesh. As for the metric accuracy of the mesh, this is directly linked to that of the point cloud since, as previously mentioned, the points in the cloud become the vertices of the polygons in the surface reconstruction mesh. However, beyond metric considerations, it is also important to evaluate certain parameters for polygonal models to assess their correctness and usability – especially in the field of high-detail 3D reconstructions –.

A well-constructed mesh should have a uniform and consistent distribution of polygons. The average polygon side length is one of the key metrics for evaluating mesh quality, and it is often the main factor accounted for the mesh (3D) resolution (see section 2.1.1 for further details on this concept). Nonetheless, a high number of polygons (or very small values for the polygons' side length) may also be the result of interpolation processes occurred either during the point cloud generation (used to construct the mesh) or in the continuous surface reconstruction step. Hence, this value must be critically evaluated to understand whether the high polygon density is a result of a robust reconstruction approach.

Additionally, automatic mesh topology analysis algorithms are employed to detect and correct common issues such as non-manifold, clustered or intersecting faces, holes, and degenerate polygons. These errors can compromise the structural integrity of the mesh, making it unsuitable for further applications like 3D printing, mesh manipulation, virtual illumination or simulations and – more generically – a consistent and robust surface inspection.

Non-manifold geometry, in particular, occurs when an edge is shared by more than two polygons, creating inconsistencies in the mesh's topology. This issue can lead to rendering errors or failures in processes that rely on mesh topology consistency, as mentioned above (Chatzivasileiadi et al., 2018). Detecting and fixing non-manifold

faces is then a crucial step to perform subsequent post-processing operations with the polygonal models.

When evaluating the outcomes of different surveying techniques – or different outputs obtained with the same instrument at different conditions/configurations – it is essential to use appropriate comparison strategies to quantify the differences between the datasets. Two commonly used methods for this aim are Cloud-to-Cloud (C2C) and Mesh-to-Mesh (M2M) distance calculations.

C2C comparison measures the Euclidean distance between neighbour points in two point clouds. It is particularly useful for assessing differences in models generated by different techniques or at different times. Tools like the open-source software CloudCompare are widely used for C2C comparisons, allowing to visualise the distance between points through colour-coded distance maps. M2M comparison, on the other hand, calculates the distances between corresponding vertices on two meshes. The results can be visualised using distance maps or histograms that show the distribution of distances across the models (figure 31). Moreover, the vertex of the mesh can be also compared with respect to the points in a cloud, producing a Mesh-to-Cloud distance estimation (CloudCompare, 2021).

Both C2C and M2M techniques rely on statistical analysis of the distance values, which typically follow a Gaussian distribution. The mean of the distribution represents the average distance between the two datasets, while the standard deviation indicates the variability. A tight distribution around zero suggests good alignment between the models, while larger deviations may point to discrepancies caused by differences in resolution, incorrect alignment procedures, or inconsistency in the datasets.

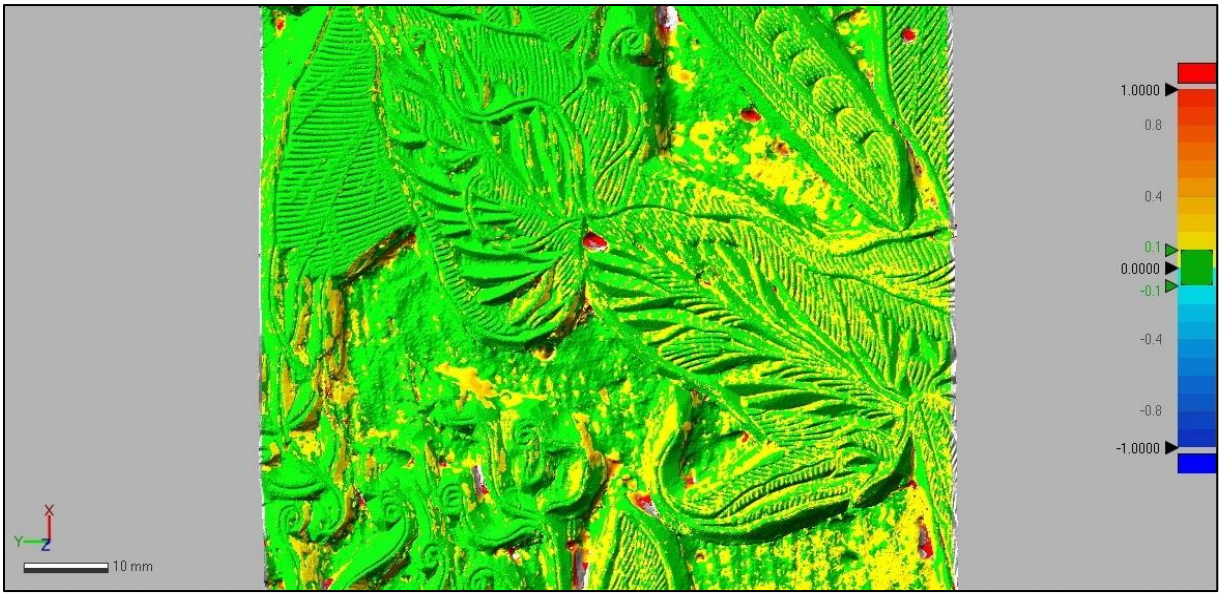

Figure 31. Two overlapped meshes compared, visualised with Mesh2Mesh result colour gradient; right: a colour scale bar showing the measured distance range (in mm)

Distance maps are an effective tool for visualising the differences between two 3D datasets. These maps use colour gradients to highlight areas where the models differ significantly, allowing for a quick visual assessment of alignment or discrepancies (Geomagic Design X, 2020). In addition to distance maps, profiles and section extraction techniques can be used to compare specific cross-sections of the models. This method is particularly useful for analysing linear features or assessing the geometric accuracy of specific areas. Profiles provide a more detailed comparison, as they allow for extracting and comparing the shape of the object at specific points, offering insights into height, curvature, and other geometric properties.

In conclusion, the evaluation and comparison of 3D point clouds and meshes require a comprehensive understanding of various quality metrics, but they are both pivotal operations to carry out in geomatic surveying. The characteristics of the digital dataset obtained, as seen, are strictly related to the strategies adopted during data processing that are, in turn, directly influenced by the methods of data acquisition in the field. The surveying phase is, in fact, crucial and presents many challenges, especially in the specific context of cultural heritage, as will be further explored in the following section.

2.6 Context-related (CH) issues in 3D surveying

The previous sections reviewed the advantages of high-detail 3D surveying in the investigation of cultural heritage (CH) properties, showcasing successful applications where technology has been effectively leveraged for this purpose. Later, a technical discussion about the most used geomatic tools in high-detail 3D surveying was offered, to provide a theoretical framework on the instruments and digital data types utilised in heritage digital reconstruction and investigation.

However, it is essential to recognise that CH represents a highly intricate and multifaceted context for Geomatics and scientific and technological disciplines in general. The challenges extend beyond purely technical considerations—such as material properties, environmental conditions during data acquisition, and practical constraints in the field—to encompass legal, ethical, and political complexities that must be carefully navigated when engaging with CH assets.

As discussed in section 1.1, the concept of "heritage" is not only vast and heterogeneous but also intertwined with theoretical, philosophical, and political dimensions. Those working with CH are not merely dealing with physical objects and sites; they are engaging with symbols and intangible elements carrying cultural, historical, and emotional significance. This section aims to outline the primary constraints faced by surveyors in the digitisation of cultural heritage (in a general sense, not only in high-detail 3D surveying), offering an outlook on these topics.

- *Materials-related constraints*

Remondino & Rizzi (2010) report – among many others – that materials-related properties of the objects represent one of the most challenging issues in heritage digitisation. These issues in the context of SLS have been already discussed in detail in a dedicated section (2.3.2), being this technique one of the most problematic in terms of materials-light interactions. The non-coherent nature of the projected light in SLS is more affected by optical challenges with respect to systems using coherent sources such as LT, or compared to passive methodologies such as photogrammetry.

This sub-section is, in fact, more generic about the main issues in digitising the already mentioned "non-cooperative" materials, but is more specific on the context of application, namely that of CH.

In this context, another complication arises from the fact that cultural assets are almost always composite and heterogeneous. Different materials exhibit varying behaviours when surveyed with sensing devices. For example, a statue made of stone, metal, and glass presents significant challenges, as these materials vary in their optical properties. The heterogeneity issue is particularly problematic in photogrammetry, which relies on the consistent detection of surface features. Surfaces with different textures or reflective properties can cause poor image matching, as discussed by Karami al. (2021).

Reflective and translucent surfaces present unique challenges. Reflective materials like metals, polished stones and ceramics can cause issues with both range-based scanning and photogrammetry due to speckle patterns in light reflection (in active scanning systems) and inhomogeneous optical behaviours when interacting with environmental lightning. These phenomena can create noise in the point cloud data acquired with laser scanners, as noted for instance by Gao et. al (2022). Translucent objects, such as wax or vitreous materials, can allow light to pass through, distorting both laser returns and complicating photogrammetric-based reconstructions (Conti et al., 2022).

- *Environmental, physical and logistical constraints*

Surveying cultural heritage sites often requires working in challenging environments that impose physical constraints, including poorly controllable lighting conditions and spatial restrictions. For photogrammetry, as observed in section 2.3.3, lighting is critical. In dimly lit environments such as cathedrals or archaeological sites, insufficient lighting can result in poor image quality, while overly bright conditions can cause reflections that compromise the quality of the survey. Gaiani et al. (2017)

note that lighting setups must be carefully managed to balance natural and artificial light, which can be logistically complex, especially in outdoor surveys.

Moreover, many heritage sites are located in confined or difficult-to-access areas, such as tombs or caves. Tanduo et. al (2023) highlight that in these cases, setting up scanning equipment like laser scanners or even photogrammetric setups can be difficult due to the sites' morphology complexity. In these cases, mobile systems such as SLAM technologies offer a solution, but these devices do not provide the same accuracy and resolution as static scanning systems.

Aside from technical and environmental limitations, other practical constraints related to logistics issues can severely impact the success of CH surveying projects. Transporting and setting up equipment in remote or difficult-to-access locations is a major logistical challenge in cultural heritage documentation. Hendrickx et al. (2011) describe the difficulties of bringing scanning equipment to archaeological sites, particularly when these sites are located in remote areas. Additionally, time constraints often limit the amount of data that can be collected as in the case, for instance, of temporary museum exhibitions (Balzani et al., 2023).

Logistical constraints in 3D surveying of heritage objects often stem from the physical impediments present in their environment, such as nearby artefacts or structural elements that cannot be moved. These obstacles limit the visibility of scanning equipment, potentially compromising the completeness of the survey. Additionally, many heritage objects themselves are immovable due to their size or fragility, or because they are part of permanent museum displays (Kesik et al., 2022). These issues further restrict the ability to reposition them for better surveying perspectives.

- *Legal and ethical constraints*

In addition to the technical and practical constraints, legal and ethical issues are also paramount in the digitisation of CH assets. Surveyors must take into account complex legal, moral, and political considerations, especially when dealing with fragile artefacts and sensitive heritage assets.

CH objects – in almost any case – cannot be touched, manipulated, or treated in any way, as legal frameworks prohibit physical contact to avoid degradation. For example, guidelines from institutions such as ICOMOS (International Council on Monuments and Sites) stipulate strict non-invasive procedures for CH documentation and investigation (ICOMOS, 2001). Despite geomatic 3D surveying systems being non-invasive, sometimes the application of markers or surface coatings is needed or would ensure better outcomes, but this type of intervention is usually forbidden. Surveyors must then strike a balance between data accuracy and assets' preservation-related issues.

The legal constraints surrounding access to heritage sites often depend on the significance of the site and the level of protection it enjoys under national and international law. For instance, UNESCO World Heritage sites are heavily regulated, requiring numerous permits and coordination with local conservation bodies to conduct any form of documentation. Surveyors are frequently required to work under the supervision of local authorities, who may impose further restrictions on how and when scans are conducted (Rüther & Palumbo, 2012).

Beyond legal restrictions, there are also significant ethical considerations when it comes to interact with cultural heritage objects, even in digital formats. Once a CH object is digitised, the resulting model can be edited, altered, or enhanced. Manipulating a heritage digital model, even for scientific or educational purposes, can inadvertently introduce historical or cultural biases. Some scholars argue that digitally modifying cultural artefacts may be equivalent to physically altering them, as it can change the public's understanding of the object.

This is particularly controversial in the context of CH assets that hold deep political or religious significance. For instance, digitally reconstructing a destroyed monument or artefact could be seen as erasing the historical context of its destruction (Khunti, 2018). In some cases, cultural heritage objects are linked to specific communities or groups that have ownership rights over the interpretation of their history. For

example, Indigenous communities may have specific rituals or beliefs about how their heritage should be treated, both physically and digitally. The unauthorised digitisation or manipulation of such objects can be viewed as a form of cultural appropriation, as discussed by Brown and Nicholas (2013). In these cases, surveyors must obtain consent from the relevant communities and ensure that the digital data is used respectfully toward cultural sensitivities.

Ethical concerns also extend to how digital models are used once they are created. Publishing digital models of lost heritage on commercial platforms introduces important questions about intellectual property rights and the commercialisation of cultural heritage. While 3D models are invaluable for education, research, and preservation, sharing them on platforms with their own regulations can lead to the commodification of cultural heritage. Alkhatib et al. (2023) highlight the risk that these digital replicas may be subjected to private platforms' terms, potentially undermining the cultural significance of the original object.

Hence, legal, ethical, and political constraints play a crucial role in shaping the practices of 3D surveying in cultural heritage contexts. These challenges must be carefully navigated to ensure that the surveying work respects the fragility, cultural significance, and ethical concerns surrounding heritage objects and sites. By adhering to strict conservation principles and engaging in dialogue with global and local communities and institutions, it can be ensured that the digitisation efforts contribute to the preservation and respectful dissemination of cultural heritage.

3. METHODOLOGY

Having clarified a number of aspects – terminological, theoretical, and technical – in this section the focus will be on describing how high-detail 3D surveying was studied and applied for the experimental part of this PhD research. First of all, the surveying instruments available at the research group and used for the experiments will be described from a technical point of view. Next, the survey and processing methodologies employed and the data analysis and comparison strategies will be discussed.

This section will provide a methodological framework for the adopted strategies in approaching the real case studies presented later. Indeed, the Geomatics and Topography research group at DICAM has long and consolidated experience in 3D surveying, even of high detail. Therefore, over the years, very well-tested and consolidated procedural approaches have been established, as well as good practices to be adopted in the operational phases. As part of this PhD research, efforts have been made to consolidate and further optimise these strategies, focusing specifically on the field of high-detail 3D surveying, particularly in its application to cultural heritage. In addition to the research group's extensive experience in this area, new solutions have been tested, and existing ones have been critically evaluated.

3.1 Geomatics instruments and software employed

- *The Laboratory of Surveying and Geomatics "LARIG" at Bologna University*

This PhD research was conducted at the Department of Civil, Chemical, Environmental and Materials Engineering (DICAM) of Bologna University, using the facilities and instruments of the Laboratory of Surveying and Geomatics (LARIG). The first Laboratory of Geodesy and Surveying was established in 1935, alongside the founding of the Faculty of Engineering (from the Royal School of Engineering) in its current location at *Viale del Risorgimento* in Bologna. The library tower of the faculty, designed as a Geodetic Observatory, still features a geodetic reference point, reflecting the long-standing commitment to topographical and geodetic studies. Over time, the

original Laboratory has built a strong collection of modern instruments while preserving historical topographic devices inherited from the past. The former Institute of Topography, Geodesy and Mining Geophysics evolved into the present-day Geomatics Area of the DICAM Department, and today LARIG specialises in geodetic, topographical, photogrammetric, 3D scanning, mapping and remote sensing projects, supporting both research and teaching.

This PhD thesis, then, has been conducted in a laboratory with a rich history, a long-standing tradition in geomatic studies, and a deep reservoir of expertise, offering an invaluable environment for advanced research.

- *Geomatic instruments and software employed for the PhD research*

Among the available devices at LARIG are also those to implement high-detail 3D surveying, namely structured-light projection scanners and photogrammetric equipment, which were employed in the experimental phase of this PhD thesis. In addition to the surveying devices, the laboratory is equipped with several high-performance workstations, which are particularly effective in handling graphic-intensive tasks. These workstations were employed to process the collected data using a combination of commercial and open-source software.

Among the commercial software utilised were *Artec Studio Professional* (version 16), the proprietary software used to pre-process the 3D data collected with the Artec structured light scanners, and *Agisoft Metashape* (various versions, now 2.1.2), which was used for Structure-from-Motion (SfM) photogrammetric processing. *Stonex Cube3D* (various versions, now 3.0.0) was also tested for 3D data processing (photogrammetry and point clouds from 3D scanning), as well as *Geomagic Design X* (version 2016.1.1). Additionally, free and open-source software such as CloudCompare (version 2.13.1), MeshLab (version 2023.12), and Blender (version 3.1) were employed for 3D data processing and modelling, while QGIS (version 3.36.3) and ImageJ (version 1.54j) were used to implement image-processing operations. The combination

of these software solutions ensured comprehensive data generation, processing and evaluation during the experimental work.

- *Structured-Light Projection Scanners*

LARIG laboratory, as mentioned, is equipped with high-end structured-light projection scanners that were tested for the experiments of this thesis. More precisely, the two devices of this kind mostly employed, EVA and Spider 3D scanners, are manufactured by *Artec3D*, based in Luxembourg (https://www.artec3d.com/it).

Artec EVA[1] is a portable, handheld SLS instrument designed to capture medium-sized objects (figure 32). It operates with a speed of 16 frames per second and records up to 2 million points per second. Key specifications of EVA include a resolution of 0.2 mm and an accuracy in the 3D points calculation of up to 0.1 mm. This tool is ideal for medium-to-small-sized objects, presenting a field of view of approximately 214 x 148 mm at the closest working distance and 536 x 371 mm at the maximum distance. The optimal working distance for EVA ranges from around 0.3 meters to 1 meter.

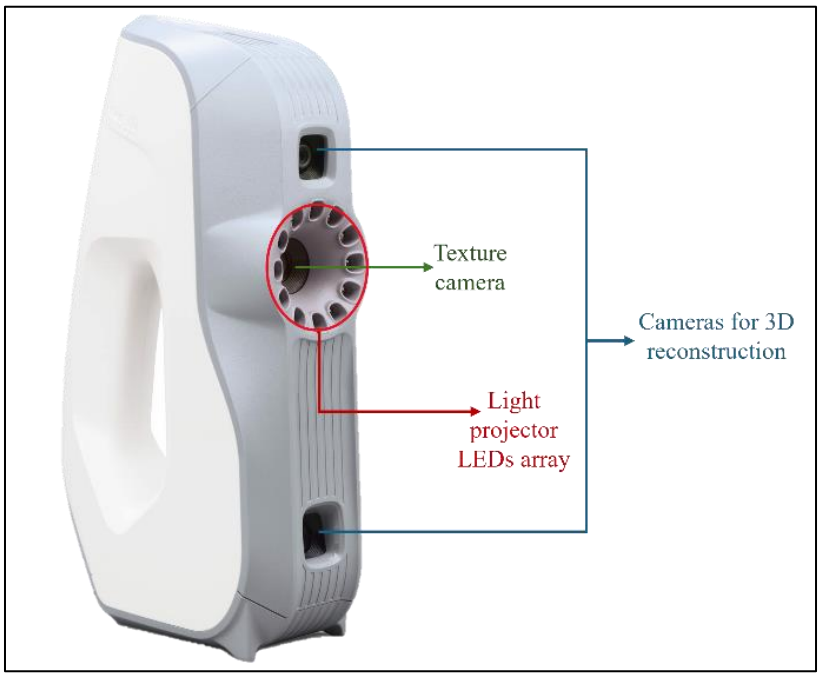

Figure 32. Artec EVA SLS scanner and its components

[1] *Artec* EVA technical specifications from the manufacturer's website

Artec Spider[2], too (figure 33), is handheld and portable, but it is designed for even smaller objects digitisation, having a field of view of approximately 180 x 140 mm and operating at closer working distances (170 mm - 350 mm). Its specifications are qualitatively higher compared to EVA, reaching 0.1 mm in terms of resolution and 0.05 mm of precision. This scanner employs a shorter wavelength of light, specifically blue LED light at around 450 nm, enabling the detection of finer details and smaller surface features compared to scanners using longer wavelengths. The smaller the wavelength, the more precise the scanner can be, as the resolution improves due to reduced diffraction effects (refer to the theoretical section 2.3.2 for further details on SLS working principles).

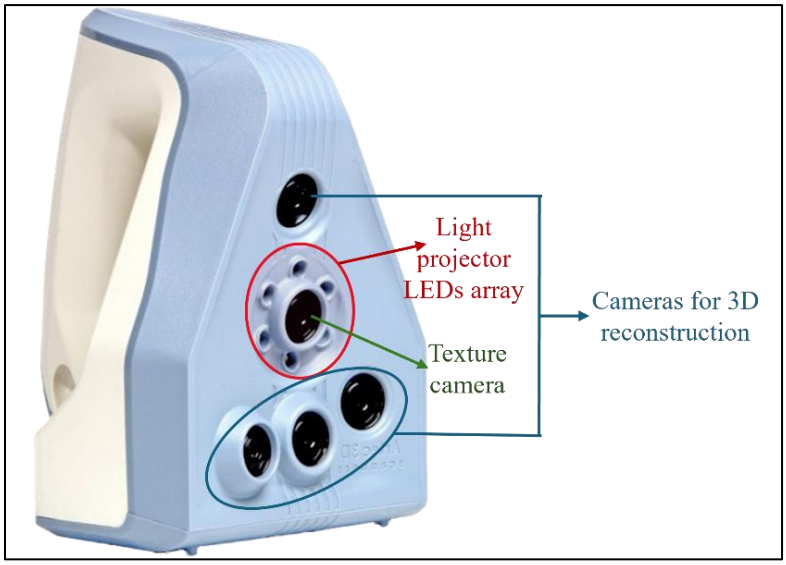

Figure 33. Artec Spider SLS scanner and its components

- *Photographic Equipment for close-up and macro photogrammetry*

The *Canon EOS 6D* and *Canon EOS 5D* Mark II cameras, both full-frame DSLR (Digital Single Lens Reflex) models, were chosen for photogrammetric data acquisition due to their high-resolution capabilities and adaptability. The EOS 6D features a 20.2 MP full-frame sensor (5472 x 3648) with a 35.8 x 23.9 mm sensor size and a pixel size of 6.5 µm. Meanwhile, the EOS 5D offers a slightly higher 21.1 MP resolution (5616 x 3744) and a smaller 6.4 µm pixel size. Both cameras use CMOS

[2] *Artec* Spider technical specifications from the manufacturer's website

(Complementary Metal-Oxide-Semiconductor) sensors, delivering high-resolution images with low noise.

To preserve the finest image details and colour accuracy, both cameras capture images in RAW format, maximising dynamic range—a crucial factor in photogrammetry. The EOS 6D offers an ISO range of up to 25,600, while the EOS 5D can reach an extended ISO of 102,400, enabling adaptability across diverse lighting conditions. For focusing precision, the EOS 5D employs a 61-point autofocus (AF) system, whereas the EOS 6D is equipped with an 11-point AF system. Both models support various lenses and focal lengths, offering flexibility in image acquisition, whether capturing broad scenes, detailed close-ups, or macro views tailored to the specific needs of each photogrammetric project.

For this thesis, the employed lens equipments are Canon 24-70 mm[3] and Canon 100 mm lenses[4]. The first is a versatile zoom lens, offering flexible focal lengths suited to capturing both wide-angle shots and detailed close-ups—ideal for varied object sizes and environments. For applications requiring high magnification and fine details, the Canon 100 mm macro lens is used. This lens enables the capture of small objects and intricate surface details, allowing for significant magnification without needing to position the camera too close to the object.

- *Equipment for micro-photogrammetry: Mic-Fi portable digital microscope*

For micro-photogrammetry applications, the *Mic-Fi* MICFIUVWIR portable digital microscope[5] was employed. This low-cost device allows to view and capture images and videos at magnification levels between 5x and 200x, making it useful for inspecting micro-level surface features. It is equipped with an optical system featuring a 1.3 MP (1280x1024) CMOS 1/4" sensor, permitting to see the results of the microscopic analysis in real-time on a computer (both via Wi-Fi or cabled

[3] https://www.canon.it/lenses/ef-24-70mm-f-2-8l-ii-usm-lens/

[4] https://www.canon.it/lenses/ef-100mm-f-2-8l-macro-is-usm-lens/

[5] https://mic-fi.it/shop/wi-fi-microscopes/micfiuvwir-white-uv-ir-light-wi-fi-microscope/?lang=en

connection) and to retrieve the micro-images in various formats including JPEG and BMP. This instrument is particularly valuable in material analysis, where surface defects, deterioration patterns, or fine textures need to be examined in detail. Moreover, it is a portable and lightweight device (88 grams), enabling *in situ* investigations, that can also be mounted on a dedicated stand to adjust the capture height.

- *Lighting Equipment*

A low-cost LED lightbox with dimensions of 30 x 30 cm is employed to provide consistent illumination for small objects during imagery acquisition. The uniform light distribution –also improved by including a diffusing panel below the led array– minimises shadows and ensures that the entire surface of the object is evenly lit, which is essential for producing uniform and high-quality images for photogrammetric 3D reconstructions. In situations where objects are too large for the lightbox or when field conditions do not allow for controlled lighting setups, low-cost portable LED lamps are also used. These lamps provide adjustable lighting conditions that can be customised to the needs of the object being captured. The portability and flexibility of these lamps make them ideal for fieldwork, where lighting conditions are often variable and less predictable.

- *Thermal Imaging Equipment - FLIR P620 Thermal Camera*

Thermal imaging is a key tool for detecting subsurface material conditions and analysing temperature variations, making it widely used in the field of heritage diagnostics – as also highlighted in the related studies section 2.2. For the aims of this thesis, the *FLIR* P620 thermal camera (figure 34) was used specifically for the 3D data integration experiment with thermal analysis (section 3.4.7). This device is an advanced thermal imaging system presenting a spatial resolution of 640 x 480 pixels and a thermal sensitivity of 40 mK at 30 °C. The camera operates in the thermal infrared wavelength range of 7.5–13 μm, enabling it to capture thermal variations across a temperature range of -40°C to 500°C with an accuracy of ±2°C or 2% of the reading.

Figure 34. FLIR P620 thermal camera in a field acquisition in Bologna

- *Calibration tools*

Colour accuracy is essential in photogrammetry and 3D scanning, particularly when the visual representation of objects is as important as their geometric details. For this thesis, the *X-RITE* colour checker was employed. This calibration checkboard provides a reference for adjusting the colour balance of images to match standardised colour values in the RGB space, ensuring that the digital reconstruction accurately represents the colours of the objects.

Moreover, to ensure accuracy in thermal imaging data, a calibration target made of a material with known emissivity is used. This target helps distinguish an object's emitted radiation from ambient reflections within the total measured radiance. Since the sensor records a combination of both, knowing the target's emissivity allows analysts to determine the proportion of emitted versus reflected radiation. This step is crucial for applying Planck's law correctly, ultimately enabling each pixel's measured radiance to be converted into accurate temperature values.

Hence, the equipment available at the LARIG lab provides comprehensive capabilities for high-detail 3D surveying, covering structured-light projection scanning, photogrammetry, thermal imaging, and additional equipment for lightning control and calibration. The integration of these technologies supports a wide range of applications and enhances the ability to conduct advanced research in Geomatics.

3.2 Surveying and processing procedures

3.2.1 Surveying and processing procedures with SLS

As highlighted in the technical section dedicated to this topic, structured-light projection scanning is a complex and powerful technology capable of producing highly detailed results. The accuracy of the instruments of this kind employed for this thesis, as mentioned earlier, can reach up to 50 microns, which makes the achievable metric accuracy nominally very high. However, this level of precision is contingent upon ideal conditions and cooperative materials, as discussed in section 2.3.2.

To mitigate these optical and material-related issues, the strategy employed has consistently been to inspect the objects to be scanned, preferably during a preliminary site visit, before conducting the actual scan. This approach allows for an assessment—though often, issues are only discovered during the scanning phase—of whether the material in question was suitable for SLS. In any case, the practice has been to also prepare an alternative image-based surveying technique to address any issues that might arise with the SLS.

From an operational perspective, the scanners tested, Artec EVA and Spider, are used in conjunction with their proprietary software during the data acquisition phase. In cases involving non-cooperative materials, attempts were made to optimise the scanning settings within the software, such as adjusting the scanner's sensitivity (though the meaning of this parameter is not fully disclosed by the manufacturer) and the brightness of the acquired frames. While tweaking these settings can sometimes improve results, in particularly challenging cases, the scan may still fail, and the image-based approach is preferred.

Moreover, as mentioned in section 2.3.2, SLS technologies can be negatively affected by the presence of non-continuous or isolated objects in the scanned regions. This issue has been frequently encountered during survey operations using SLS, particularly when dealing with objects that are either too small relative to the pattern

coverage or are discontinuous. To address this, external objects were sometimes introduced into the scene to serve as "reference masses", enhancing continuity. However, as will be detailed in the case study in section 3.4.1, this approach can introduce additional complexities during data processing.

In addition, the practical limitation discussed in section 2.6, regarding the inability to move cultural artefacts from their original positions, has often posed an additional operational challenge. These scanners have specific instrumental ranges (see section 3.1 for technical specifications), and beyond certain working distances, scanning becomes unfeasible. The immovability of objects has, in some cases, significantly impacted the feasibility of the survey. In such instances, the solution has been to capture as much data as possible from all accessible angles and then merge the various scans during post-processing, sometimes supplementing with photogrammetric surveys.

The alignment of different datasets—which must all be oriented within the same reference system—typically employs the ICP algorithm (refer to section 2.5.1). However, this approach can introduce errors due to the rotations and translations applied to the 3D datasets. Consequently, whenever feasible, it was preferred to acquire complete data in a single scan to prevent any adverse effects on metric accuracy or geometric detail from post-processing alignment procedures.

Another "good practice" for data acquisition with SLS has been to control, as much as possible, the ambient lighting conditions. As noted in section 2.3.2, fluctuations in environmental brightness can negatively impact the quality of the scan. In some cases, it was noted that some artificial lights would produce higher noise levels in the surface reconstructions; in these instances, the lights were completely switched off, operating in a completely dark environment (figure 35).

Figure 35. Data acquisition with SLS of an archaeological asset in a dark environment – The artificial external lights were negatively interacting with the projected light pattern.

Additionally, efforts were made to gather a sufficient—and, in more complex cases, redundant—amount of data to cover the entire surface of the objects surveyed. During the processing phase, only the points with the highest robustness were retained, eliminating any redundant ones.

In the processing phase, as mentioned earlier, the data collected with the scanners used for this thesis can only be pre-processed with proprietary software from the manufacturer, which reads data in a proprietary format. This software workflow includes an alignment—or, as many refer to it, "registration"—process for the various geometric elements acquired. The registration algorithms used in the workflow become progressively more refined, aiming to accurately align all internal elements of each individual scan relative to one another. The individual scans are then aligned first by manually selecting homologous points on shared features across distinct datasets and subsequently with the software's "global registration" algorithm, which employs a "best-fitting" strategy.

Another step involves surface noise reduction, eliminating geometric elements that constitute so-called outliers or elements detached from a continuous reference surface. This is followed by the reconstruction of a continuous polygonal surface, during which

the 3D resolution of the final mesh can be adjusted. This step is critical because an excessively high 3D resolution, relative to both the scanner's resolution and the robustness of the alignment process, can result in interpolated surfaces. Therefore, a "conservative" approach has always been adopted, remaining within the scanners' resolution capabilities and considering the quality of the registration procedures (which, in this software, is represented by a dimensionless error value with an unspecified meaning).

In conclusion, SLS scanning and processing strategies have been carefully designed, taking into account the capabilities of the tools used, operational constraints, specific survey requirements, and the characteristics of various operational contexts. In all cases, pre-survey planning has proven essential to the successful outcome of the project.

3.2.2 Surveying and processing procedures in DP

A different issue is the surveying and processing workflow conducted for photogrammetric reconstructions. In using image-based techniques, precise planning of the survey was always a crucial step, but this was conducted differently with respect to SLS, considering theoretical and methodological principles in photogrammetry.

Initially, the GSD (see section 2.1.1) is calculated considering the available optical equipment, focal lengths, and potential acquisition distances in accordance with the survey's metric accuracy and geometric detail requirements. Based on the necessary detail level and, where applicable, on the Nyquist-Shannon sampling theorem (as discussed in section 2.3.3), an achievable GSD range is determined for various sensor-lens-distance configurations. Additionally, based on these factors, the area covered in each image is calculated to ensure consistent spacing between images, targeting an overlap of at least 70% as recommended in close-range photogrammetric surveys (see section 2.3.3). These theoretical considerations are essential for planning an effective

survey strategy, adapting to the specific requirements of each object or environment, and anticipating potential output quality.

For scaling objects in photogrammetric surveys, black-and-white coded photogrammetric targets—printed at 600 DPI (Dots Per Inch) with laser technology for optimal resolution and contrast—are used. These targets are often attached to small blocks of various sizes to position them at consistent depths relative to the surveyed objects' surfaces (figure 36). Ensuring that the upper surfaces of objects and targets are approximately at the same level proves especially beneficial in macro-photogrammetry, where, as discussed, depth of field can be notably shallow. These targets serve as control points to reinforce the external orientation of images within the Structure from Motion workflow and as scale bar points for model scaling. Further use of these targets as metric control points is discussed in section 3.3.

Figure 36. Cube-shaped targets for photogrammetric survey during a survey campaign in Palazzo Poggi collection (Bologna)

Once the targets are appropriately distributed across the scene to strengthen the constraint network, the survey proceeds. Image acquisition is carried out with attention to the specified GSD, maintaining consistent distances for nadiral images (oriented orthogonally to the reference surface). As indicated, an overlap of at least 70% is sought between successive images during both x-y plane shifts and tilted image captures. Additionally, variable capture heights are utilised to ensure comprehensive scene coverage (ideally capturing all targets within single images) and close-up

captures to enhance GSD through closer acquisition distances (figure 37). For raking images, a full 360° rotation around the object is conducted when feasible, given any physical constraints, with the camera positioned at two distinct tilt angles. This approach reinforces the capture scheme, covering occluded and recessed areas that may be difficult to visualise.

Capturing raking images in macro photography presents unique challenges due to the reduced depth of field at close range, where elements near the focal plane may appear in focus while others do not. Aperture settings are balanced carefully—narrower apertures are preferable to enhance depth of field—while considering sensitivity settings (ISO, International Organisation for Standardisation) to manage noise. Lower ISO values help reduce noise, but increasing it may be necessary for narrower apertures to achieve adequate exposure, requiring a balance between aperture, ISO, and exposure to optimise image quality.

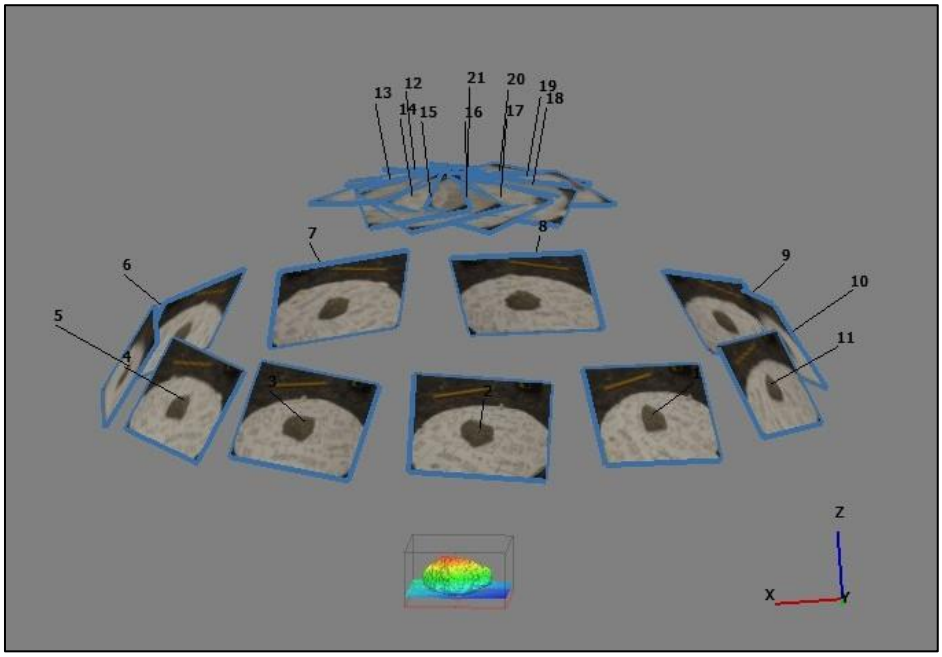

Figure 37. An example of imagery acquisition scheme for photogrammetric purposes, in this case for the reconstruction of a small rock specimen (ca. 6.5 x 6 cm)

Lighting control is also critical. When object size permits, a portable light box is used. For larger objects unsuitable for the light box, LED panels are positioned to ensure even illumination across the photographed surfaces (refer to section 3.1).

After image acquisition, the processing phase begins. Before importing into the SfM photogrammetry software, colour calibration is conducted using a colour checker to ensure consistency in RGB values. Within the SfM software, an image quality assessment is then performed, evaluating sharpness, lighting, and focus. This step identifies images with potential quality deficiencies that could compromise the final model, allowing for the removal of lower-quality images from the dataset to strengthen alignment and reconstruction. Masks are applied to portions of images with blurring, uneven lighting, or extraneous objects, isolating relevant scene sections. Manual collimation of control points and scale bars follows, with alignment adjustments made based on reprojection error calculations.

During image alignment, settings are calibrated based on the object's characteristics, generally preferring parameters to avoid image oversampling or undersampling, thus preserving their original resolution. After the external orientation of the images, an initial points set is generated, representing all the extracted tie points matched among the extracted features. These points are evaluated by inspecting the metric error residuals on the scale bars or control points and by the reprojection errors in pixels. If these values exceed acceptable thresholds (varying according to the type of instrument used for the control points coordinate generation, as well as the image resolution and characteristics) calibration and alignment parameters are modified to attempt to reduce errors.

For dense point cloud and mesh generation, in cases of fine depth discontinuities in the surveyed objects (as shallow engravings), depth filtering is disabled to avoid loss of information. Once generated, the dense clouds undergo a filtering procedure to remove outliers, often using a confidence map to facilitate the exclusion of less robust points. During mesh construction, interpolation is typically disabled to prevent artefacts, preserving the accuracy of the object's surface representation. Finally, texture mapping – if needed – is performed, ensuring uniform lighting across images to create a seamless texture on the 3D models.

3.3 Combined approaches

As previously mentioned, it is often essential in Geomatics to combine the advantages of multiple techniques. In cultural heritage studies, obtaining both a high level of geometric detail and a faithful visual representation of objects is often critical. This consideration becomes even more relevant when using 3D models for the study and analysis of cultural heritage assets. To combine the metric accuracy and resolution of range-based scanning devices with photorealistic textures, an integrated approach between instruments of different types is adopted.

In this thesis, the established approach was to survey the geometry with SLS while also conducting a photogrammetric survey to be used—when the metric outputs were proven superior—exclusively for texturing purposes. To facilitate this, targets were placed within the scene captured both by the SLS scanners and during imaging acquisition (figure 38). This allowed for the collimation of targets in the images during processing, associating each with a set of coordinates derived from the targets in the metric model. This method not only ensures that the two models are aligned within the same reference system—discounting alignment phase errors—but also assigns metric information to the photogrammetric models.

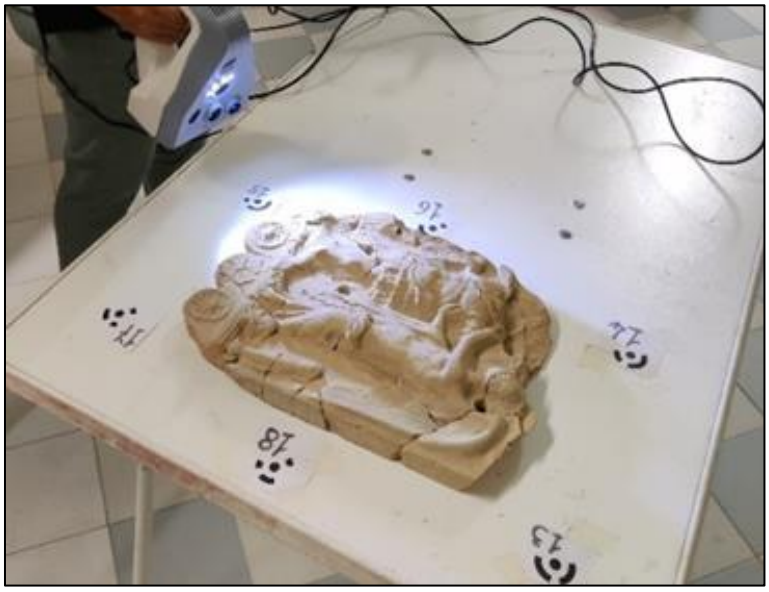

Figure 38. Scanning with SLS in Riccione Museum, capturing the coded targets for registration with DP

Beyond photo-texturing applications, this procedure was also used to compare the geometric detail between SLS and DP models. When it was not possible to create a unified reference system for the range-based and image-based surveys, the datasets acquired at different times and with various techniques were manually aligned. This process typically involves identifying common points in both datasets, which serve as constraints for the roto-translation applied to align one model to the reference model. Alignment based on homologous points is then refined using algorithms such as the previously mentioned ICP and evaluated by calculating the distance between points in the different clouds or meshes.

When combining digital data from different domains, such as 3D data with 2D data from imaging analysis and processing, the process becomes more complex. In these cases, various strategies are employed depending on the output characteristics in terms of quality and quantity, as well as the specific objectives of the survey. These issues are further complicated by the evident differences in terms of spatial resolution between imagery datasets acquired with, for instance, high-resolution cameras and low-medium-resolution imaging devices such as thermal cameras. This aspect will be discussed in the dedicated section among the experimental case studies (3.4.7).

In conclusion, this set of practices in surveying with SLS, DP, and combined techniques represents the culmination of refined methodologies for high-detail 3D surveying developed throughout the doctoral experience. This section aims to illustrate how theory—outlined in previous chapters—is intricately linked to practice, and a successful survey cannot disregard essential theoretical and methodological considerations. These processes have been optimised for high-detail surveying in the field of cultural properties investigation, enabling the successful application of dedicated geomatic techniques and procedures across a range of case studies. Some of them are described and analysed in the following section.

3.4 Applications of high-detail surveying and processing for heritage science

In this section, some case studies addressed for this PhD research will be presented in which high-detail 3D surveying has been employed for the digital documentation and study of cultural heritage. Examples will be proposed in which surveying and processing strategies were tested and evaluated, with a view to both experimenting with the technologies available for high-detail surveying and understanding the potential of the outputs in the investigation of cultural heritage. Nonetheless, it is important to note that laser triangulators, which are described as one of the methodologies for high-detail surveying, were not used in these experimentations on real case studies. The focus will, therefore, be on 3D data processing survey methodologies acquired with light projection structure scanners (described in the previous section) and with close-range digital photogrammetry.

Moreover, at the end of this section, two case studies will be presented in which the high-detail 3D surveying output was integrated with non-geomatic tools (i.e. image analysis operations and thermography imaging). These tests were carried out to investigate the potential of combined approaches to enrich the knowledge of heritage artefacts from various points of view, taking advantage of both the detailed investigation of surface 3D morphology but also of the information provided by techniques of other domains. Examples of this kind are present in the scientific literature (see section 2.2), and in the final part of this PhD research, experiments in this sense were carried out.

Nonetheless, the main focus of this section is on the methodologies involved in geomatic high-detail 3D surveying, data processing strategies and the potential of these tools in the study of heritage assets.

3.4.1 Operative issues in SLS surveying for museum assets documentation

As outlined in previous sections discussing methodologies in structured-light projection scanning, this geomatic technique offers numerous advantages in the field of heritage digitisation. In recent years, such scanners have been widely adopted across various contexts due to their rapid and efficient data acquisition, their versatility, and their capability to achieve sub-millimetre accuracies and resolutions.

However, as discussed in section 2.3.2, the numerous advantages of this technique are accompanied by a range of challenges that arise in specific, non-standard contexts. These include the digitisation of morphologically and materially complex objects and the presence of adverse environmental conditions during data acquisition, especially in terms of uneven lightning. Moreover, as explained, the projected light patterns can be incorrectly or incompletely detected in the presence of discontinuous or isolated elements in the scanned scene.

Such issues were encountered during the acquisition of certain objects exhibited in the "*Aldrovandi, l'Altro Rinascimento"* exhibition at the Palazzo Poggi collection, part of the University of Bologna's Museum System. This collection comprised hundreds of objects of various types (from manuscripts to woodcut matrices to zoological and natural specimens) used by the Bolognese naturalist (Ulisse Aldrovandi, 1522-1605, to whom the exhibition was dedicated) for the study of animals, plants, and natural phenomenon.

A national project (*"CHANGES"*[6]) in which the University of Bologna participated aimed to create a complete digital twin of this exhibition. As part of this effort, the majority of the objects in the collection were captured in 3D to create a virtual environment, thereby digitally and permanently preserving the temporary museum exhibition (Balzani et al., 2023). Within the scope of this project, the Topography and

[6] https://www.fondazionechanges.org/pnrr/

Geomatics group of DICAM was also involved and participated in the acquisition of approximately 60 artefacts.

Among these, one emblematic case was the tooth of a narwhal. This object was particularly elongated (approximately 2 metres) but very narrow (with a base diameter of max 5 cm) and presented a helical shape (figure 39). Consequently, it featured unique geometric characteristics and posed challenges for structured light scanning in two distinct ways: firstly, its vertical extension exceeded the vertical coverage of the selected SLS scanner (Artec EVA, with a field of view of approximately 536 × 371 mm at the maximum working distance), while its width was too narrow for the instrument's horizontal coverage. Additionally, the helical shape, which defined a repeated pattern, coupled with a very uniform texture devoid of distinctive visual features, proved particularly problematic.

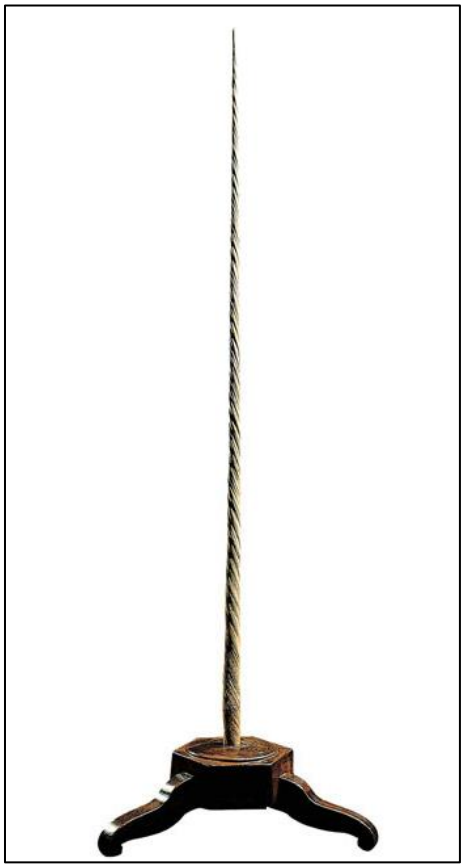

Figure 39. The narwhal tooth conserved at the Palazzo Poggi collection (image credits: https://storie.ivipro.it/db/museo-di-palazzo-poggi/)

However, given the need to digitalise a large number of objects in that context and within a limited time frame, the EVA scanner was nevertheless chosen. This scanner was deemed appropriate in terms of accuracy and 3D resolution (0.1 mm) and also allowed for rapid data acquisition. Yet, as soon as the scanning operations commenced, the aforementioned challenges became immediately apparent. Firstly, the narrow diameter of the object caused it to appear isolated from the rest of the scene, preventing real-time alignment of the acquired geometry frames because the light pattern was incorrectly detected by the cameras. Furthermore, the vertical extension of the object far exceeded the area covered by the instrument.

To address the first issue, additional elements were introduced into the scene to provide "bridge" features, which would assist the scanner in obtaining more comprehensive detection of the pattern elements. As for the second problem, it became clear from the outset that the only viable solution was to perform multiple scans, followed by aligning the various portions during post-processing. To facilitate this task, a rigid panel was placed behind the narwhal tooth, allowing the use of visual markers drawn on it as common reference points between the different scans, given that, as previously mentioned, the object's surface itself lacked distinctive features that could be used as notable points of reference.

Upon the completion of the laborious scanning phase, the data were processed using proprietary software developed by the same company that produced the scanners, namely Artec Studio Professional. This software enables the processing of raw data acquired through its devices in a proprietary format. The individual data elements, referred to as "scans," consist of a series of "frames" that already contain the three-dimensional information captured by the scanner. Initially, an attempt was made to semi-automatically align the scans corresponding to different parts of the object, using the visible elements of the panel behind the narwhal tusk as reference points (figure 40a).

However, this strategy proved ineffective, as the automatic alignment algorithms succeeded in merging the frames of the panel but failed when it came to the helical structure of the object (figure 40b). As a result, extensive manual intervention was required to align the various parts of the geometry through rotation and translation, attempting to join the different sections based on the few visible and recognisable features on the object's surface.

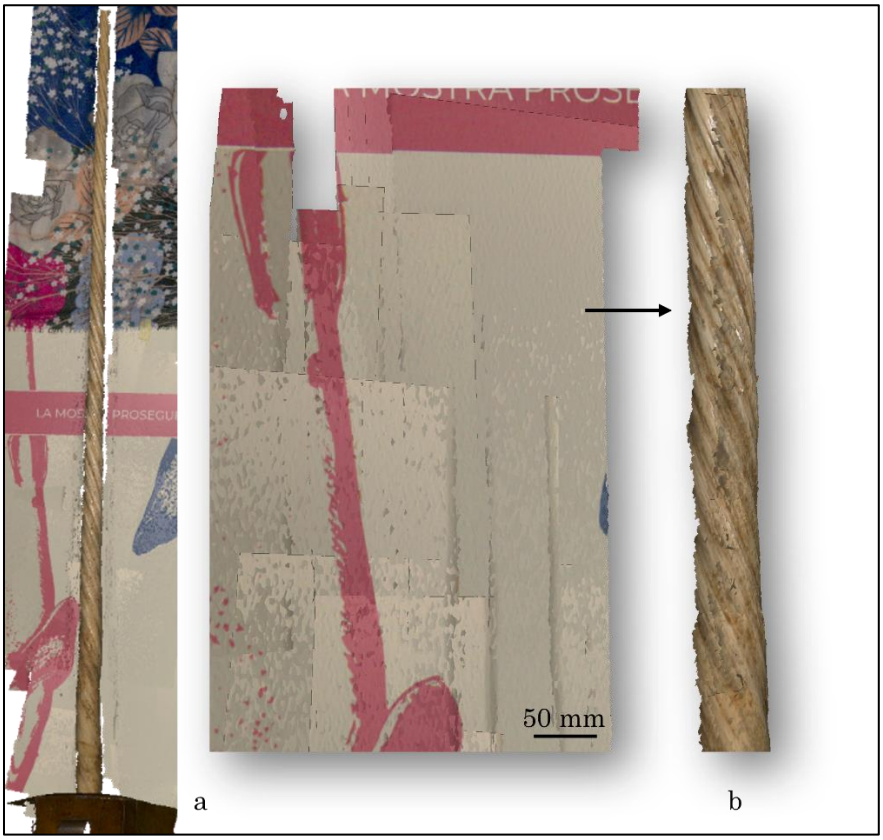

Figure 40. a) Raw scan data from SLS acquisition of the narwhal tooth and the panel behind it; b) A close-up view of one scan: the frames related to the panel are correctly aligned, while those associated with the narwhal tooth are slightly misaligned

Additionally, the introduction of additional elements to the scene, which were necessary to enable real-time data acquisition of an object isolated in space, posed further complications during post-processing. Specifically, these objects had to be removed manually from the scene, paying attention not to remove significant portions of the narwhal toot's model. This procedure significantly increased the time required for the processing.

Nonetheless, the final model was ultimately obtained by fusing all the manually aligned scans in a continuous mesh and setting a resolution of 1 mm not to introduce interpolation in the data, and a texture map was created using the texture frames acquired by the scanner (figure 41).

In conclusion, it is important to point out that this example is not directly attributable to the context of "high-detail" surveying, as the digital twin of the exhibition was created for documentation purposes rather than the investigation of individual artefacts. However, it was included for two main reasons: first, the narwhal tooth serves as an example of an extremely challenging and uncooperative object for SLS scanning. This object, as discussed, presented a range of characteristics that highlighted the limitations of this technique, necessitating a series of acquisition and processing strategies to address these issues. Furthermore, it represents a case of the operational challenges that may arise in museum contexts, highlighting context-specific issues encountered in the surveying of museum artefacts.

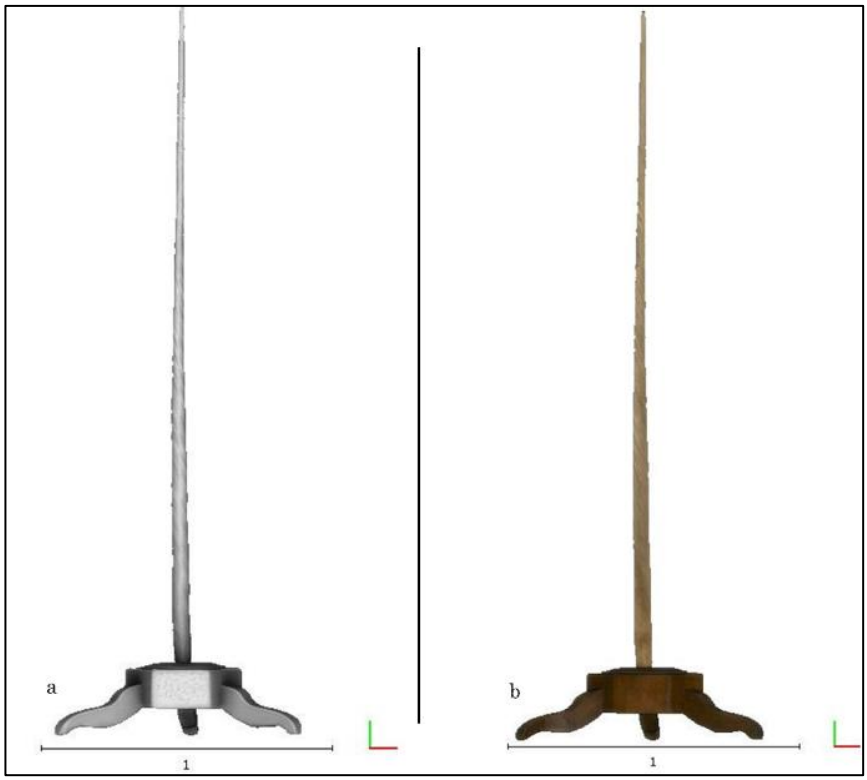

Figure 41. The narwhal tooth final 3D model visualised with a shader (a) and with the applied texture (b)

3.4.2 Surveying and processing operations to enhance museum digital data

As previously emphasised, high-detail 3D surveying can be a valuable tool for documenting, studying, and enhancing museum assets, contributing to both scholarly research and the broader appreciation of cultural heritage. In this context, a project was conducted at the "Luigi Ghirotti" Territory Museum of Riccione (Italy), which has recently implemented digital strategies to enhance visitor engagement and accessibility. As part of these efforts, a surveying campaign focused on creating tactile replicas of Roman-era fictile slabs for an Augmented Reality application for visually impaired visitors (Bitelli et al., 2025). The campaign generated a significant amount of digital data, leading to additional processing beyond the initial digitisation required by the museum to further enhance the collected information.

First, the 3D survey methodological approach relied on two primary techniques: SLS and high-resolution imaging. The range-based instruments employed included both EVA and Spider *Artec* scanners, to capture both the overall geometry and smaller features. In addition, the *Canon* EOS 6D DSLR camera was employed to capture high-resolution images for texturing purposes, since the accuracy and time-effectiveness of the SLS equipment was considered a more adequate solution for the geometry acquisition in the context of this project. The images were captured with a photogrammetric approach, as described in section 3.3, in order to cover the surface of the objects exhaustively and to ensure robustness in the texture application.

The processing of the geometry data obtained with SLS resulted in a series of 3D models with a resolution varying from 0.1 mm to 0.3 mm, according to the objects' size and complexity (figure 42). The texturing procedure (conducted to ensure a comprehensive representation of the objects, yet not necessary for the physical replicas' creation with 3D printing) was performed using an automatic photo-registration algorithm (available in the proprietary software of the scanners) that identifies common points between the 3D geometry coordinates and the pixels in the images (figure 43).

Figure 42. The final 3D models obtained for the Riccione Territorial Museum project: a), b), c) "Potnia theròn" slab fragments; d) "Winged Victories" slab; e) "Damnatio Memoriae" inscribed table; f) "Miliarium" (modified from Bitelli et al., 2025)

Figure 43. Texture 3D model of the "Winged Victories" slab (modified from Bitelli et al., 2025)

After completing the physical replicas, as anticipated, it was decided to further exploit the extensive high-resolution digital dataset of the archaeological properties to conduct additional digital operations. Some objects underwent experimental post-processing to explore further the capabilities of digital restoration and analysis in archaeology. One of them involved a marble inscribed table which had undergone a *Damnatio memoriae*, a Roman practice of erasing names from public monuments. The table's inscription, which originally included the name of Emperor Domitian, had been partially erased following his condemnation by the Senate.

This experiment aimed to recover the erased inscription by a digital approach. Using the 3D model of the table, which was scanned at a resolution of 0.1 mm, lighting models were applied – in free processing software – to emphasise the surface contours of the engraving. By focusing the light on the affected areas, it was possible to recover the original lettering and reconstruct the missing portion of the inscription (figure 44). The next step involved aligning the recovered letters with similar characters from other parts of the table's inscription, using the cleavage left by the erased letters as reference points. The final output was a new 3D model in which the erased inscription had been digitally restored, revealing the name *"Domitianus Aug. Germanicus".*

Another experiment involved the milestone (*"Miliarium",* figure 42f), which bore several inscriptions. Due to the state of preservation of the stone, some of them were difficult to read, particularly because of the cylindrical shape of the object. To address this, a geometric projection technique was applied, which involved unrolling the milestone's surface onto a flat plane. First, a cylindrical primitive was fitted to the 3D model of the milestone to obtain precise measurements of its radius. Using this data, the lateral surface of the cylinder was geometrically projected to create a flat, unrolled version of the milestone, using the free software CloudCompare. This procedure allowed to view all the inscriptions at once, improving their legibility. The projected model was then further enhanced with digital lighting to highlight the engraved text (figure 45).

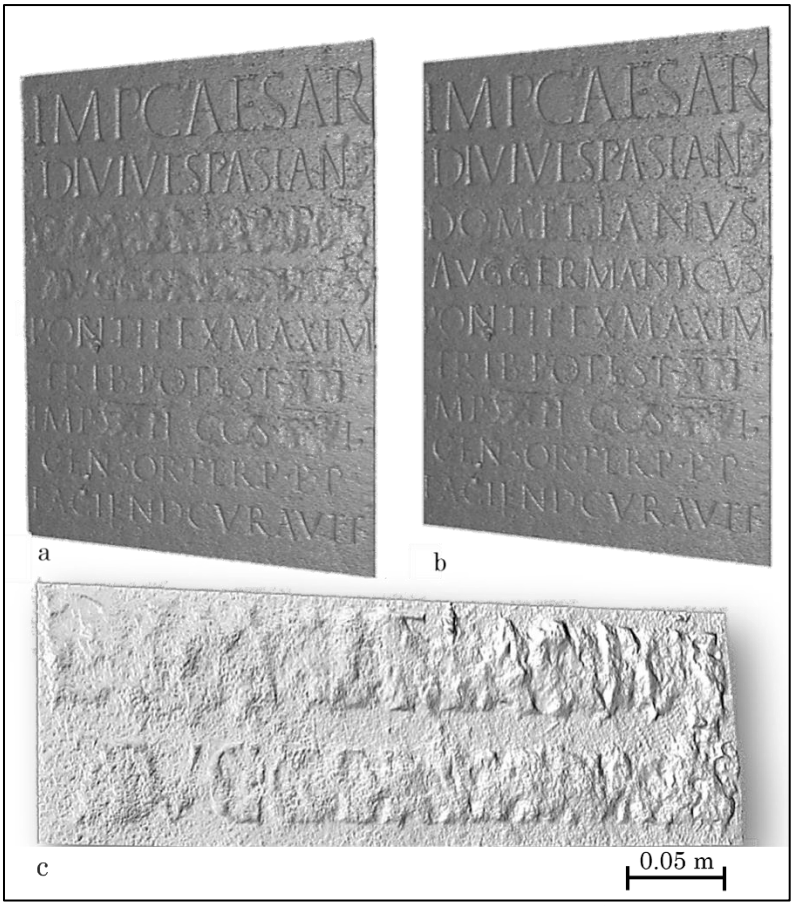

Figure 44. a) 3D model of the table before reconstruction; b) Proposal of reconstruction of the missing inscriptions; c) A detail of the erased inscription, visualised with a shader

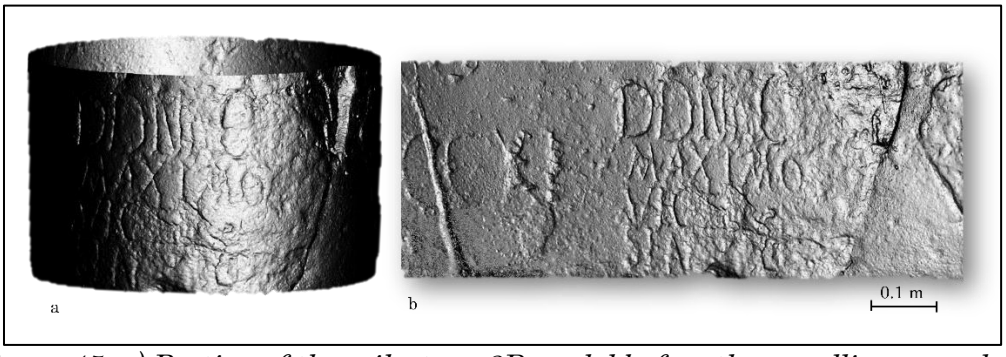

Figure 45. a) Portion of the milestone 3D model before the unrolling procedure; b) The same portion after unrolling, visualised with a shader (Bitelli et al., 2025)

In conclusion, this work demonstrated the potential of digital post-processing techniques for archaeological analysis. The combination of different high-detail 3D surveying techniques allowed to reconstruct, interpret, and enhance the archaeological artefacts with detail and accuracy, providing digital support for scholarly research and for museum assets valorisation.

3.4.4 Evaluating and comparing SLS and DP for virtual restoration purposes

As discussed in the literature review section, 3D surveying enables a range of valuable operations for the virtual restoration of damaged, fragile, or fragmented cultural objects. The example presented here falls within this context, though it has its own distinctive characteristics. Firstly, the object in question was not technically damaged; rather, it was in a state of altered preservation due to the passage of time and non-ideal conservation conditions.

The tested methodology of virtual restoration was applied to a pearwood xylographic matrix (~20 x 15 cm), created by Ulisse Aldrovandi (a Bolognese naturalist who lived between the 16t^{h} and 17th centuries), which was historically used to imprint illustrations of the species described in his botanical and zoological works (figure 46). The Aldrovandian matrices, preserved at the Palazzo Poggi collection of the University of Bologna, have, as anticipated, undergone a process of deterioration over the centuries, leading to alterations in their geometry.

Figure 46. The Aldrovandi xylographic stamp considered for the experiment

The objective of this experiment, carried out in collaboration with SMA (*Sistema Museale di Ateneo*) of Bologna University, was then to generate a highly accurate digital model of the original object, virtually correct the deformation by restoring the flatness of the engraved surface, and then produce a "non-deformed" copy through 3D printing, which could be used as a matrix for printing onto paper. Nonetheless, in the context of this thesis, the virtual restoration procedure will be just briefly described, while the focus will be on subsequent operations of surveying techniques comparison.

First, to achieve a high-quality 3D model, SLS was initially employed using the Artec Spider scanner. Upon completing the delicate processing phase, a triangular mesh consisting of approximately 31 million polygons with a 3D resolution of 0.1 mm was produced. The model highlighted the slight deformation of the stamp, which – when compared to a best-fitting tangent plane – resulted in being non-planar (figure 47a).

Then, in order to proceed with the digital restoration of the object planarity, a set of points (~ 7000) corresponding to the peaks of the engravings were manually extracted from this mesh, and a curvature surface was then created and interpolated to describe the geometry of the uppermost section, using a terrain analysis software. Subsequently, the height difference between this surface and a horizontal plane positioned above the model was calculated. This Δz value was then applied to the vertices of the mesh, directly modifying the .Obj file to preserve the original topology.

As illustrated in figure 47, it was evident that, prior to the virtual restoration, the upper surface of the matrix (where the illustrations are engraved) was not flat (figure 47c) and, as a result, not all the peaks were at the same height, preventing a complete imprint of the engraving. After the tested procedure, instead, all the peaks were aligned on the same plane, allowing the design to "emerge" in its entirety (figure 47c). Finally, the digitally corrected model of the stamp was 3D printed using resin technology, in order to preserve the geometric resolution obtained through the scan.[7]

[7] A more detailed description of this work will be published in an article in course of realisation

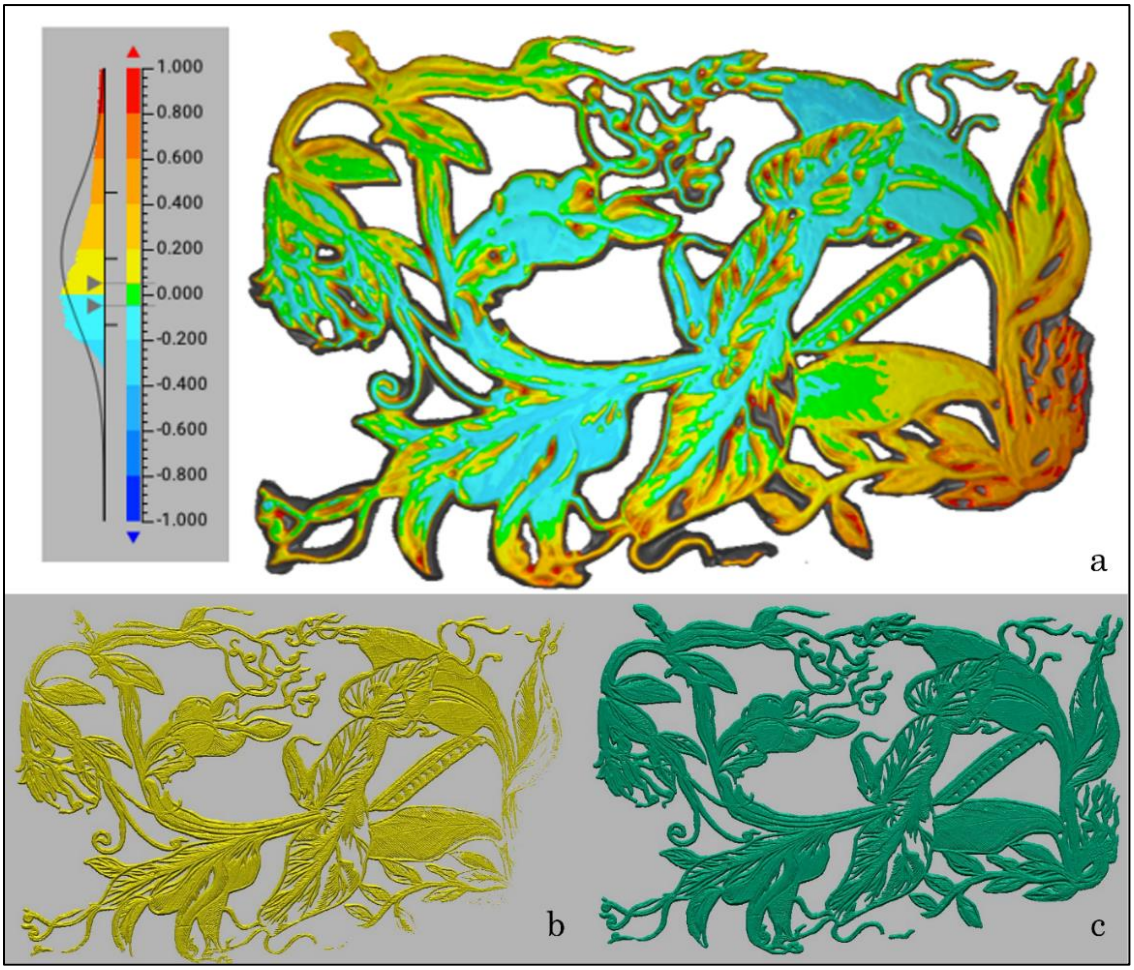

Figure 47. (a): Colour gradient and bar showing the distance values (between -1 and 1 mm) of the stamp mesh with respect to a best-fit tangent plane; (b): a longitudinal section of the upper surface showing its non-planarity; (c): the same section of the upper surface realised after the digital restoration

Additionally, a macro-photogrammetry strategy was chosen for the Aldrovandi matrix to explore the feasibility of applying image-based techniques to such a complex object. For this purpose, a Canon EOS 5D camera paired with a 100 mm macro lens was used. Approximately 150 images – then selected and reduced – were captured from nadiral and oblique perspectives (figure 48). However, for the oblique images, the limited depth of field—despite the aperture set at f/22—posed a challenge on an object of considerable dimensions (around 20 cm in width and 15 cm in height), resulting in out of focus areas, subsequently masked in pre-processing. The nadir images, taken from a distance of about 15 cm from the object and presenting a GSD of around 10 microns, captured impressive details, barely visible to the naked eye (figure 49).

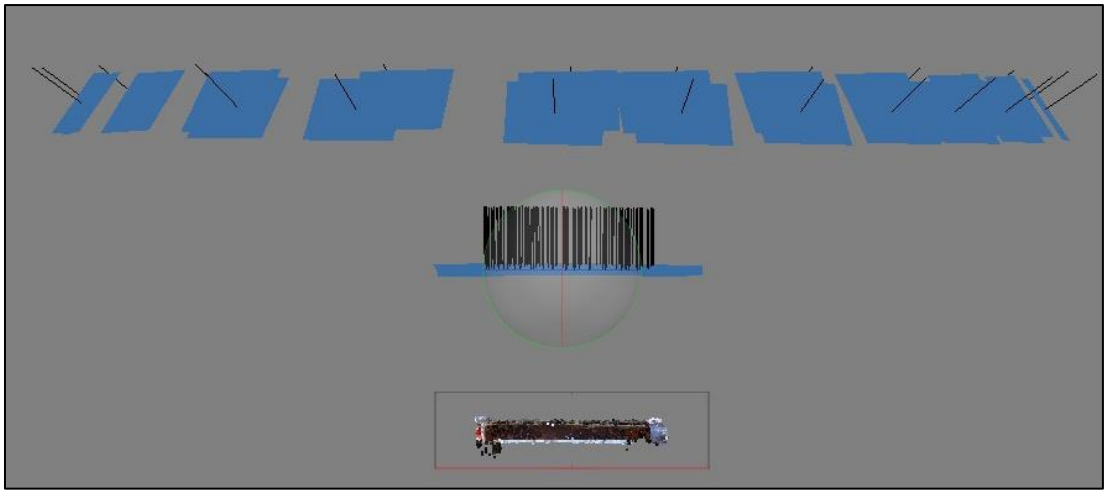

Figure 48. Camera poses as estimated by the SfM software, showing both oblique and nadiral images

Figure 49. One of the macro-images acquired for the photogrammetric reconstruction of Aldrovandian stamps (the original image resolution was resampled)

This level of detail allowed the software to extract an exceptionally high number of keypoints and subsequently tie points (~1.2 millions) in the sparse geometry reconstruction. In addition, to scale the model and orient it in the same reference system of the mesh obtained with SLS, a set of 3D coordinates were extracted from the metrical dataset and assigned to five points in the images (figure 50).

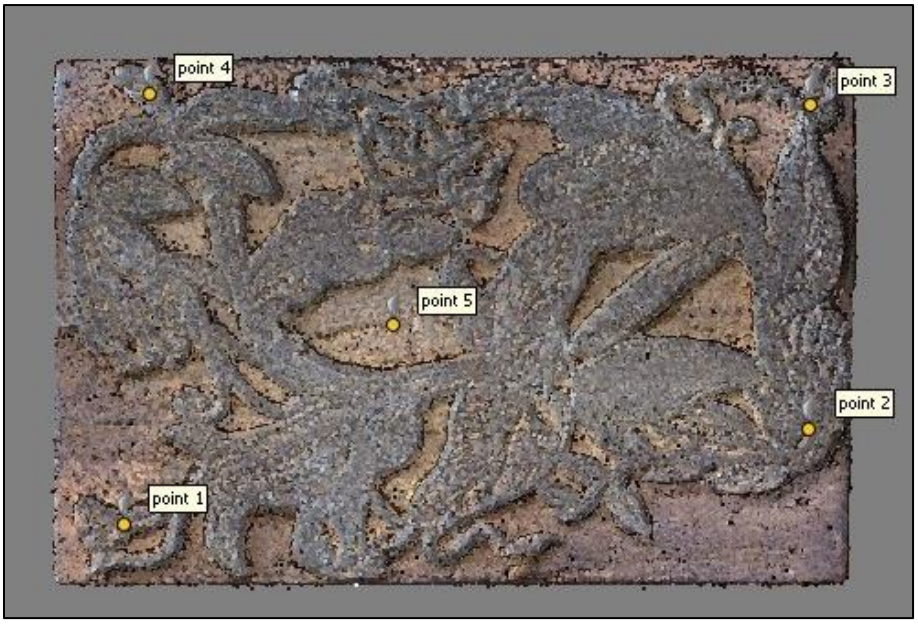

Figure 50. Tie points used to orient the images in the SfM software (or the "sparse" cloud), and the control points from the SLS coordinates used to orient and scale the model

The accuracy in the image orientation and geometry reconstruction was evaluated by considering both the reprojections errors in the collimation of the control points in the images and the RMSE associated with their metrical residuals. As seen in table 2, the average metrical error of the points is 0.081 mm, in accordance with the accuracy of the metrical dataset used to align and scale the model (the Artec Spider, as said, presents an accuracy of 0.05 mm and a resolution of 0.1 mm). This result is particularly notable, as it demonstrates that the data obtained from macro-photogrammetry is highly comparable to that from SLS,

Points (5)	**X error (mm)**	**Y error (mm)**	**Z error (mm)**	**Total (mm)**	**Reprojection errors (pix)**
Point 1	-0.0201968	0.0507926	-0.00548377	0.0549352	0.727
Point 2	0.0546076	0.0145398	0.0296497	0.0638161	0.743
Point 3	0.0344176	-0.000309027	-0.0162967	0.0380829	0.657
Point 4	0.0393909	-0.0939771	0.0217711	0.104198	0.558
Point 5	-0.108219	0.0290348	-0.0296403	0.115901	0.832
Total	0.0597286	0.0499323	0.0224824	*0.0810321*	0.704

Table 2. RMSE of the residuals associated with the control points (in mm) and reprojection errors for each of them (in pixel)

Subsequent to tie points extraction and filtering according to their associated errors, a dense points cloud was obtained, constating in ~100 mln points. This was further optimised by eliminating the points with low confidence values (as explained in section 2.5.1, this is a metric of reliability computed by the SfM software for tie points estimation, reflecting primarily the number of matching images, figure 51). In addition, a DEM was generated by the SfM software that highlights how this reconstruction was able to represent the deformation in the object shape, observed also in the SLS-derived model (figure 52).

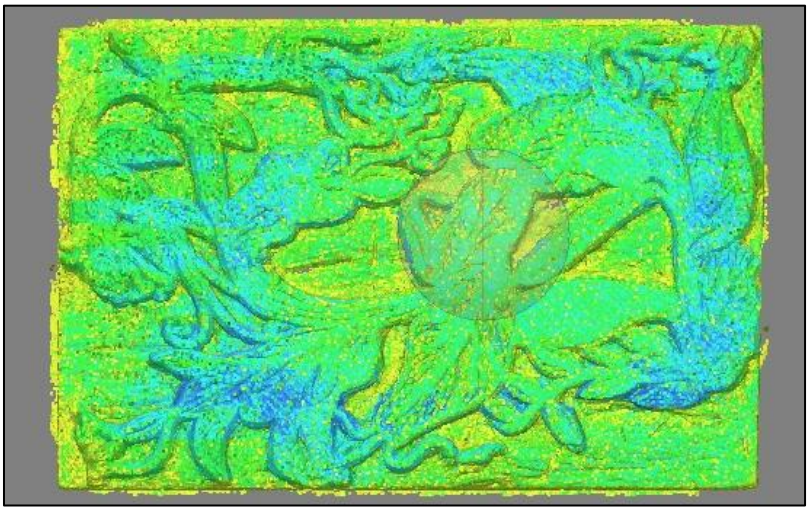

Figure 51. Dense 3D point cloud visualised with the "confidence" values colour gradient

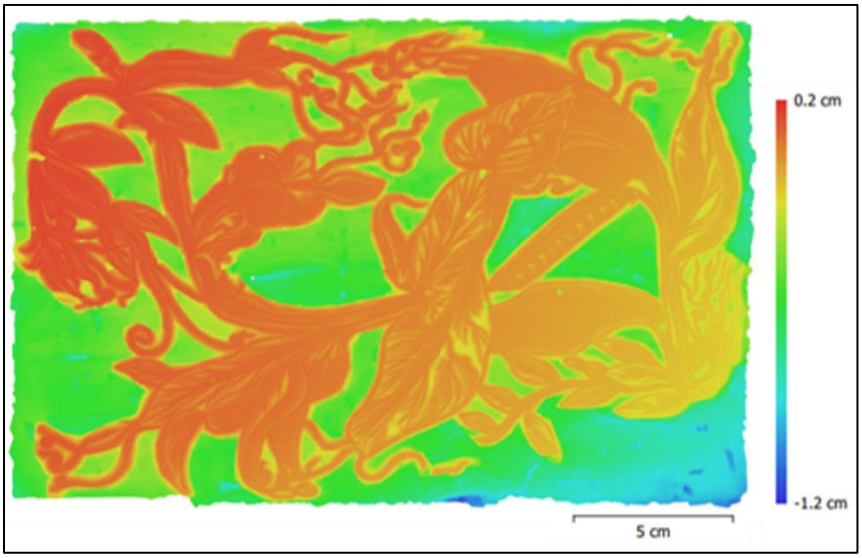

Figure 52. A DEM of the stamp obtained by photogrammetry visualised with a height ramp colour gradient: this visualisation highlights the same surface deformation seen from the SLS model

Ultimately, a 3D mesh was extracted from the dense point cloud (figure 53a). This final outcome was evaluated from different perspectives and compared to the SLS-obtained dataset (figure 53b). First, the mean value of the triangles' side length was estimated, resulting in being 0.035 mm; hence, the mesh obtained with DP presented a higher 3D resolution compared to that obtained from SLS (0.1 mm).

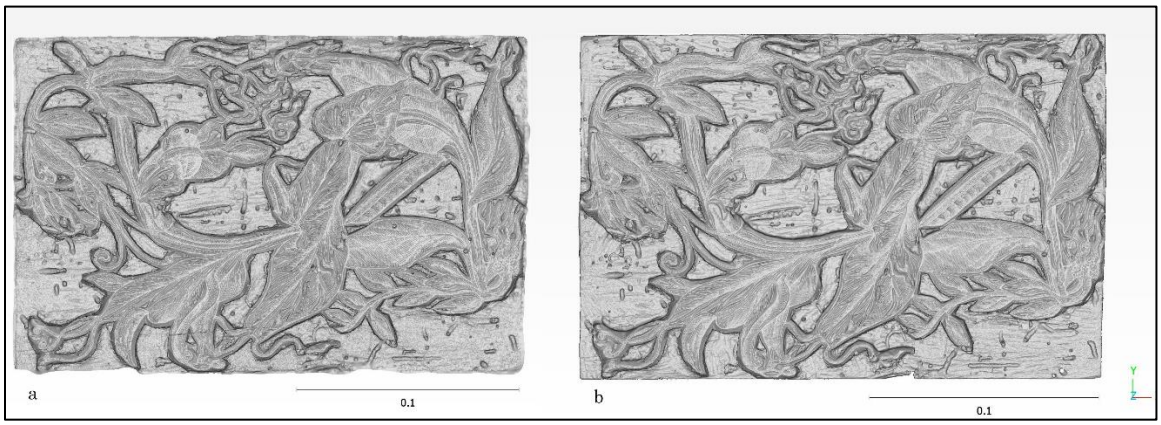

Figure 53. a) Final 3D mesh obtained with DP; b) Final 3D mesh obtained with SLS

Subsequently, some considerations were made in terms of surface reconstruction quality. First, the roughness estimation was conducted in CloudCompare, which measures local variations in surface geometry relative to an ideal smooth reference. (figure 54). From this calculation, the SLS mesh exhibits lower roughness values (0.00058 versus 0.00078 as maximum values) with respect to DP mesh, suggesting lower irregularity in the reconstructed surface with the range-based technique.

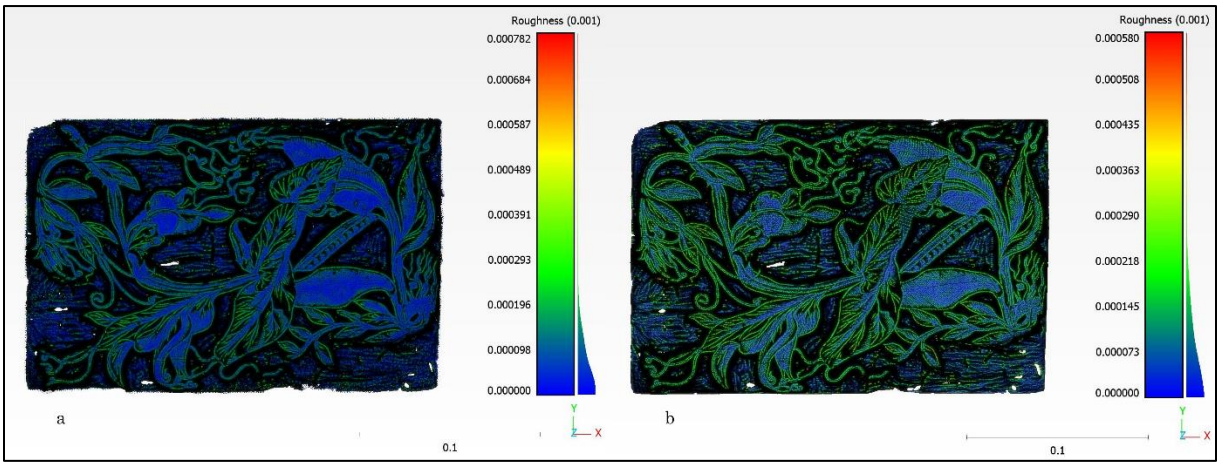

Figure 54. The two meshes visualised with the colour gradient of the estimated roughness. The values associated with DP (a) are slightly higher compared to SLS (b)

At a closer look of the mesh details, however, the DP mesh appears slightly smoother, while the SLS mesh looks more irregular, despite the latter having lower roughness values. This discrepancy likely arises due to differences in resolution and reconstruction processes. The higher roughness values in DP may be influenced by its finer resolution (35 microns vs. 100 microns in SLS), as a denser mesh can capture more local surface variations, increasing roughness measurements. Additionally, photogrammetric processing often introduces depth estimation noise, contributing to greater numerical roughness, even if the final mesh appears smoother due to inherent smoothing effects. Conversely, the lower resolution of the SLS mesh may filter out some of these micro-variations, resulting in lower roughness values while still appearing more irregular upon close inspection.

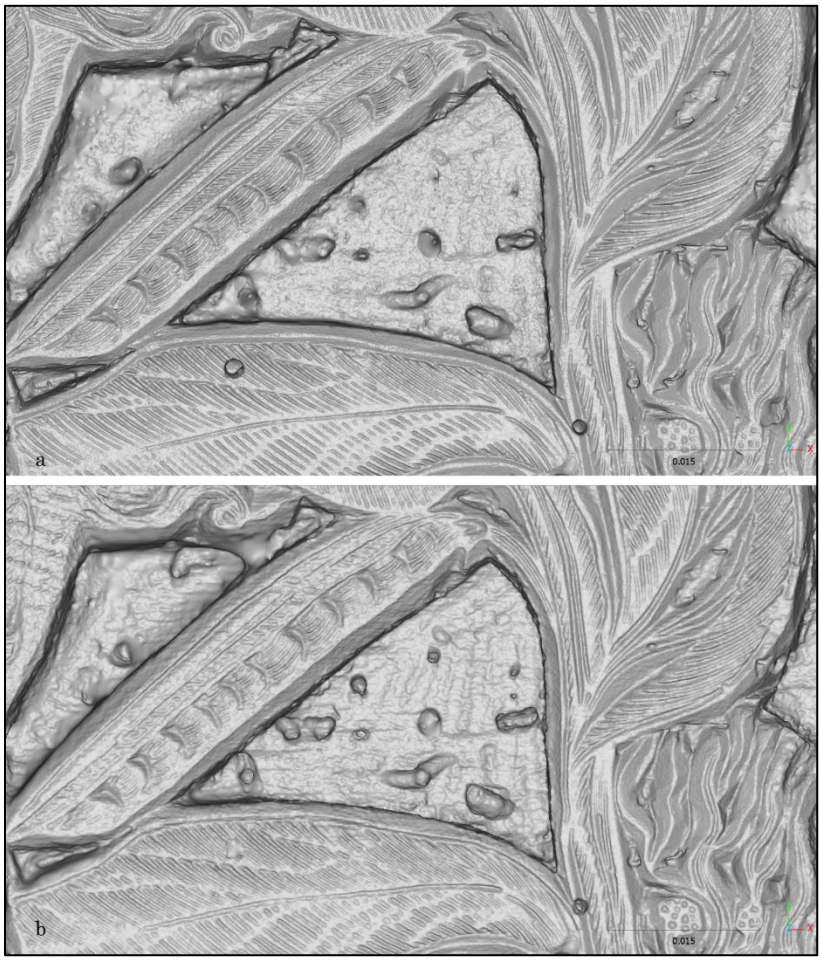

Figure 55. A close-up detail of the two meshes obtained with DP (a) and SLS (b). The view highlight the high level of detail obtained in both, but a slightly smoother appearance in DP-derived mesh

Nonetheless, it is important to point out that this kind of mesh topology evaluation must be correlated to the strategy adopted by the software in the surface reconstruction process. As seen previously, there are different algorithms that aim at constructing solid surfaces from 3D point clouds. In both case of the SfM and SLS software used, it is not clearly specified which strategy is adopted for this task. This compromises the completeness and correctness of this comparison and leaves room for empirical evaluations.

In addition, the meshes obtained with the two techniques were also compared relatively. This was achieved by conducting Cloud-to-cloud distance comparisons between the vertexes of the two meshes (figure 56). The results were then evaluated for the global C2C distance values, those along the XY plane, and those concerning the Z variations, and Gaussian-fitted histograms were produced (figure 57).

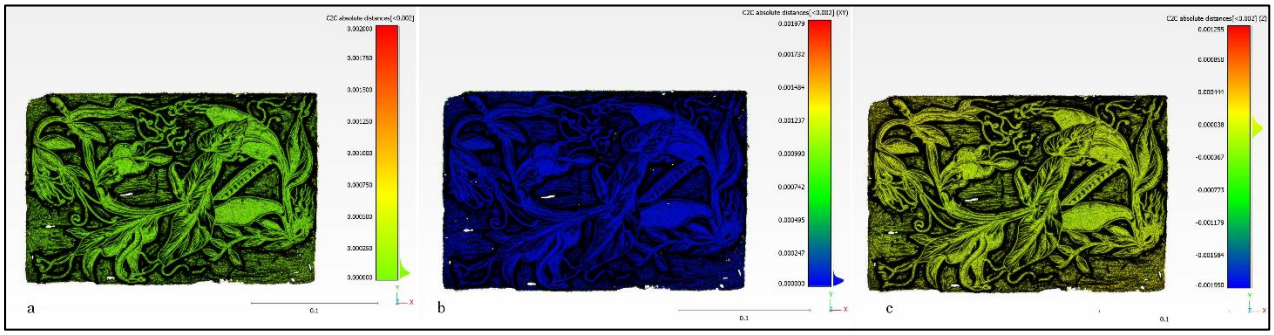

Figure 56. C2C results: a) global variation; b) Variation on the XY plane; c) variation along the Z axis

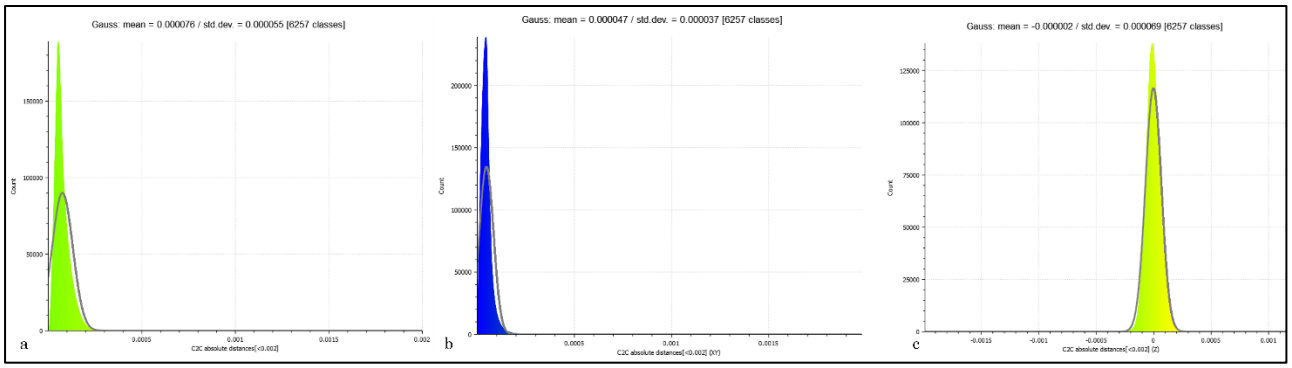

Figure 57. C2C results - Gauss-fitted histograms of the values for the global (a), XY plane (b) and Z (c) comparisons

The C2C analysis reveals that the two point clouds are generally well-aligned, with minor variations. The global mean absolute deviation is 0.000076 m, with a standard deviation of 0.000055, indicating that most points are closely matched. In the XY plane, the alignment is particularly stable, with a lower mean deviation (0.000047 m) and standard deviation (0.000037), as confirmed by the colour gradient map, which shows minimal variation. Conversely, in the Z axis, the deviations are more pronounced, with a higher standard deviation (0.000069), though the mean remains close to zero (-0.000002 m), suggesting that the variations are evenly distributed rather than systematically biased. The colour gradient map reflects this greater variation, particularly in certain regions, yet the symmetrical histogram indicates that these differences balance out. While the XY alignment is more consistent, the Z variations highlight local topographical differences, which are captured differently by the two methods but remain within an acceptable range.

The results concerning the global C2C distance estimation were also reported synthetically in table 3, explaining more clearly the significance of each value. The table summarising arithmetic mean values, standard deviation, and RMS (Root Mean Square) distance provides a complementary statistical perspective. Unlike the histograms, which represent data through Gaussian fitting, the table reports purely numerical values, confirming that the average global deviation is 75.8 μm, with a standard deviation of 55.4 μm, and an RMS error of 93.9 μm. These values reinforce the previous considerations, indicating that most point deviations are small but with occasional larger discrepancies affecting the overall RMS value.

Metric	Description	Value (m)	Value (μm)
Mean	Arithmetic mean of all point-to-point distances, indicating the average separation between corresponding points.	7.57665e-05 m (0.0000758 m)	75.8 μm
Standard deviation (σ)	Indicates how tightly the distances cluster around the mean	5.53951e-05 m (0.0000554 m)	55.4 μm
RMS	Emphasises larger deviations by taking the square root of the mean of squared distances; a common measure of overall "error."	9.38572e-05 m (0.0000939 m)	93.9 μm

Table 3. Global C2C distance estimation metrics, presenting arithmetic mean, standard deviation, and RMS values to quantify point cloud alignment without Gaussian fitting

These results highlight the importance of considering both statistical analysis and visual inspection when evaluating point cloud comparisons. While histograms provide an objective numerical assessment of accuracy, false-colour visualisations help pinpoint the spatial distribution of deviations, offering a clearer understanding of where errors are most significant. The combination of both methods is crucial for assessing the accuracy and reliability of different 3D acquisition techniques, ensuring a comprehensive evaluation of their performance.

This analysis led to another important observation: while SLS proved highly effective in capturing an accurate and detailed model, it encountered difficulties in certain areas, particularly on the shinier, more reflective surfaces. Consistent with known material-induced limitations in SLS, this phenomenon resulted in increased surface noise, which required meticulous cleaning to avoid data loss (figure 58). In contrast, photogrammetry was less affected by this phenomenon, yielding a more homogeneous and continuous reconstruction with less noise.

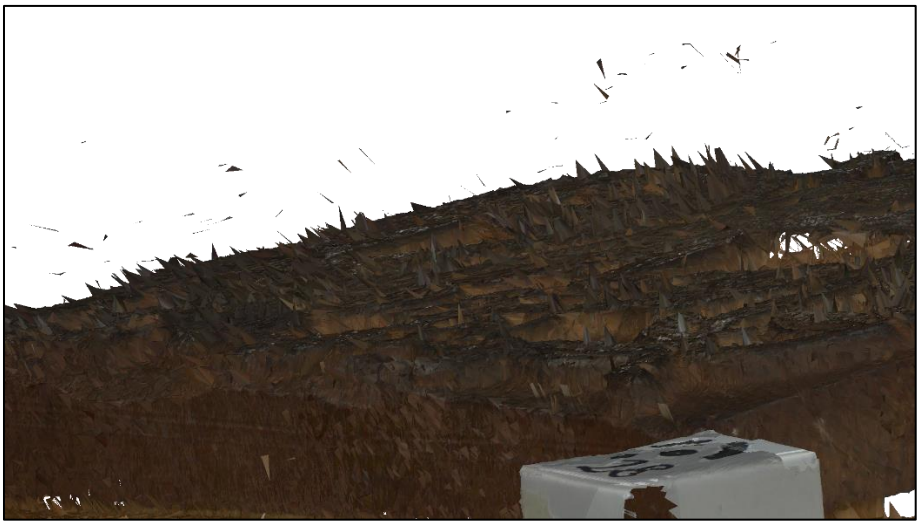

Figure 58. Outliers and noise in the SLS raw scan data

This finding raises an additional consideration for 3D modelling, particularly for physical replica printing: the potential of macro-photogrammetry as an alternative to more expensive methods like SLS. However, operational aspects are also noteworthy; while photogrammetry in this case demonstrated considerable advantages, the range-based technique proved significantly faster in data acquisition.

The time required for data collection differs vastly between the two methods: approximately one hour for range-based scanning compared to several days for image acquisition and processing in the image-based approach. This limitation becomes especially apparent in non-research contexts, where extended hours for photogrammetric setup under optimal conditions may not be feasible. Furthermore, SLS was found to be considerably more "pragmatic" compared to photogrammetry, which required tripods, turntables, and portable LED lights to illuminate the scene. Such logistical aspects are essential considerations in this comparison.

Nonetheless, this work demonstrates, consistent with other cases in the literature (see section 2.4), that photogrammetry—particularly in its macro configuration—is an exceptionally powerful 3D reconstruction technique. Following a meticulous survey design phase and presuming a robust theoretical and practical knowledge, photogrammetry can deliver remarkable results, comparable to, and in some respects superior to, range-based techniques.

3.4.5 Experiments in micro-photogrammetry with a low-cost equipment

An additional experiment in detailed photogrammetry, specifically micro-photogrammetry, was conducted on archaeological gemstones preserved at the Archaeological Museum of Bologna. These gemstones are of extremely small dimensions (less than two centimetres in width and height) and feature very fine surface engravings. In this section, one of the tested cases is presented: an Egyptian gemstone shaped like a scarabaeus, measuring approximately 2.3 x 1.8 cm (figure 59). The objective of this survey was not a detailed morphological investigation but, similar to the narwhal tooth case described earlier, focused on digital documentation for the creation of a digital twin for a temporary museum exhibition. Nevertheless, this experiment is here reported to highlight the potential and limitations of the micro-photogrammetry methodology used.

The survey was conducted using a low-cost portable digital microscope (described in the instrument section). The gemstone was positioned approximately 5 cm from the

microscope lens and was rotated and translated while the image-capturing device remained stationary (figure 60). Additionally, angled images were captured by slightly tilting the microscope and rotating the gemstone 360°. As discussed in the theoretical section on photogrammetry, angled images help strengthen the geometric framework of the survey and gather more information about occluded parts, especially in the concavities of the engravings. Throughout both the orthogonal and angled image captures, the object was rotated and translated ensuring an image overlap of approximately 70%.

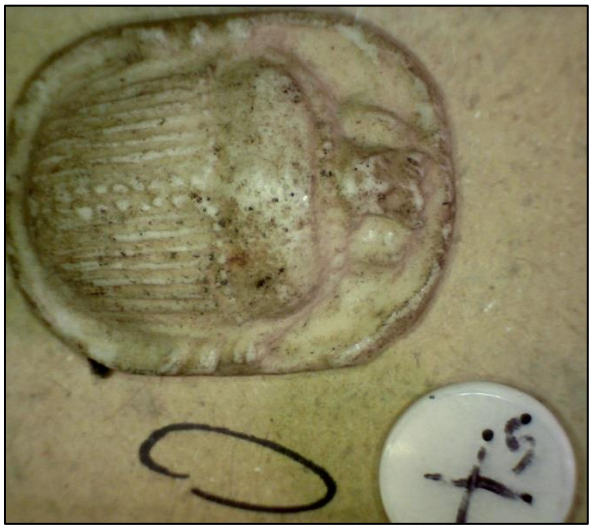

Figure 59. The scarabeus gem conserved at Bologna Archaeological Museum

Figure 60. The portable digital microscope acquiring images of the gem

The microscope's field of view on the object was limited, but sufficient to capture the entire gemstone in a single frame. The GSD of the images, as calculated using the formula presented in section 2.1.1, was approximately 0.025 mm, which was adequate for the purposes of this survey. A total of 60 images were captured (later reduced after selecting the best quality ones) at a resolution of 1024 x 1024 pixels, the maximum obtainable with this low-cost digital microscope.

The data was processed using the multi-view SfM software Agisoft Metashape. To scale the object, four adjustable-height targets were placed around it, consisting of pins with a cross and a number drawn on them (one of them is visible in figure 59). These targets were necessary to maintain a reference height parallel to the surface of the gemstone, as the depth of field in microphotography is very shallow and can cause focusing problems when objects are at different distances on the plane by only a few millimetres. The "pin" targets were manually aligned within the SfM software, and the distances between their centres were measured with a calibrated ruler to scale the 3D model of the gemstone using scale-bars.

The image alignment procedure was then performed, ensuring that there was no limit on the extraction of tie points from the images (which were analysed by the software without any subsampling). This approach was taken because the starting resolution of the images was low, as previously mentioned (1024 pixels), so a sparse point cloud was generated containing all possible extractable information from the images.

After the external orientation of the images, a sparse point cloud of approximately 70,000 points was produced, with a density (average distance between points) of about 0.3 mm. This value is consistent with the starting GSD of the acquired images. The reprojection error on the manually aligned targets was about 0.8 pixels, while the average metric error on the targets was 0.2 mm. The resulting point cloud, after its filtering and cleaning, was then used to create a continuous polygonal surface, with a density (average triangle size) of approximately 0.35 mm, consistent with the average point-to-point distance (figure 61).

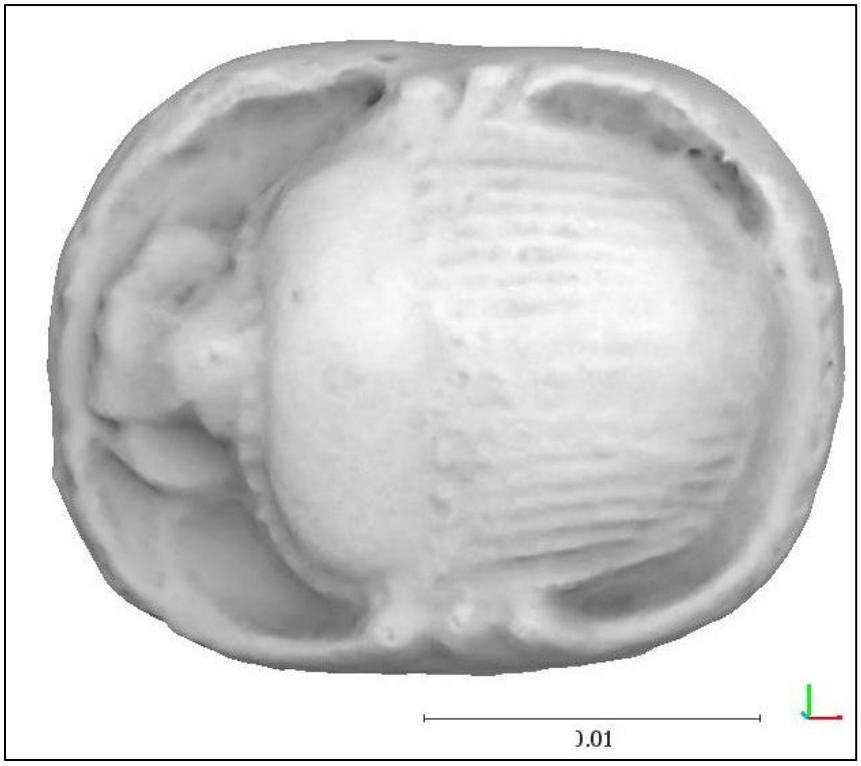

Figure 61. Final mesh of the scarabaeus gem, visualised with a shader

Furthermore, to gain insight into the geometrical correctness of the reconstruction with micro-photogrammetry, a comparison was made aligning the obtained model to a mesh of the object obtained with SLS. The results of the Cloud-to-cloud comparison on the meshes vertex is shown in figure 62, as well as the histogram of the gaussian distribution of the values, reporting a mean deviation of 95 microns. This is in line with the accuracy of the scanner to which the photogrammetric model was aligned, and highlight a very good results in terms of comparability of the two techniques.

In conclusion, this micro-photogrammetry experiment was successful in meeting the survey's goals from both a metrical and detail perspective. The obtained 3D resolution was sufficient to make the small discontinuities on the object's surface visible in the final mesh. In addition, the comparison with a range-based derived model highlighted a promising result in terms of reconstruction robustness and level of detail.

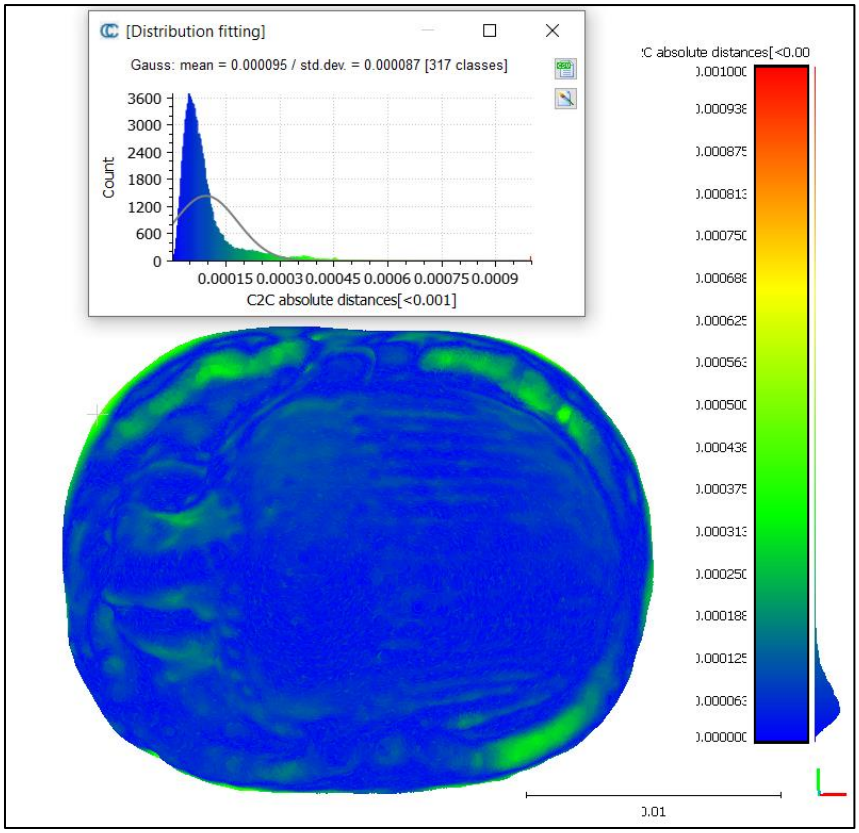

Figure 62. Cloud-to-Cloud comparison between the SLS mesh and the micro-photogrammetry-derived model of the scarabeus gem

However, this experiment also revealed certain technical challenges: firstly, using a microscope results in a very shallow depth of field. This becomes problematic when objects have a geometry that does not allow all (or nearly all) of their portions to be in focus simultaneously. This issue can be mitigated by applying masks to the out-of-focus parts of the images to prevent the extraction of incorrect features and tie points in the point cloud, but this would significantly increase processing time. In this case, masking was unnecessary because the object had a height of about 5 mm, which fell within the microscope's depth of field.

Moreover, the shallow focus depth proved particularly problematic for angled images, where the nearest portions of the object were in focus while the more distant parts were not. This issue is significant in photogrammetry, as a robust capture geometry requires angled photos, and it is not always possible to work with such shallow depths of field. Additionally, the microscope used was a low-cost model, which introduces

several limitations: many optical parameters, such as aperture and exposure time, cannot be adjusted. This becomes an obstacle when ambient lighting conditions produce unwanted optical effects on reflective or overly homogeneous materials. In this case, these issues did not significantly affect the survey, and the results were still successful for the aims of the project. However, in more complex objects or acquisition conditions, the methodology used may require adjustments or may not work at all.

Despite these challenges, the experiment demonstrated the potential of the method: although the resolution of the acquired images was not optimal, the density of the point cloud and the resulting model was still very satisfactory, achieving a 3D resolution of 0.35 mm. This result is significant because it suggests that micro-photogrammetry with a low-cost device could be a viable alternative, at least for very small objects like this one, to more expensive systems such as macro-photogrammetry or structured light projection scanning.

3.4.6 Combining SLS and Image Processing for philological analysis

The section presents a detailed application of high-precision 3D surveying and post-processing techniques on an ancient Egyptian engraved wooden tablet, part of the University Library of Bologna ("BUB") collection. The tablet, measuring 3.6 x 12.8 cm, bears Greek inscriptions on both sides, which have been difficult to interpret due to the wear and damage over time (figure 63). The wax surface on which the text was engraved has been remarkably preserved, though fractures and incomplete inscriptions have complicated efforts to decipher the text. The tablet, paleographically dated to the 2nd century CE, records monetary payments and dates, though its full context remains unclear.

The 3D survey employed Artec Spider structured-light projection scanner. Multiple scans were taken from different angles to ensure full coverage, including both the "A" and "B" sides, as well as the thin edges. A bridging scan was also performed to capture parts of both sides in a single frame, ensuring that the data sets from each side could be merged by aligning homologous points.

Figure 63. The engraved Egyptian tablet from Bologna University Library, both sides (Credits: BUB staff)

The acquired data were processed using the scanner's proprietary software. Automatic noise removal algorithms were applied to refine the surface, followed by a meshing procedure that generated a detailed 3D polygonal model. The final 3D model consisted of 3.2 million triangles and achieved a resolution of 0.1 mm (figure 64). For texturing, two approaches were tested. First, the scanner's internal colour data were used. Then, a higher-quality texture was created from a series of high-resolution images taken by the library's technical staff. These images were converted to grayscale and enhanced through contrast adjustment and histogram stretching to improve visibility of the fine details. The enhanced images were applied to the 3D model, combining the detailed geometry with high texture resolution (figure 65).

As part of the methodology, an additional texturing procedure was tested using image-analysis techniques. Specifically, Principal Component Analysis (PCA) was applied to the high-resolution RGB images of the tablet. PCA, a statistical method

often used in image processing, works by transforming correlated variables (in this case, the three RGB bands) into a set of uncorrelated components known as principal components. This process helps to highlight subtle differences in the data by emphasising variations that may not be immediately visible across the individual RGB bands.

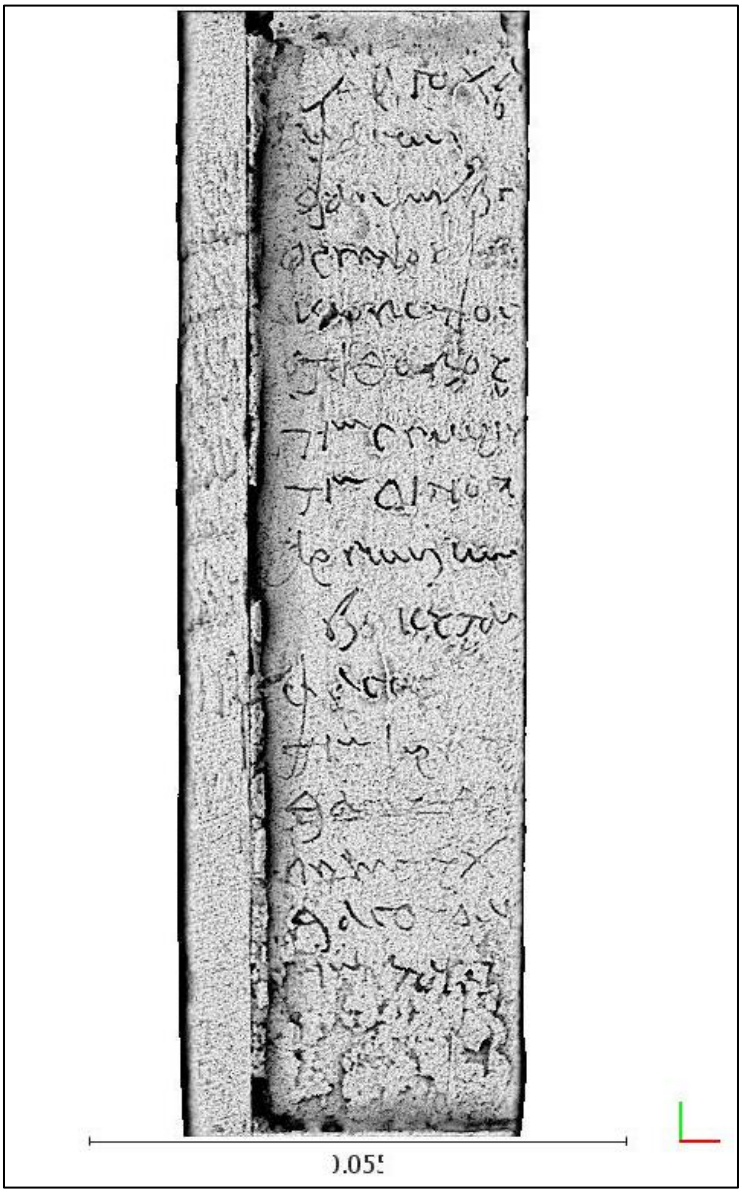

Figure 64. The final 3D mesh of the tablet for side A, visualised with a shader

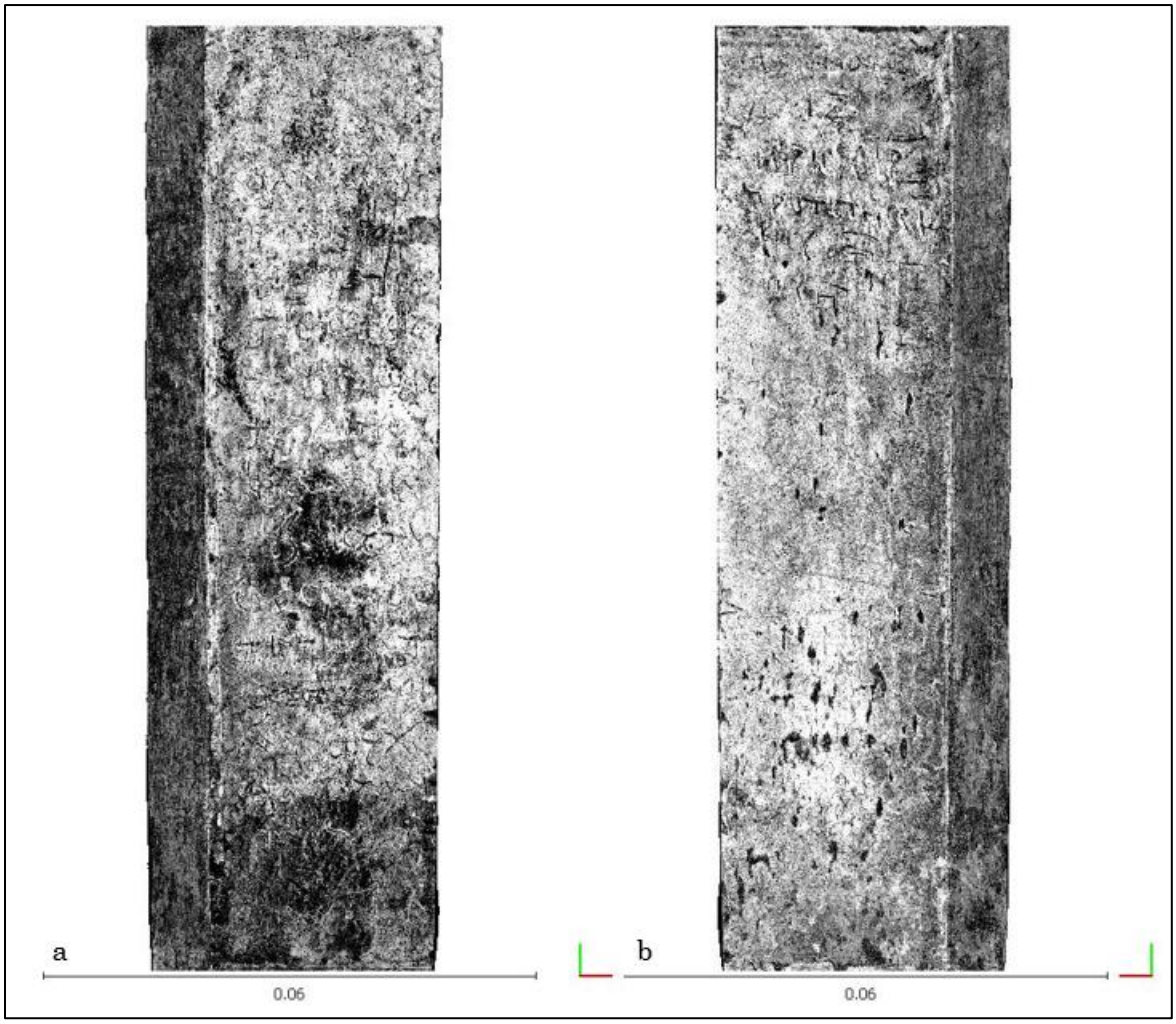

Figure 65. The tablet 3D model of both side A (a) and side B (b), textured with high-resolution enhanced images

Although PCA is typically applied to multispectral images, in this case, it was used on the standard three-band RGB visible spectrum images. Despite this, the strategy proved beneficial for the investigation. By applying PCA, three principal components were extracted from the original RGB bands, revealing additional fine details that were not as apparent in the raw colour data. From these components, false-colour (FC) images were created by combining the principal components in different ways, generating new RGB visualisations that enhanced the surface characteristics of the tablet (figure 66). These false-colour images were particularly useful for further inspecting the engraved surface, revealing subtle variations in texture and depth.

Additionally, the false-colour images were applied as textures to the high-detail 3D model of the tablet using the photo-registration procedure in MeshLab. This process combined the benefits of high-detail surface inspection with the analytical insights derived from the image-analysis approach. By using both the detailed 3D geometry and the enhanced image data, the methodology maximised the information contained in the high-resolution image set provided by the museum, allowing for a more thorough investigation of the tablet's surface.

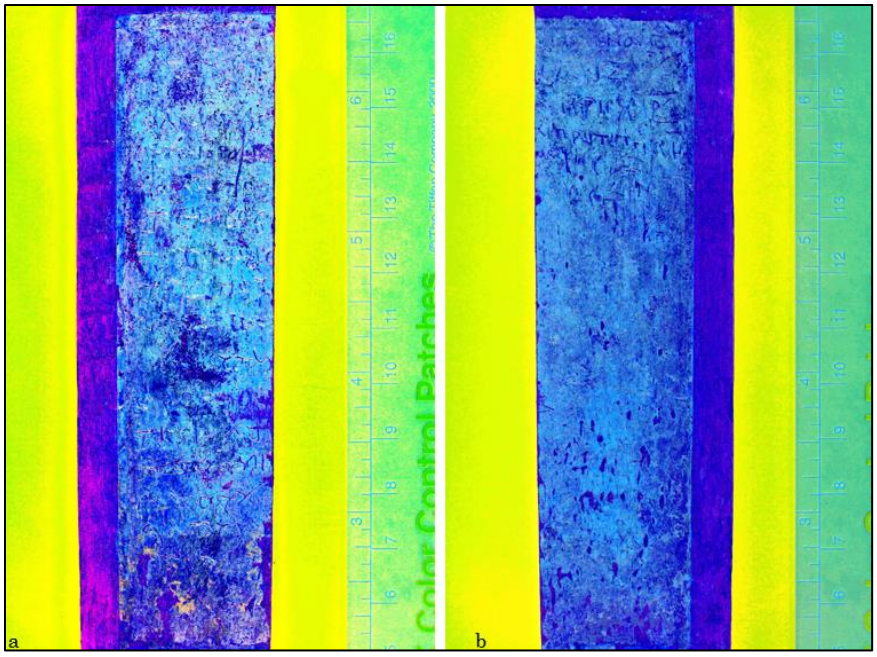

Figure 66. False colour images of side A (b) and B (b) of the tablets generated with the PCA components-derived bands

Following the completion of these digital operations, the resulting 3D model was presented to a professor of papyrology for inspection. Upon close examination of the high-detail model, the professor was able to gain new insights into the text content, identifying subtle features that had previously gone unnoticed. This led to a more enriched interpretation of the engravings, further clarifying the significance of personal names and monetary amounts mentioned in the inscriptions. The collaboration between digital technology and papyrological expertise highlighted how advanced imaging techniques can enhance traditional text analysis, contributing to a deeper understanding of the artefact's historical context.

3.4.7 Testing 3D and diagnostic data integration strategies

The final case study presented in this collection involves the integration of a three-dimensional dataset with thermographic analysis. This methodology was tested on a part of a historic building (early 20th century) at the University of Bologna, which showed signs of biological degradation (presence of mould and lichen) and structural damage (cracks and fissures). While this case study is not of particular interest in itself, it served as a test subject for applying the proposed methodology.

First, a high-detail 3D survey was conducted using close-up photogrammetry (Canon EOS 6D with a 20 MP sensor and a 24-70 mm lens). Detailed and wide-angle photos of the wall were taken to achieve a GSD of approximately 0.5 mm, allowing the morphological characteristics potentially indicating degradation phenomena to be appreciated in the images. Simultaneously, a thermographic survey was conducted using the FLIR P-620 thermal camera (as described in section 3.1) to detect possible moisture infiltration or capillary water rise (figure 67).

Approximately 20 thermal images were acquired, covering the entire surface of interest and maintaining some coherence with the image acquisition scheme of the high-resolution RGB images. Subsequently, the thermal images were calibrated using a reflectance target placed in the scene, producing 32-bit grayscale images where pixel values indicated the measured temperatures.

Figure 67. Thermal imaging on the site

The images were then converted to 16-bit in the open-source software QGIS because the SfM photogrammetry software could not correctly interpret the 32-bit image data. These grayscale images were then oriented along with the high-resolution RGB images, using homologous points manually aligned in both the thermal and RGB image sets (figure 68). The alignment was carried out with no limits on feature extraction from the images used as tie points, as the thermal images were low-resolution (600 pixels).

The alignment was successful, and the RGB and thermal image camera poses were estimated by the SfM software, as well as oriented relatively to the RGB imagery dataset. The reprojection error on the manually aligned points was about 1.1 pixel, an acceptable value given the resolution difference between the RGB and thermal images.

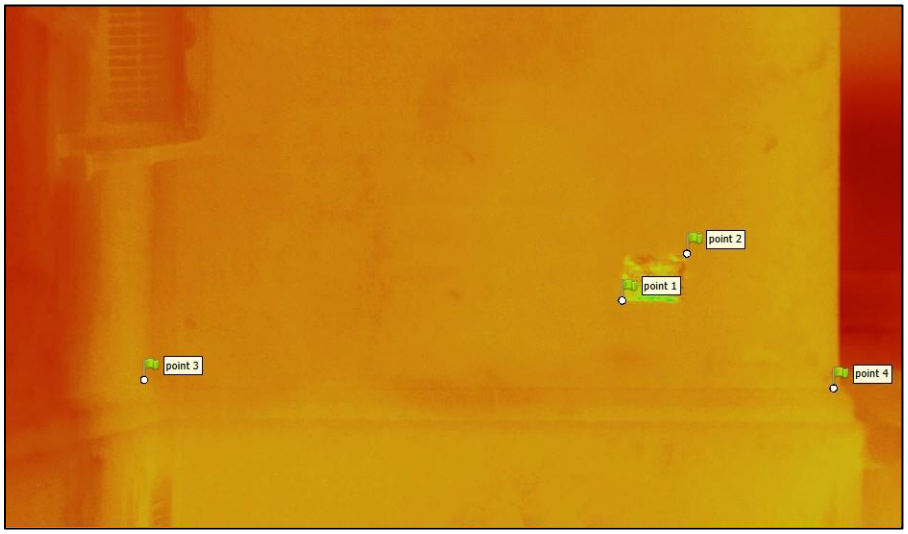

Figure 68. Control points associated to notable features in the thermal imaging imagery

Next, a few control points were added by identifying natural points in the scene and associating them with spatial coordinates acquired from a terrestrial laser scanner point cloud. This procedure helped strengthen the alignment and scaled the photogrammetric model. The RMSE on the targets was about 2 mm, consistent with the precision of the laser scanner used (Leica RTC 360, with a point precision of 1.9 mm at a distance of 10 metres).

The dense point cloud generation was then based solely on the high-resolution RGB image set, with the thermal images deactivated. This decision followed previous examples from the literature (Patrucco et al., 2022), which demonstrated that the low resolution of thermal images and their variability (due to different acquisition conditions, causing slight variations in temperature readings) can lead to inaccuracies or distortions in geometry construction. The dense point cloud was initially generated with a resolution of 0.5 mm (consistent with the GSD of the input images) and accurately represented the surface discontinuities of the surveyed wall.

However, this point cloud was later decimated, reducing the resolution (average point-to-point distance) to 1 mm. This reduction was necessary because the spatial resolution of the thermal images was not comparable to that of the RGB images. Using thermal images to calculate the point cloud colours would have introduced a significant disparity between the geometric resolution of the point cloud and the resolution of the thermal images. After simplifying the geometry, the colour of the point cloud was calculated by deactivating all the RGB images and using only the single bands thermal images.

The resulting point cloud was thus coloured with the grayscale thermal images (which had been oriented together with the visible images), with a single band representing the colour value. This produced a dense and detailed point cloud (with a resolution of 1 mm, as mentioned), but it was coloured using temperature values extracted from the single-band thermal images. The cloud contained X, Y, Z coordinates and an additional scalar field that, in this case, represented the temperature values stored in each pixel. This scalar field can be then visualised with different colour gradients, adjusting the threshold to a specific values range, and inspected to see the associated temperature value to each point in the cloud (figure 69 and 70).

This approach allowed for a detailed 3D visualisation of the wall surface, enriched by the temperature data derived from the thermographic survey.

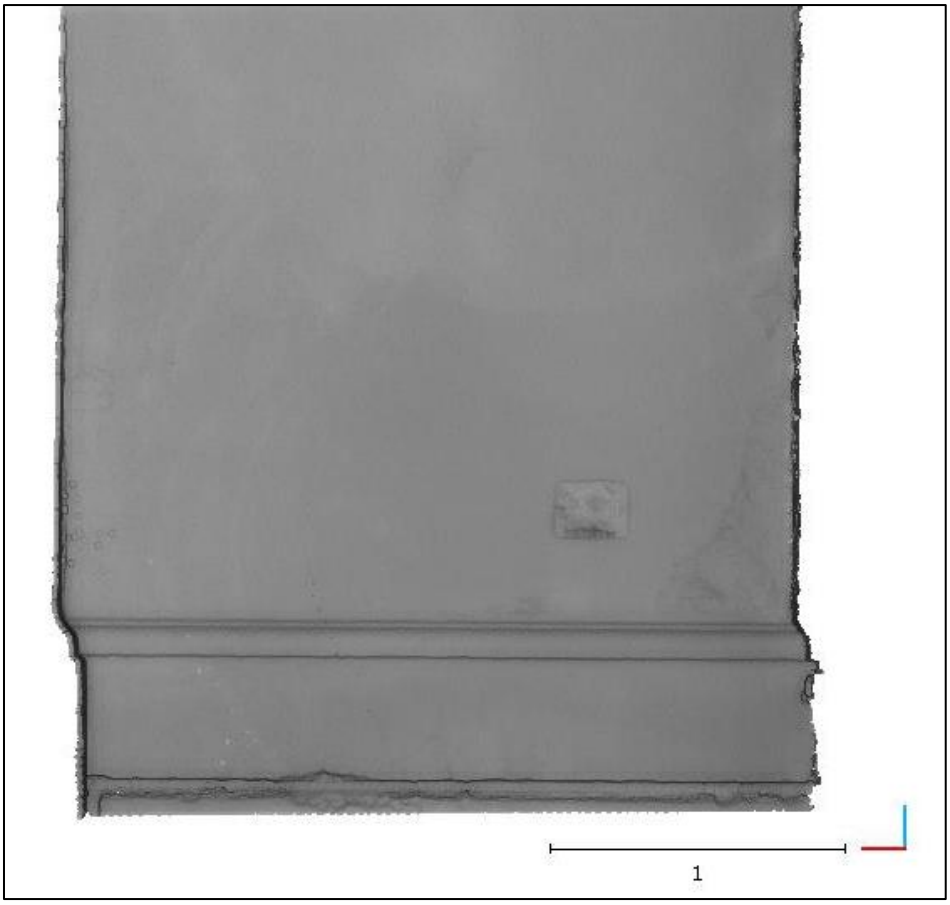

Figure 69. The obtained thermal point cloud visualised with the scalar field in grey levels

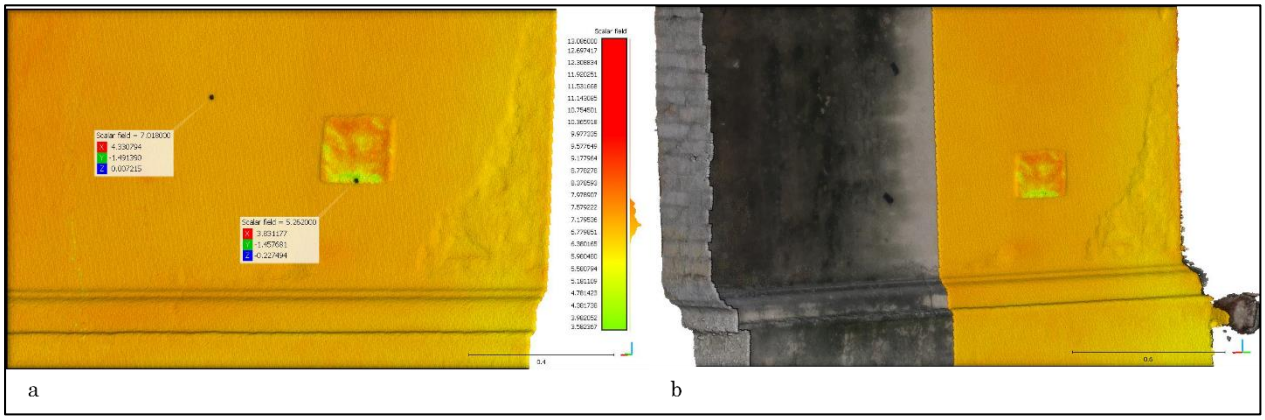

Figure 70. a) A portion of the cloud, with the scalar field of the temperature visualised in false colours and showing the temperature values associated with the points; b) The point clouds obtained with RGB images compared with the aligned thermal cloud

4. DISCUSSION

4.1 Proposing high-detail 3D surveying as a tool for assets' investigation

This thesis has aimed to provide a comprehensive discussion of high-detail 3D surveying, addressing both terminological issues as well as theoretical and technological challenges, with a focus on its promising applications in cultural heritage analysis. High-detail 3D survey methodologies offer in fact several advantages to meet the demanding requirements of cultural heritage studies, despite a persistent underlying challenge of conceptual and lexical inconsistency.

There are numerous exemplary cases demonstrating the successful use of geomatic techniques within this context. As illustrated by examples discussed in section 2.2, along with the case studies examined in this research, high-detail 3D surveying proves to be a valuable investigative tool, making a substantial contribution to heritage science. The sub-millimetric, and even micrometric, accuracy and resolution achieved by these geomatic instruments reveal surface details that may otherwise be invisible or indistinguishable to the human eye.

Beyond that, the digital format serves as an ideal platform for visualisation, permitting analytical approaches that are not feasible in the physical realm, as previously explored. The post-survey digital processes—such as surface enhancement, diagnostic integration, and advanced 3D modelling—further extend the potential of high-detail digital reconstructions, opening up significant avenues for heritage research and preservation.

The case studies section has presented a series of examples demonstrating that sub-millimetric and 3D morphological surface analysis can yield significant insights for historical-archaeological studies, virtual restoration, and philological investigation. Concurrently, this work has highlighted the practical considerations inherent in such surveys; while the advantages and potential are substantial, they present notable

challenges that demand rigorous planning, a solid theoretical foundation, and robust methodological frameworks.

Nevertheless, alongside these opportunities, several limitations remain. Theoretical challenges persist, as certain concepts and aspects, despite efforts made in this and other research works, still require further clarification within the scientific literature. This need for greater theoretical rigour underscores the importance of ongoing scholarship, as detailed in the relevant sections of this thesis.

Moreover, on a methodological level, while professionals from various fields have increasingly adopted 3D surveying practices—expanding their utility as extensively discussed—numerous operational aspects still lack standardised approaches or unified guidelines. These methodological inconsistencies reveal an urgent need for continued research, aiming to refine these techniques for broader and more reliable use. Further exploration of these issues and proposed directions for future studies will be discussed in the concluding section on future perspectives.

In summary, high-detail 3D surveying offers a rich investigative toolset, unlocking a wide array of applications across fields such as diagnostics, historical research, archaeological contextualisation, and material analysis. These facets hold particular relevance within cultural heritage work, where the accurate preservation, study, and interpretation of artefacts are paramount. High-detail 3D surveying, then, has the capacity to significantly and meaningfully enhance our understanding of cultural heritage, contributing to its documentation, protection, and appreciation on a deeper level.

4.2 Considerations on the advantages and disadvantages of surveying methodologies

As already emphasised, high-detail 3D surveying can represent a key investigative tool within heritage science. The use of both range-based and image-based geomatic techniques offers promising results in achieving high geometric accuracy and detailed

digital reconstructions of artefacts. However, their effectiveness depends on their specific technical characteristics, operational constraints, and the documentation objectives. A methodological exploration of these techniques highlights not only their individual strengths and limitations but also the advantages of integrating them into a complementary workflow.

As discussed from the outset of this thesis in relation to terminological challenges, high-detail range-based 3D surveying technologies—specifically laser triangulators and structured-light projection scanning —have undergone significant advancements due to developments by private companies. This has led, on the one hand, to terminological and theoretical inconsistencies, and on the other, to their widespread adoption and increasing user-friendliness. Various case studies from the literature review demonstrated that both LT and SLS can achieve remarkable levels of geometric accuracy and detail, making them essential in heritage documentation.

Despite their advantages, LT systems present significant challenges. While they provide superior micrometric levels of accuracy, they are among the most expensive surveying instruments, making them less accessible for heritage projects operating under financial constraints. Their operational drawbacks are further compounded by their large size, which complicates field deployment and limits their usability beyond controlled environments. Furthermore, LT systems are primarily employed for geometric reconstruction without integrated texture acquisition, a notable disadvantage in cultural heritage documentation where both geometric and visual fidelity are crucial for interpretation and study. However, their use of laser light extends their applicability to non-cooperative surfaces such as metals, which frequently pose challenges for other range-based methods, including SLS.

SLS, in contrast, is the most commonly employed range-based technique in cultural heritage applications. It achieves sub-millimetre accuracy while remaining more practical and portable than LT. Its capability to generate high-resolution geometric documentation is particularly effective for objects featuring fine surface

discontinuities, such as inscribed or engraved artefacts. However, SLS performance is highly contingent on optimal scanning conditions, particularly regarding lighting and material properties. Non-cooperative materials, as well as complex object geometries, can introduce significant challenges. This was evident for instance in the case of the narwhal tooth (section 3.4.1), where its elongated structure necessitated an intensive target strategy both during scanning and post-processing, significantly increasing operational complexity and processing time. Similarly, structured light projection can introduce surface noise or alignment artefacts, particularly when scanning reflective objects, necessitating meticulous post-processing to refine the final model. These factors underscore the importance of careful planning when applying SLS to artefacts with heterogeneous material and geometric properties.

The issue of reconstructing non-cooperative surfaces using active techniques can, however, be mitigated by passive, image-based methods such as close-range photogrammetry. This approach offers exceptional flexibility across a wide range of survey scenarios and material types while providing robust visual reconstructions through precise control of imaging parameters. Particularly in macro and micro configurations, close-range photogrammetry can achieve micrometric resolutions, often surpassing those obtainable with SLS. This was demonstrated in this thesis through the case study of Aldrovandi's xylographic matrices, presented in Section 3.4.4. This example showed that, with meticulous acquisition and processing, exceptionally high levels of detail—down to a few tens of microns—can be achieved, even for complex and small surfaces. Furthermore, as observed in this case study, surface reconstructions obtained through careful photogrammetric processing can appear smoother and cleaner than those generated by SLS.

From a metrological perspective, rigorous camera calibration and the use of high-accuracy control points enable remarkable results. In terms of cost, high-end cameras range from a few hundred to several thousand euros, and commercial Structure-from-Motion software falls within a similar price range, making photogrammetry the most economical technique among those analysed. However, it presents greater operational

complexities, requiring extensive manual intervention. Controlling ambient lighting is crucial, though this challenge can be mitigated with the use of lightboxes or portable lights, as demonstrated in this thesis. Moreover, in certain situations, adhering to the strict acquisition protocols required for multi-view photogrammetry may not be feasible, particularly when objects cannot be moved due to spatial constraints. Additionally, depth-of-field limitations in macro and micro configurations can compromise the sharpness of certain object areas, requiring supplementary techniques such as focus stacking or masking the problematic areas in post-processing.

A further distinguishing feature of photogrammetry, especially in very close-range configurations, is the direct impact of theoretical knowledge on the quality of results. Despite the significant technological advancements that have made photogrammetric software increasingly user-friendly, methodological rigour and adherence to fundamental theoretical principles remain essential for achieving high-quality outcomes. However, when a strong theoretical and methodological foundation is applied, close-range photogrammetry proves to be a highly effective technique for high-detail surveying, even for complex objects requiring extreme precision and accuracy.

The observations made so far have been summarised in table 4, including practical and operational aspects of the three technologies analysed. As evidenced by the table and the preceding discussion, there is no single "perfect" technique for high-detail surveying, as each of the surveyed techniques presents distinct advantages and constraints. As is often the case in surveying, integrating multiple instruments and planning the workflow according to specific requirements are essential for obtaining reliable results, and the suitability of each approach depends on the specific characteristics of the artefact and objectives.

Technique	Accuracy and detail levels	Operational complexity	Theoretical knowledge required	Acquisition time	Processing time	Costs
Laser Triangulators	Microns	Medium	Medium	Medium	High	High (€€€€€-€€€€€€)
Structured-light projection scanning	Tenths of mm	Medium-low	Low	Low	Medium	Medium (€€€€-€€€€€)
Close-range digital photogrammetry	Tenths of mm	Medium-High	High	Medium-High	High	Low (€€€-€€€€)

Table 4. Different high-detail 3D surveying techniques compared

Beyond 3D documentation, integrating techniques of different types supports advanced analytical applications and multidisciplinary investigations. Combining detailed geometric data with high-resolution imaging, for instance, can enhance the study of engraved surfaces, revealing faint inscriptions or worn details that might otherwise remain undetected. This multi-modal strategy proved particularly effective in the study of an engraved Egyptian tablet (section 3.4.6), where the application of image-processing techniques further improved the legibility of surface features.

Moreover, integrating thermographic imaging with 3D data (as seen in section 3.4.7) can facilitate a more comprehensive analysis of material integrity, enabling to correlate surface morphology with structural conditions and degradation phenomena. The same considerations apply to other types of data that can be better analysed if coupled with three-dimensional geometry: we are referring to infrared, multispectral, hyperspectral, or even geophysical investigations. Nonetheless, the integration of digital outcomes obtained with techniques of different domains can present unique challenges such as, as mentioned, the differences in terms of resolution (both 2D and 3D). Moreover, the integration of technologies belonging to different disciplines entails the risk of using data in an improper or incorrect manner. To prevent this from happening, it is important to emphasise the importance of collaboration between experts from different fields who can not only combine data efficiently, but also draw meaningful conclusions about the results of the integration.

5. CONCLUSIONS

5.1 Conclusions and innovative aspects of the PhD Thesis

This thesis has explored the theoretical and practical dimensions of high-detail 3D surveying within the geomatic domain, with a particular focus on its application in the documentation and investigation of small-scale heritage assets. While the literature provides numerous examples of 3D surveying methodologies, few studies offer a comprehensive and structured analysis dedicated to high-detail surveying of individual objects aimed at studying and investigating surface geometry. This work aimed at filling this gap by providing an exhaustive examination of geomatic techniques, demonstrating their potential beyond documentation and extending into analytical applications within heritage science.

A contribution of this study was its clarification of ambiguities within this specialised branch of Geomatics, particularly regarding terminological inconsistencies. An effort was made to clarify certain ambiguities within high-detail 3D surveying, supported by an extensive literature review. The latter provided structured conceptual foundations for disciplines that are increasingly viewed as tools, risking the dilution of their theoretical basis. Addressing this issue requires targeted strategies and cross-disciplinary collaborations to ensure that both the technical and conceptual aspects of high-detail surveying are adequately understood and applied.

This work also underscored the necessity of a standardised lexical framework to enhance scholarly communication and improve methodological clarity. The literature review further outlined the technological landscape of high-detail 3D surveying, analysing three primary techniques: laser triangulators, structured-light projection scanning, and close-range digital photogrammetry. Each method's advantages and limitations were examined, with particular emphasis on SLS and DP.

The methodological section illustrated how survey practices, grounded in both theoretical and practical knowledge, could yield robust and meaningful results. An in-

depth analysis of survey tools, software, and processing strategies was provided, validating their practical implementation through original case studies. The outcomes of the tested methodologies confirmed that high-detail 3D surveying and processing can contribute to heritage investigation from multiple perspectives, including historical and archaeological research, digital restoration, and philological interpretation. Experiences and practices were reported and discussed, such as the digitisation of highly complex objects using SLS and DP, the development of adaptive and targeted practices, the combination of range-based and image-based techniques, and the integration with image analysis and thermal imaging. Although these applications existed in the literature, they were not widely documented, leaving considerable room for further research.

Despite the achieved results, several challenges were identified and discussed, pertinent to the complex and multifaceted world of heritage high-detail digitisation. As seen, this specific context poses several challenges, such as the balancing between data resolution and completeness with manageability, the integration of data from different domains, the careful evaluation of the digital products obtained from a geometrical point of view, and more. This research identified good practices advocating for the careful planning of the survey and the optimisation of data processing techniques to achieve high-resolution models while considering operational constraints and context-specific issues.

In conclusion, this study demonstrated how robust approaches balancing theoretical foundations with practical considerations can yield significant results, even in unconventional 3D surveying scenarios. By presenting original examples, the development of adaptive methodologies, and the integration of various techniques, this thesis underscored the potential of high-detail 3D surveying to contribute meaningfully to cultural heritage studies. Ultimately, by bridging methodological gaps and proposing structured approaches, this research provided a foundation for future advancements in the field, reinforcing the role of Geomatics as a rigorous and advantageous tool in heritage science.

5.2 Open Issues and Future Perspectives

Despite the insights gained into high-detail 3D surveying for documenting and analysing cultural heritage, several limitations became apparent through the literature review and experimental methodologies of this thesis, indicating areas for further exploration.

A key limitation was the narrow scope of comparative analyses between digital photogrammetry and structured-light projection scanning. Though informative, these initial comparisons were confined to specific case studies and controlled conditions, limiting their applicability to diverse artefact types and settings. Future research should expand these comparisons to include a wider range of lighting conditions, surface textures, object complexities, and various instruments of both techniques. Such broader studies would clarify the optimal use cases for each method.

The lack of empirical testing with laser triangulators was another notable limitation. Future studies that include LT could provide a more comprehensive comparison with DP and SLS, clarifying its operational challenges—such as calibration complexities and costs—relative to its high accuracy. This would offer a fuller perspective on practical trade-offs and help identify the most effective method in different scenarios.

In addition, integrating 3D data with image analysis and thermal data was acknowledged but only minimally explored. Further work should focus on refining procedures for effectively utilise data from different domains in integrated approaches.

Balancing high-detail outputs with manageable computational demands remains a significant challenge. Oversampling can lead to excessive data, complicating post-processing and analysis. Future research should investigate adaptive sampling methods that optimise the resolution based on surface complexity, while also exploring scalable data processing solutions could support smaller teams and institutions, encouraging broader adoption of high-detail 3D surveying.

As 3D surveying technologies become more accessible, the perceived need for rigorous scientific expertise can diminish, potentially leading to inconsistent practices or misuse. Targeted training programs that combine theoretical and practical knowledge are needed to address this issue. Collaboration between Geomatics experts and conservators would further encourage a multidisciplinary approach, enhancing both reliability and effectiveness in 3D documentation.

Developing international guidelines and best practices for high-detail 3D surveying in heritage science is also crucial. These standards should outline technical protocols for data acquisition and processing, ensuring consistency and comparability across projects. They must also address ethical considerations surrounding the use and dissemination of digital models, especially for culturally sensitive artefacts, to promote responsible use of technology.

In conclusion, while this thesis has clarified certain aspects of high-detail 3D surveying for heritage science, continued work is needed to address existing challenges. Refining integration procedures, expanding comparative analyses to include DP, SLS, and LT, and promoting cross-disciplinary collaboration can advance both precision and accessibility. Establishing clear guidelines, best practices, and robust data workflows will further support consistent, ethical, and efficient documentation of cultural heritage.

BIBLIOGRAPHY

1. Abdel-Wahab, M., Wenzel, K., & Fritsch, D. 2012. Efficient reconstruction of large unordered image datasets for high accuracy photogrammetric applications. ISPRS Annals of the Photogrammetry, Remote Sensing and Spatial Information Sciences, I-3, 1–6. https://doi.org/10.5194/isprsannals-I-3-1-2012.

2. Adamczyk, M., Kamiński, M., Sitnik, R., Bogdan, A., & Karaszewski, M., 2014. Effect of temperature on calibration quality of structured-light three-dimensional scanners. Applied Optics, 53(23), 5154-5162. https://doi.org/10.1364/AO.53.005154

3. Adami, A., Balletti, C., Fassi, F., Fregonese, L., Guerra, F., Taffurelli, L., Vernier, P., 2015. The bust of Francesco II Gonzaga: from digital documentation to 3D printing. ISPRS Ann. Photogramm. Remote Sens. Spatial Inf. Sci. II-5/W3, 9–15. https://doi.org/10.5194/isprsannals-II-5-W3-9-2015

4. Agin, G.J., & Binford, T.O., 1973. Computer Description of Curved Objects. IEEE Transactions on Computers, C-25, 439-449.

5. Agisoft LLC., 2024. Agisoft Metashape Professional Edition: User Manual (Version 2.1.3). Agisoft. Retrieved from https://www.agisoft.com/downloads/user-manuals/. Last accessed: Oct. 2024.

6. Agüera-Vega, F., Carvajal-Ramírez, F., Martínez-Carricondo, P., 2017. Assessment of photogrammetric mapping accuracy based on variation ground control points number using unmanned aerial vehicle. Measurement 98, 221–227. https://doi.org/10.1016/j.measurement.2016.12.002

7. Albarelli, A., Cosmo, L., Bergamasco, F., Torsello, A., 2014. High-Coverage 3D Scanning through Online Structured Light Calibration, in: 2014 22nd International Conference on Pattern Recognition. Presented at the 2014 22nd International Conference on Pattern Recognition (ICPR), IEEE, Stockholm, Sweden, pp. 4080–4085. https://doi.org/10.1109/ICPR.2014.699

8. Aliaga, D.G., Yi Xu, 2008. Photogeometric structured light: A self-calibrating and multi-viewpoint framework for accurate 3D modeling, in: 2008 IEEE Conference on Computer Vision and Pattern Recognition. Presented at the 2008 IEEE Conference on Computer Vision and Pattern Recognition (CVPR), IEEE, Anchorage, AK, USA, pp. 1–8. https://doi.org/10.1109/CVPR.2008.4587709

9. Alkhatib, Y.J., Forte, A., Bitelli, G., Pierdicca, R., Malinverni, E., 2023. Bringing Back Lost Heritage into Life by 3D Reconstruction in Metaverse and Virtual Environments: The Case Study of Palmyra, Syria, in: De Paolis, L.T., Arpaia, P.,

Sacco, M. (Eds.), Extended Reality, Lecture Notes in Computer Science. Springer Nature Switzerland, Cham, pp. 91–106. https://doi.org/10.1007/978-3-031-43404-4_7

10. Allen, E. and Triantaphillidou, S., 2010. The Manual of Photography, 10th ed. Oxford, U.K.: Elsevier/Focal Press

11. Almroth, U., 1985. Digital photogrammetry, pixel size, image quality, noise considerations. No. TRITA-FMI-2-51. Report No. CM-P00067749.

12. ASPRS (American Society for Photogrammetry and Remote Sensing), 2023. ASPRS Positional Accuracy Standards for Digital Geospatial Data, Edition 2, Version 1.0. ASPRS, Bethesda, MD. Available at: https://publicdocuments.asprs.org/2023-PositionalAccuracyStd.

13. Amir, Y.M., Thörnberg, B., 2017. High Precision Laser Scanning of Metallic Surfaces. International Journal of Optics 2017, 4134205. https://doi.org/10.1155/2017/4134205

14. Angheluță, L.M., Rădvan, R., 2019. Macro photogrammetry for the damage assessment of artwork painted surfaces. Int. Arch. Photogramm. Remote Sens. Spatial Inf. Sci. XLII-2/W15, 101–107. https://doi.org/10.5194/isprs-archives-XLII-2-W15-101-2019

15. Angheluta, L., Radvan, R., 2020. 3D Digitization of translucid materials in Cultural Heritage objects: a comparative study between laser scanning and photogrammetry. Romanian Journal of Physics 65, 1.

16. Antinozzi, S., Ronchi, D., Fiorillo, F., Barba, S., 2021. 3Dino: Configuration for a Micro-Photogrammetric Survey - Applying Dino-Lite microscope for the digitalisation of a cuneiform tablet. Presented at the eCAADe 2021: Towards a New, Configurable Architecture, Novi Sad, Serbia, pp. 211–222. https://doi.org/10.52842/conf.ecaade.2021.2.211

17. Antinozzi, S., Fiorillo, F., 2022. Optimized configurations for micro-photogrammetric surveying adaptable to macro optics and digital microscope. Int. Arch. Photogramm. Remote Sens. Spatial Inf. Sci. XLVI-2/W1-2022, 25–32. https://doi.org/10.5194/isprs-archives-XLVI-2-W1-2022-25-2022

18. Antinozzi, S., Fiorillo, F., Surdi, M., 2022. Cuneiform Tablets Micro-Surveying in an Optimized Photogrammetric Configuration. Heritage 5, 3133–3164. https://doi.org/10.3390/heritage5040162

19. Antinozzi, S., Fiorillo, F., Surdi, M., 2023. Geometrical Feature Identification of Cuneiform Signs on Micro-Survey Reconstruction, in: Brooks, A.L. (Ed.), ArtsIT, Interactivity and Game Creation, Lecture Notes of the Institute for Computer Sciences, Social Informatics and Telecommunications Engineering. Springer Nature Switzerland, Cham, pp. 78–88. https://doi.org/10.1007/978-3-031-28993-4_6

20. Arbace, L., Sonnino, E., Callieri, M., Dellepiane, M., Fabbri, M., Iaccarino Idelson, A., Scopigno, R., 2013. Innovative uses of 3D digital technologies to assist the restoration of a fragmented terracotta statue. Journal of Cultural Heritage 14, 332–345. https://doi.org/10.1016/j.culher.2012.06.008

21. Arriaza, M.C., Yravedra, J., Domínguez-Rodrigo, M., Mate-González, M.Á., García Vargas, E., Palomeque-González, J.F., Aramendi, J., González-Aguilera, D., Baquedano, E., 2017. On applications of micro-photogrammetry and geometric morphometrics to studies of tooth mark morphology: The modern Olduvai Carnivore Site (Tanzania). Palaeogeography, Palaeoclimatology, Palaeoecology 488, 103–112. https://doi.org/10.1016/j.palaeo.2017.01.036

22. Awange, J., Kiema, J., 2019. Environmental Geoinformatics: Extreme Hydro-Climatic and Food Security Challenges: Exploiting the Big Data, Environmental Science and Engineering. Springer International Publishing, Cham. https://doi.org/10.1007/978-3-030-03017-9

23. Azlan, K.A., Omar, M.R., Hussin, M.S.F., Abdullah, M.I.H.C., Chinniah, E.S., 2020. Measurement Accuracy Assessment for Laser Triangulation 3D Scanning Machine. IJRTE 8, 2789–2793. https://doi.org/10.35940/ijrte.F8394.038620

24. Balzani, R., Barzaghi, S., Bitelli, G., Bonifazi, F., Bordignon, A., Cipriani, L., Colitti, S., Collina, F., Daquino, M., Fabbri, F., Fanini, B., Fantini, F., Ferdani, D., Fiorini, G., Formia, E., Forte, A., Giacomini, F., Girelli, V.A., Gualandi, B., Heibi, I., Iannucci, A., Manganelli Del Fà, R., Massari, A., Moretti, A., Peroni, S., Pescarin, S., Renda, G., Ronchi, D., Sullini, M., Tini, M.A., Tomasi, F., Travaglini, L., Vittuari, L., 2023. Saving temporary exhibitions in virtual environments: The Digital Renaissance of Ulisse Aldrovandi – Acquisition and digitisation of cultural heritage objects. Digital Applications in Archaeology and Cultural Heritage 32, e00309. https://doi.org/10.1016/j.daach.2023.e00309

25. Barazzetti, L., 2017. Network design in close-range photogrammetry with short baseline images. ISPRS Ann. Photogramm. Remote Sens. Spatial Inf. Sci. IV-2/W2, 17–23. https://doi.org/10.5194/isprs-annals-IV-2-W2-17-2017

26. Barber, D., Mills, J., 2007. 3D Laser Scanning for Heritage: Advice and Guidance to Users on Laser Scanning in Archaeology and Architecture, 1st ed. Swindon Historic England. UK

27. Barbieri, E., Franzoni, E., Lambertini, A., Pizzigatti, C., Trevisiol, F., Bitelli, G., 2023. 3D Data Management and Thermographic Studies as a Knowledge Base for the Conservation of a Rationalist Architecture, in: Furferi, R., Governi, L., Volpe, Y., Gherardini, F., Seymour, K. (Eds.), The Future of Heritage Science and Technologies, Lecture Notes in Mechanical Engineering. Springer International Publishing, Cham, pp. 3–15. https://doi.org/10.1007/978-3-031-17594-7_1

28. Barone, S., Paoli, A., Razionale, A., 2013. A Coded Structured Light System Based on Primary Color Stripe Projection and Monochrome Imaging. Sensors 13, 13802–13819. https://doi.org/10.3390/s131013802

29. Bell, T., Li, B., Zhang, S., 2016. Structured Light Techniques and Applications, in: Webster, J.G. (Ed.), Wiley Encyclopedia of Electrical and Electronics Engineering. Wiley, pp. 1–24. https://doi.org/10.1002/047134608X.W8298

30. Beraldin, J.-A., Blais, F., Cournoyer, L., Godin, G., Rioux, M., 2000. Active 3D sensing. Quaderni 10, Centro di Ricerche Informatiche per i Beni Culturali, Scuola Normale Superiore, Pisa, Italy.be

31. Besl, P.J., 1988. Active, optical range imaging sensors. Machine Vision and Applications, Springer. 1, 127-152

32. Bitelli, G., Girelli, V. A., Remondino, F., & Vittuari, L., 2006. Surface modelling of complex archaeological structures by digital close-range photogrammetry. Bar International Series, 1568(321), 80.

33. Bitelli, G., Girelli, V., Vittuari, L., 2007. Accurate survey of the Stela from Tilmen Höyük by digital photogrammetry and 3D modelling. In: Refik Duru'ya Armağan - Studies in Honour of Refik Duru, pp. 169-173.

34. Bitelli, G., Balletti, C., Brumana, R., Barazzetti, L., D'Urso, M.G., Rinaudo, F., Tucci, G., 2017. Metric documentation of cultural heritage: research directions from the Italian GAMher project. Int. Arch. Photogramm. Remote Sens. Spatial Inf. Sci. XLII-2/W5, 83–90. https://doi.org/10.5194/isprs-archives-XLII-2-W5-83-2017

35. Bitelli, G., Borghi, B., Francolini, C., Galletti, F., 2020. New hypotheses and interpretations regarding the Longobard Basin in the "Jerusalem" of Bologna

supported by 3D surveying methodologies. Journal of Cultural Heritage 46, 226–234. https://doi.org/10.1016/j.culher.2020.04.005

36. Bitelli, G., Forte, A., Tini, M.A., Belfiori, F., Tirincanti, A., 2025. High-Detail 3D Reconstruction and Digital Strategies for the Enhancements of Archaeological Properties in Museums. Heritage 8, 49. https://doi.org/10.3390/heritage8020049

37. Boehler, W., Marbs, A., 2001. The potential of non-contact close range laser scanners for cultural heritage recording. CIPA XIX International Symposium, XVIII-2001, Potsdam and IAPRS 34.

38. Bortolotto, C., 2007. From Objects to Processes: UNESCO'S 'Intangible Cultural Heritage'. Journal of Museum Ethnography, (19), 21-33.

39. Boyer, K.L., Kak, A.C., 1987. Color-Encoded Structured Light for Rapid Active Ranging. IEEE Trans. Pattern Anal. Mach. Intell. PAMI-9, 14–28. https://doi.org/10.1109/TPAMI.1987.4767869

40. Brown, D. C., 1971. Close-range camera calibration. Photogrammetric Engineering, 37(8), 855–866.

41. Brown, D., Nicholas, G., 2012. Protecting indigenous cultural property in the age of digital democracy: Institutional and communal responses to Canadian First Nations and Māori heritage concerns. Journal of Material Culture 17, 307–324. https://doi.org/10.1177/1359183512454065

42. Cabrelles, M., Lerma, J.L., Villaverde, V., 2020. Macro Photogrammetry & Surface Features Extraction for Paleolithic Portable Art Documentation. Applied Sciences 10, 6908. https://doi.org/10.3390/app10196908

43. Callieri, M., Ranzuglia, G., Dellepiane, M., Cignoni, P., & Scopigno, R., 2012. Meshlab as a complete open tool for the integration of photos and colour with high-resolution 3D geometry data. Comput Appl Quant Methods Archaeol, 406-16.

44. Campbell, J.B., Wynne, R.H., 2011. Introduction to Remote Sensing, Fifth Edition. Guilford Publications.

45. Cantó, A., Lerma, J.L., Martínez Valle, R., Villaverde, V., 2022. Multi-light photogrammetric survey applied to the complex documentation of engravings in Palaeolithic rock art: the Cova de les Meravelles (Gandia, Valencia, Spain). Herit Sci 10, 169. https://doi.org/10.1186/s40494-022-00815-1

46. Cao, M., Jia, W., Lv, Z., Zheng, L., & Liu, X. 2018. Evaluation of local features for Structure from Motion. Multimedia Tools and Applications, 77(9), 10979–10993. https://doi.org/10.1007/s11042-018-5864-1.

47. Chatzivasileiadi, A., Wardhana, N., Jabi, W., Aish, R., Lannon, S., 2018. Characteristics of 3D Solid Modeling Software Libraries for Non-Manifold Modeling. CAD&A 16, 496–518. https://doi.org/10.14733/cadaps.2019.496-518

48. Chen, C.S., Hung, Y.-P., Chiang, C.-C., Wu, J.L., 1997. Range data acquisition using color structured lighting and stereo vision. Image and Vision Computing 15, 445–456. https://doi.org/10.1016/S0262-8856(96)01148-1

49. Chen, F., Brown, G.M., Song, M., 2000. Overview of three-dimensional shape measurement using optical methods. Optical Engineering 39, 10. https://doi.org/10.1117/1.602438

50. Chen, T., Lensch, H.P.A., Fuchs, C., Seidel, H.-P., 2007. Polarization and Phase-Shifting for 3D Scanning of Translucent Objects, in: 2007 IEEE Conference on Computer Vision and Pattern Recognition. Presented at the 2007 IEEE Conference on Computer Vision and Pattern Recognition, IEEE, Minneapolis, MN, USA, pp. 1–8. https://doi.org/10.1109/CVPR.2007.383209

51. Cignoni, P., Callieri, M., Corsini, M., Dellepiane, M., Ganovelli, F., Ranzuglia, G., 2008. MeshLab: an Open-Source Mesh Processing Tool. Eurographics Italian Chapter Conference. https://doi.org/10.2312/localchapterevents/italchap/italianchapconf2008/129-136

52. CloudCompare v2.6.1, User manual. Retrieved from: https://www.cloudcompare.org/doc/qCC/CloudCompare v2.6.1 - User manual.pdf; Last accessed: Sept. 2024

53. Colizzi, L., De Pascalis, F., Fassi, F., 2006. 3D Visualisation and Virtual Reality for Cultural Heritage Diagnostic, in: Abdul-Rahman, A., Zlatanova, S., Coors, V. (Eds.), Innovations in 3D Geo Information Systems, Lecture Notes in Geoinformation and Cartography. Springer Berlin Heidelberg, Berlin, Heidelberg, pp. 629–639. https://doi.org/10.1007/978-3-540-36998-1_48

54. Conati, F., 1977. Real-time measurement of three-dimensional multiple rigid body motion. Master of Science thesis at the Massachusetts Institute of Technology, Department of Mechanical Engineering.

55. Conti, A., Fiorini, L., Tucci, G., 2022. The Ambon of Sant 'Andrea in Pistoia: a comparison between laser scanner and photogrammetric digitization of marble

surfaces. Int. Arch. Photogramm. Remote Sens. Spatial Inf. Sci. XLVI-2/W1-2022, 159–166. https://doi.org/10.5194/isprs-archives-XLVI-2-W1-2022-159-2022

56. Cristina, S.; P. Camilleri, K. and Galea, T. (2011). Multi-view 3D data acquisition using a single uncoded light pattern. In Proceedings of the 8th International Conference on Informatics in Control, Automation and Robotics - Volume 1: ICINCO; ISBN 978-989-8425-75-1; ISSN 2184-2809, SciTePress, pages 317-320. DOI: 10.5220/0003545203170320

57. Cui, B., Tao, W., Zhao, H., 2021. High-Precision 3D Reconstruction for Small-to-Medium-Sized Objects Utilizing Line-Structured Light Scanning: A Review. Remote Sensing 13, 4457. https://doi.org/10.3390/rs13214457

58. Davies, A., 2009. Close-Up and Macro Photography. 1st ed., Routledge. https://doi.org/10.4324/9780080959047

59. De Paolis, L.T., De Luca, V., Gatto, C., D'Errico, G., Paladini, G.I., 2020. Photogrammetric 3D Reconstruction of Small Objects for a Real-Time Fruition, in: De Paolis, L.T., Bourdot, P. (Eds.), Augmented Reality, Virtual Reality, and Computer Graphics, Lecture Notes in Computer Science. Springer International Publishing, Cham, pp. 375–394. https://doi.org/10.1007/978-3-030-58465-8_28

60. Deetjen, M.E., Lentink, D., 2018. Automated calibration of multi-camera-projector structured light systems for volumetric high-speed 3D surface reconstructions. Opt. Express 26, 33278. https://doi.org/10.1364/OE.26.033278

61. Dostal, C., Yamafune, K., 2018. Photogrammetric texture mapping: A method for increasing the Fidelity of 3D models of cultural heritage materials. Journal of Archaeological Science: Reports 18, 430–436. https://doi.org/10.1016/j.jasrep.2018.01.024

62. Fang, X., Wang, J., Li, B., Zeng, W., Yao, Y., 2015. On total least squares for quadratic form estimation. Studia Geophysica et Geodaetica 59, 366–379. https://doi.org/10.1007/s11200-014-0267-x

63. Fassi, F., 2007. 3D modelling of complex architecture integrating different techniques–a critical overview. 3D-ARCH 2007 Proceedings: 3D Virtual Reconstruction and Visualization of Complex Architectures, ETH Zurich, International Archives of Photogrammetry, Remote Sensing and Spatial Information Sciences, 36, 5.

64. Ferrer-González, E., Agüera-Vega, F., Carvajal-Ramírez, F., Martínez-Carricondo, P., 2020. UAV Photogrammetry Accuracy Assessment for Corridor Mapping Based

on the Number and Distribution of Ground Control Points. Remote Sensing 12, 2447. https://doi.org/10.3390/rs12152447

65. Ficker, T., Martišek, D., 2015. 3D Image Reconstructions and the Nyquist–Shannon Theorem. 3D Res 6, 23. https://doi.org/10.1007/s13319-015-0057-4

66. Figueiredo, M., Rodrigues, J.I., Silvestre, I., Veiga-Pires, C., 2014. Web3D Visualization of High Detail and Complex 3D-mesh Caves Models, in: 2014 18th International Conference on Information Visualisation. Presented at the 2014 18th International Conference on Information Visualisation (IV), IEEE, Paris, France, pp. 275–280. https://doi.org/10.1109/IV.2014.15

67. Fisseler, D., Weichert, F., Müller, G.G.W., Cammarosano, M., 2014. Extending Philological Research with Methods of 3D Computer Graphics Applied to Analysis of Cultural Heritage. Eurographics Workshop on Graphics and Cultural Heritage. https://doi.org/10.2312/GCH.20141314

68. Fonseca Moro, L.A., Perez Pavón, J.L., 2024. A newly discovered engraved aurochs in Siega Verde, Salamanca (Spain). Documentation by combining low-cost and macro photogrammetry. Journal of Archaeological Science: Reports 53, 104302. https://doi.org/10.1016/j.jasrep.2023.104302

69. França, J.G.D.M., Gazziro, M.A., Ide, A.N., Saito, J.H., 2005. A 3D scanning system based on laser triangulation and variable field of view, in: IEEE International Conference on Image Processing 2005. Presented at the 2005 International Conference on Image Processing, IEEE, Genova, Italy, p. I–425. https://doi.org/10.1109/ICIP.2005.1529778

70. Francolini, C., 2021. 3D high resolution techniques applied on small and medium size objects: from the analysis of the process towards quality assessment. PhD Thesis, Alma Mater Studiorum Università di Bologna. PhD in Civil, chemical, environmental and materials engineering, cycle XXXIII. 10.48676/unibo/amsdottorato/9489.

71. Freeman Gebler, O., Goudswaard, M., Hicks, B., Jones, D., Nassehi, A., Snider, C., Yon, J., 2021. A comparison of structured light scanning and photogrammetry for the digitisation of physical prototypes. Proc. Des. Soc. 1, 11–20. https://doi.org/10.1017/pds.2021.2

72. Fryer, J., Mitchell, H., Chandler, J.H., 2007. Applications of 3D Measurement from Images, Applications of 3D Measurement from Images. Whittles Publishing

73. Gaiani, M., Apollonio, F., Ballabeni, A., Remondino, F., 2017. Securing Colour Fidelity in 3D Architectural Heritage Scenarios. Sensors 17, 2437. https://doi.org/10.3390/s17112437

74. Galantucci, L.M., Guerra, M.G., Lavecchia, F., 2018. Photogrammetry Applied to Small and Micro Scaled Objects: A Review, in: Ni, J., Majstorovic, V.D., Djurdjanovic, D. (Eds.), Proceedings of 3rd International Conference on the Industry 4.0 Model for Advanced Manufacturing, Lecture Notes in Mechanical Engineering. Springer International Publishing, Cham, pp. 57–77. https://doi.org/10.1007/978-3-319-89563-5_4

75. Gallo, A., Muzzupappa, M., Bruno, F., 2014. 3D reconstruction of small sized objects from a sequence of multi-focused images. Journal of Cultural Heritage 15, 173–182. https://doi.org/10.1016/j.culher.2013.04.009

76. Gao, R., Li, M., Yang, S.-J., Cho, K., 2022. Reflective Noise Filtering of Large-Scale Point Cloud Using Transformer. Remote Sensing 14, 577. https://doi.org/10.3390/rs14030577

77. Garcia, R.R., Zakhor, A., 2012. Consistent Stereo-Assisted Absolute Phase Unwrapping Methods for Structured Light Systems. IEEE J. Sel. Top. Signal Process. 6, 411–424. https://doi.org/10.1109/JSTSP.2012.2195157

78. Gajski, D., Solter, A., Gašparovic, M., 2016. Applications of macro photogrammetry in archaeology. Int. Arch. Photogramm. Remote Sens. Spatial Inf. Sci. XLI-B5, 263–266. https://doi.org/10.5194/isprsarchives-XLI-B5-263-2016

79. Geng, J., 2011. Structured-light 3D surface imaging: a tutorial. Adv. Opt. Photon. 3, 128. https://doi.org/10.1364/AOP.3.000128

80. Geomagic Design X, User manual. Retrieved from: https://www.engineering.pitt.edu/contentassets/52314f399aba40fa86709314a569641c/geomagicdesignx2014userguide.pdf; Last accessed: Sept. 2024

81. Georgopoulos, A., Ioannidis, C., Valanis, A., 2010. Assessing the performance of a structured light scanner. International Archives of Photogrammetry, Remote Sensing and Spatial Information Sciences, Vol. XXXVIII, Part 5 Commission V Symposium, Newcastle upon Tyne, UK.

82. Ghilani, C.D., Wolf, P.R., 2012. Elementary Surveying: An Introduction to Geomatics. 13th ed., Prentice Hall.

83. Giacomo, P., 1976. Lasers in metrology. Soviet Journal of Quantum Electronics, 6(4), 477.

84. Girelli, V.A., Tini, M.A., Dellapasqua, M., Bitelli, G., 2019. High resolution 3D acquisition and modelling in cultural heritage knowledge and restoration projects: the survey of the fountain of Neptune in Bologna. Int. Arch. Photogramm. Remote Sens. Spatial Inf. Sci. XLII-2/W11, 573–578. https://doi.org/10.5194/isprs-archives-XLII-2-W11-573-2019

85. Gomes, L., Regina Pereira Bellon, O., Silva, L., 2014. 3D reconstruction methods for digital preservation of cultural heritage: A survey. Pattern Recognition Letters 50, 3–14. https://doi.org/10.1016/j.patrec.2014.03.023

86. Gonzalez, R.C., Woods, R.E., 2008. Elaborazioni delle immagini digitali,. 3rd edition, Pearson Prentice Hall

87. Grifoni, E., Bonizzoni, L., Gargano, M., Melada, J., Ludwig, N., Bruni, S., Mignani, I., 2022. Hyper-dimensional Visualization of Cultural Heritage: A Novel Multi-analytical Approach on 3D Pomological Models in the Collection of the University of Milan. J. Comput. Cult. Herit. 15, 1–15. https://doi.org/10.1145/3477398

88. Guarnieri, A., Pirotti, F., Vettore, A., 2010. Cultural heritage interactive 3D models on the web: An approach using open source and free software. Journal of Cultural Heritage 11, 350–353. https://doi.org/10.1016/j.culher.2009.11.011

89. Guendulain-García, S.D., Lopez-Beltran, A., Banaszak, A.T., Álvarez-Filip, L., Ramírez-Chávez, E., García-Medrano, D., Sellares-Blasco, R., López-Pérez, A., 2023. Photogrammetry for coral structural complexity: What is beyond sight? Coral Reefs 42, 635–644. https://doi.org/10.1007/s00338-023-02368-6

90. Guidi, G., Remondino, F., 2012. 3D Modelling from Real Data, in: Alexandru, C. (Ed.), Modelling and Simulation in Engineering. InTech. https://doi.org/10.5772/30323

91. Guidi, G., Shafqat Malik, U., Micoli, L.L., 2020. Optimal Lateral Displacement in Automatic Close-Range Photogrammetry. Sensors 20, 6280. https://doi.org/10.3390/s20216280

92. Gupta, M., Nayar, S.K., 2012. Micro Phase Shifting, in: 2012 IEEE Conference on Computer Vision and Pattern Recognition. Presented at the 2012 IEEE Conference on Computer Vision and Pattern Recognition (CVPR), IEEE, Providence, RI, pp. 813–820. https://doi.org/10.1109/CVPR.2012.6247753

93. Hameeuw, H., & Willems, G., 2011. New visualization techniques for cuneiform texts and sealings. Akkadica, 132(2), 163-178.

94. Harrison, R., 2013. Heritage: critical approaches. 1st ed, Heritage studies, Routledge.

95. Hartley, R., Zisserman, A., 2004. Multiple view geometry in computer vision, Second edition. ed. Cambridge University Press, Cambridge, UK.

96. Hendrickx, M., Gheyle, W., Bonne, J., Bourgeois, J., De Wulf, A., Goossens, R., 2011. The use of stereoscopic images taken from a microdrone for the documentation of heritage – An example from the Tuekta burial mounds in the Russian Altay. Journal of Archaeological Science 38, 2968–2978. https://doi.org/10.1016/j.jas.2011.06.013

97. Herzlinger, G., Goren-Inbar, N., Grosman, L., 2017. A new method for 3D geometric morphometric shape analysis: The case study of handaxe knapping skill. Journal of Archaeological Science: Reports 14, 163–173. https://doi.org/10.1016/j.jasrep.2017.05.013

98. Hess, Mona, 2017. Digital techniques for documenting and preserving cultural heritage, Collection Development, Cultural Heritage, and Digital Humanities. ARC Humanities Press, Kalamazoo, MI.

99. Higueras, M., Calero, A.I., Collado-Montero, F.J., 2021. Digital 3D modelling using photogrammetry and 3D printing applied to the restoration of a Hispano-Roman architectural ornament. Digital Applications in Archaeology and Cultural Heritage 20, e00179. https://doi.org/10.1016/j.daach.2021.e00179

100. Hodač, J., Kovářová, K., Cihla, M., Matoušková, E., Frommeltová, E., 2023. Photogrammetric Documentation of Stone Surface Topography Changes as a Tool in Conservation Praxis. Buildings 13, 439. https://doi.org/10.3390/buildings13020439

101. Horn, B.K.P., 1986. Robot vision, MIT electrical engineering and computer science series. MIT Press

102. Hsieh, Y.-C., 2001. Decoding structured light patterns for three-dimensional imaging systems. Pattern Recognition 34, 343–349. https://doi.org/10.1016/S0031-3203(99)00224-1

103. ICCROM, 2019. Heritage Science definition. Retrieved from https://www.iccrom.org/section/heritage-science. Last accessed: sept. 2024

104. ICOMOS, 2003. Charter on the Principles for the Analysis, Conservation and Structural Restoration of Architectural Heritage. Retrieved from https://www.icomos.org/en/about-the-centre/179-articles-en-

francais/ressources/charters-and-standards/165-icomos-charter-principles-for-the-analysis-conservation-and-structural-restoration-of-architectural-heritage. Last accessed: sept. 2024

105. Jalandoni, A., Kottermair, M., 2018. Rock art as microtopography. Geoarchaeology 33, 579–593. https://doi.org/10.1002/gea.21677

106. Jecić, S., & Drvar, N., 2003. The assessment of structured light and laser scanning methods in 3D shape measurements. In Proceedings of the 4th International Congress of Croatian Society of Mechanics, 237-244.

107. Johnson, A.E., Hebert, M., 1998. Control of Polygonal Mesh Resolution for 3-D Computer Vision. Graphical Models and Image Processing 60, 261–285. https://doi.org/10.1006/gmip.1998.0474

108. Karami, A., Menna, F., Remondino, F., 2021. Investigating 3D reconstruction of non-collaborative surfaces through photogrammetry and photometric stereo. Int. Arch. Photogramm. Remote Sens. Spatial Inf. Sci. XLIII-B2-2021, 519–526. https://doi.org/10.5194/isprs-archives-XLIII-B2-2021-519-2021

109. Kazo, C., Hajder, L., 2012. High-quality structured-light scanning of 3D objects using turntable, in: 2012 IEEE 3rd International Conference on Cognitive Infocommunications (CogInfoCom), Kosice, Slovakia, pp. 553–557. https://doi.org/10.1109/CogInfoCom.2012.6422042

110. Keferstein, C.P., Marxer, M., 1998. Testing bench for laser triangulation sensors. Sensor Review 18, 183–187. https://doi.org/10.1108/02602289810226408

111. Keerativittayanun, S., Kondo, T., Sira-uksorn, P., Phatrapornant, T., Sato, M., 2011. 3D scan of a color object using a color structured light pattern, in: 2011 IEEE 7th International Colloquium on Signal Processing and Its Applications. Presented at the its Applications (CSPA), IEEE, Penang, Malaysia, pp. 460–463. https://doi.org/10.1109/CSPA.2011.5759922

112. Kęsik, J., Żyła, K., Montusiewicz, J., Miłosz, M., Neamtu, C., Juszczyk, M., 2022. A Methodical Approach to 3D Scanning of Heritage Objects Being under Continuous Display. Applied Sciences 13, 441. https://doi.org/10.3390/app13010441

113. Khalil, A.M., Two-dimensional displacement measurement using static close range photogrammetry and a single fixed camera, Alexandria Engineering Journal,Volume 50, Issue 3,2011,Pages 219-227,ISSN 1110-0168, https://doi.org/10.1016/j.aej.2011.07.003

114. Khunti, R., 2018. The Problem with Printing Palmyra: Exploring the Ethics of Using 3D Printing Technology to Reconstruct Heritage. SDH 2, 1–12. https://doi.org/10.14434/sdh.v2i1.24590

115. Kim, S.H., Jo, Y.H., Song, J., Kim, D.S., Kim, H.S., 2023. A study on convergence modelling of cultural artefact using X-ray computed tomography and three-dimensional scanning technologies. Int. Arch. Photogramm. Remote Sens. Spatial Inf. Sci. XLVIII-M-2–2023, 851–856. https://doi.org/10.5194/isprs-archives-XLVIII-M-2-2023-851-2023

116. Kolluri, R., Shewchuk, J.R., O'Brien, J.F., 2004. Spectral surface reconstruction from noisy point clouds, in: Proceedings of the 2004 Eurographics/ACM SIGGRAPH Symposium on Geometry Processing. Presented at the SGP04: Symposium on Geometry Processing, ACM, Nice France, pp. 11–21. https://doi.org/10.1145/1057432.1057434

117. Kraus, K., 2007. Geometry from Images and Laser Scans. De Gruyter, Berlin, Boston. https://doi.org/doi:10.1515/9783110892871

118. Kurita, T., 2019. Principal Component Analysis (PCA), in: Computer Vision: A Reference Guide. Springer International Publishing, Cham, pp. 1–4. https://doi.org/10.1007/978-3-030-03243-2_649-1

119. Lastilla, L., Ravanelli, R., Ferrara, S., 2019. 3D high-quality modelling of small and complex archaeological inscribed objects: relevant issues and proposed methodology. Int. Arch. Photogramm. Remote Sens. Spatial Inf. Sci. XLII-2/W11, 699–706. https://doi.org/10.5194/isprs-archives-XLII-2-W11-699-2019

120. Lerma, J.L., Muir, C., 2014. Evaluating the 3D documentation of an early Christian upright stone with carvings from Scotland with multiples images. Journal of Archaeological Science 46, 311–318. https://doi.org/10.1016/j.jas.2014.02.026

121. Levoy, M., Pulli, K., Curless, B., Rusinkiewicz, S., Koller, D., Pereira, L., Ginzton, M., Anderson, S., Davis, J., Ginsberg, J., Shade, J., Fulk, D., 2000. The Digital Michelangelo Project: 3D Scanning of Large Statues. Proceedings of the 27th Annual Conference on Computer Graphics and Interactive Techniques (SIGGRAPH 2000), 131–144. https://doi.org/10.1145/344779.344849

122. Lin, H., Gao, J., Mei, Q., He, Y., Liu, J., Wang, X., 2016. Adaptive digital fringe projection technique for high dynamic range three-dimensional shape measurement. Opt. Express 24, 7703. https://doi.org/10.1364/OE.24.007703

123. Liu, B., Wu, R., & Liu, Y., 2020. Calibration algorithm for error screening based on line structured light. International Journal on Artificial Intelligence Tools, 29(07n08), 2040013.

124. Luhmann, T., Chizhova, M., Gorkovchuk, D., Hastedt, H., Chachava, N., Lekveishvili, N., 2019. Combination of terrestrial laser scanning, UAV and close-range photogrammetry for 3D reconstruction of complex churches in Georgia. Int. Arch. Photogramm. Remote Sens. Spatial Inf. Sci. XLII-2/W11, 753–761. https://doi.org/10.5194/isprs-archives-XLII-2-W11-753-2019

125. Luhmann, T., Robson, S., Kyle, S., Boehm, J., 2023. Close-Range Photogrammetry and 3D Imaging, De Gruyter STEM. De Gruyter.

126. Malzbender, T., Gelb, D., Wolters, H., 2001. Polynomial texture maps, in: Proceedings of the 28th Annual Conference on Computer Graphics and Interactive Techniques, SIGGRAPH '01. Association for Computing Machinery, New York, NY, USA, pp. 519–528. https://doi.org/10.1145/383259.383320

127. Malzbender, T., Wilburn, B., Gelb, D., & Ambrisco, B., 2006. Surface enhancement using real-time photometric stereo and reflectance transformation. Proceedings of the Eurographics Workshop on Rendering Techniques, 245-256.

128. Mancuso, A., Pasquali, A., 2015. Digital Micro-Photogrammetry, in: Proceedings of the 20th International Conference on Cultural Heritage and New Technologies 2015 (CHNT 20, 2015) Vienna 2016. Ed. Museen der Stadt Wien, Stadtarchäologie

129. Marani, R., Roselli, G., Nitti, M., Cicirelli, G., D'orazio, T., Stella, E. 2013. A 3D vision system for high resolution surface reconstruction. 2013 Seventh International Conference on Sensing Technology (ICST) 157–162.

130. Marziali, S., Marziali, E., 2017. Focus-Stacking Technique in Macro-Photogrammetry.

131. McGlone, J.C., 2004. Manual of Photogrammetry, 5th ed. American Society for Photogrammetry and Remote Sensing.

132. Mejia-Parra, D., Lalinde-Pulido, J., Sánchez, J.R., Ruiz-Salguero, O., Posada, J., 2019. Perfect Spatial Hashing for Point-cloud-to-mesh Registration. Spanish Computer Graphics Conference (CEIG) 10 pages. https://doi.org/10.2312/CEIG.20191202

133. Murphy, D., Davidson, M., 2012. Fundamentals of Light Microscopy and Electronic Imaging: Murphy/Light Microscopy 2E. https://doi.org/10.1002/9781118382905

134. Norouzi, M., Shirin, M.B., 2021. Investigating the precision of 3D scanner systems based on digital fringe projection method for biomedical engineering applications, in: 2021 28th National and 6th International Iranian Conference on Biomedical Engineering (ICBME), Tehran, Iran, pp. 58–64. https://doi.org/10.1109/ICBME54433.2021.9750299

135. Ogle, K.N., 1951. On the Resolving Power of the Human Eye. J. Opt. Soc. Am. 41, 517–520. https://doi.org/10.1364/JOSA.41.000517

136. OpenStax, 2022. College Physics 2e. OpenStax, Houston. Retrieved from: https://openstax.org/books/college-physics-2e/pages/26-4-microscopes; Last accessed: Sept. 2024

137. Patrucco, G., Gómez, A., Adineh, A., Rahrig, M., Lerma, J.L., 2022. 3D Data Fusion for Historical Analyses of Heritage Buildings Using Thermal Images: The Palacio de Colomina as a Case Study. Remote Sensing 14-22. 5699. https://doi.org/10.3390/rs14225699

138. Patrucco, G., Bambridge, P., Giulio Tonolo, F., Markey, J., Spano, A., 2023. Digital replicas of British museum artefacts. The International Archives of the Photogrammetry, Remote Sensing and Spatial Information Sciences XLVIII-M-2–2023, 1173–1180. https://doi.org/10.5194/isprs-archives-XLVIII-M-2-2023-1173-2023

139. Peng, T., 2006. Algorithms and models for 3-D shape measurement using digital fringe projections. PhD Thesis at the University of Maryland, Department of Mechanical Engineering and Institute for Systems Research

140. Penney, C. M., & Thomas, B., 1989. High performance laser triangulation ranging. Journal of Laser Applications, 1(2), 51-58.

141. Pham, D., Ha, M., Xiao, C., 2022. Color Structured Light Stripe Edge Detection Method Based on Generative Adversarial Networks. Applied Sciences 13, 198. https://doi.org/10.3390/app13010198

142. Previti, G., Luci, B., Lemorini, C., 2024. Micro-photogrammetry and traceology: new on-site documentation approaches using portable digital microscopes. Journal of Archaeological Science 168, 106004. https://doi.org/10.1016/j.jas.2024.106004

143. Pruitt, J.B., Clement, N.G., Tapanila, L., 2016. Laser and Structured Light Scanning to Acquire 3-D Morphology. Paleontol. Soc. Pap. 22, 57–69. https://doi.org/10.1017/scs.2017.8

144. Rahrig, M., Lerma, J.L., 2022. Multispectral imaging for the documentation of graffiti in an urban environment, in: Proceedings of the 5th Joint International Symposium on Deformation Monitoring - JISDM 2022. Editorial de la Universitat Politècnica de València. https://doi.org/10.4995/JISDM2022.2022.13942

145. Rahrig, M., Herrero Cortell, M.Á., Lerma, J.L., 2023. Multiband Photogrammetry and Hybrid Image Analysis for the Investigation of a Wall Painting by Paolo de San Leocadio and Francesco Pagano in the Cathedral of Valencia. Sensors 23, 2301. https://doi.org/10.3390/s23042301

146. Re, C., Robson, S., Roncella, R., Hess, M., 2011. Metric Accuracy Evaluation of Dense Matching Algorithms in Archeological Applications. Geoinformatics FCE CTU 6, 275–282. https://doi.org/10.14311/gi.6.34

147. Remondino, F., Guarnieri, A., Vettore, A., 2005. 3D modeling of close-range objects: photogrammetry or laser scanning?, in: Beraldin, J.-A., El-Hakim, S.F., Gruen, A., Walton, J.S. (Eds.), . Presented at the Electronic Imaging 2005, San Jose, CA, p. 216. https://doi.org/10.1117/12.586294

148. Remondino, F., Fraser, C.S., 2006. Digital camera calibration methods: Considerations and comparisons. The International Archives of the Photogrammetry, Remote Sensing and Spatial Information Sciences, 36, 266-272.

149. Remondino, F., Menna, F., 2008. Image-Based Surface Measurement for Close-Range Heritage Documentation. https://doi.org/10.3929/ETHZ-B-000011994

150. Remondino, F., Girardi, S., Rizzi, A., Gonzo, L., 2009. 3D modelling of complex and detailed cultural heritage using multi-resolution data. J. Comput. Cult. Herit. 2, 1–20. https://doi.org/10.1145/1551676.1551678

151. Remondino, F., Rizzi, A., 2010. Reality-based 3D documentation of natural and cultural heritage sites—techniques, problems, and examples. Appl Geomat 2, 85–100. https://doi.org/10.1007/s12518-010-0025-x

152. Rieke-Zapp, D., & Royo, S., 2017. Structured light 3D scanning. In A. Bentkowska-Kafel & L. MacDonald (Eds.), Digital Techniques for Documenting and Preserving Cultural Heritage (pp. 247-252). Arc Humanities Press. https://doi.org/10.2307/j.ctt1xp3w16

153. Rinaudo, F., Bornaz, L., & Ardissone, P., 2007. 3D high accuracy survey and modelling for Cultural Heritage Documentation and Restoration. Vast 2007–future technologies to empower heritage professionals, 26-29.

154. Rocchini, C., Cignoni, P., Montani, C., Pingi, P., Scopigno, R., 2001. A low cost 3D scanner based on structured light. Computer Graphics Forum 20, 299–308. https://doi.org/10.1111/1467-8659.00522

155. Rodríguez-Martín, M., Rodríguez-Gonzálvez, P., Lagüela, S., González-Aguilera, D., 2016. Macro-photogrammetry as a tool for the accurate measurement of three-dimensional misalignment in welding. Automation in Construction 71, 189–197. https://doi.org/10.1016/j.autcon.2016.08.016

156. Rüther, H., Palumbo, G., 2012. 3D Laser Scanning for Site Monitoring and Conservation in Lalibela World Heritage Site, Ethiopia. International Journal of Heritage in the Digital Era 1, 217–231. https://doi.org/10.1260/2047-4970.1.2.217

157. Saleh, B.E.A., & Teich, M.C., 2019. Fundamentals of Photonics. 3rd ed., Wiley Series in Pure and Applied Optics, Wiley.

158. Salman, N., Yvinec, M., Merigot, Q., 2010. Feature Preserving Mesh Generation from 3D Point Clouds. Computer Graphics Forum 29, 1623–1632. https://doi.org/10.1111/j.1467-8659.2010.01771.x

159. Salvi, J., Pagès, J., Batlle, J., 2004. Pattern codification strategies in structured light systems. Pattern Recognition 37, 827–849. https://doi.org/10.1016/j.patcog.2003.10.002

160. Salvi, J., Fernandez, S., Pribanic, T., Llado, X., 2010. A state of the art in structured light patterns for surface profilometry. Pattern Recognition 43, 2666–2680. https://doi.org/10.1016/j.patcog.2010.03.004

161. Samaan, M., Deseilligny, M.P., Heno, R., Vaissière, E.D.L., Roger, J., 2016. Close-Range Photogrammetric Tools for Epigraphic Surveys. J. Comput. Cult. Herit. 9, 1–18. https://doi.org/10.1145/2966985

162. Sapirstein, P., 2018. A high-precision photogrammetric recording system for small artefacts. Journal of Cultural Heritage 31, 33–45. https://doi.org/10.1016/j.culher.2017.10.011

163. Schenk, T., 1999. Digital Photogrammetry, Digital Photogrammetry. TerraScience.

164. Schmidt, N., Boochs, F., Schütze, R., 2010. Capture and Processing of High Resolution 3D-Data of Sutra Inscriptions in China, in: Ioannides, M., Fellner, D., Georgopoulos, A., Hadjimitsis, D.G. (Eds.), Digital Heritage, Lecture Notes in Computer Science. Springer Berlin Heidelberg, Berlin, Heidelberg, pp. 125–139. https://doi.org/10.1007/978-3-642-16873-4_10

165. Selami, Y., Tao, W., Gao, Q., Yang, H., Zhao, H., 2018. A Scheme for Enhancing Precision in 3-Dimensional Positioning for Non-Contact Measurement Systems Based on Laser Triangulation. Sensors (Basel, Switzerland) 18. https://doi.org/10.3390/s18020504

166. Shannon, C. E., 1949. Communication in the presence of noise. Proceedings of the IRE, 37(1), 10-21.

167. Shen, S. 2013. Accurate multiple view 3D reconstruction using patch-based stereo for large-scale scenes. IEEE Transactions on Image Processing, 22(5), 1901–1914. https://doi.org/10.1109/TIP.2013.2237921.

168. Silvester, C.M., Hillson, S., 2020. A critical assessment of the potential for Structure-from-Motion photogrammetry to produce high fidelity 3D dental models. American J Phys Anthropol 173, 381–392. https://doi.org/10.1002/ajpa.24109

169. Sims-Waterhouse, D., Piano, S., Leach, R., 2017. Verification of micro-scale photogrammetry for smooth three-dimensional object measurement. Meas. Sci. Technol. 28, 055010. https://doi.org/10.1088/1361-6501/aa6364

170. Skublewska-Paszkowska, M., Milosz, M., Powroznik, P., Lukasik, E., 2022. 3D technologies for intangible cultural heritage preservation—literature review for selected databases. Herit Sci 10, 3. https://doi.org/10.1186/s40494-021-00633-x

171. Smith, K. B., and Zheng, Y. F., 1998. Accuracy Analysis of Point Laser Triangulation Probes Using Simulation. ASME. J. Manuf. Sci. Eng. 120(4): 736–745. https://doi.org/10.1115/1.2830214

172. Snavely, N., Seitz, S. M., & Szeliski, R. 2007. Modeling the world from internet photo collections. International Journal of Computer Vision, 80(2), 189–210. https://doi.org/10.1007/s11263-007-0107-3

173. Song, L., Tang, S., Song, Z., 2017. A robust structured light pattern decoding method for single-shot 3D reconstruction, in: 2017 IEEE International Conference on Real-Time Computing and Robotics (RCAR). Presented at the 2017 IEEE International Conference on Real-time Computing and Robotics (RCAR), IEEE, Okinawa, pp. 668–672. https://doi.org/10.1109/RCAR.2017.8311940

174. Svelto, O., 2010. Properties of Laser Beams, in: Svelto, O. (Ed.), Principles of Lasers. Springer US, Boston, MA, pp. 475–504. https://doi.org/10.1007/978-1-4419-1302-9_11

175. Tanduo, B., Chiabrando, F., Coluccia, L., Auriemma, R., 2023. Underground heritage documentation: the case study of grotta Zinzulusa in Castro (Lecce-Italy).

Int. Arch. Photogramm. Remote Sens. Spatial Inf. Sci. XLVIII-M-2–2023, 1527–1534. https://doi.org/10.5194/isprs-archives-XLVIII-M-2-2023-1527-2023

176. Thompson, R., 2017. Close-up and Macro Photography: Its Art and Fieldcraft Techniques. Routledge.

177. Trevisiol, F., Barbieri, E., Bitelli, G., 2022. Multitemporal Thermal Imagery Acquisition and Data Processing on Historical Masonry: Experimental Application on a Case Study. Sustainability 14, 10559. https://doi.org/10.3390/su141710559

178. Triggs, B., McLauchlan, P., Hartley, R., & Fitzgibbon, A., 1999. Bundle Adjustment - A Modern Synthesis. , 298-372. https://doi.org/10.1007/3-540-44480-7_21.

179. Tucci, G., Bonora, V., Conti, A., Fiorini, L., 2017. High-quality 3D models and their use in a cultural heritage conservation project. Int. Arch. Photogramm. Remote Sens. Spatial Inf. Sci. XLII-2/W5, 687–693. https://doi.org/10.5194/isprs-archives-XLII-2-W5-687-2017

180. UNESCO, 1954. Haugue Convention for the Protection of Cultural Property in the Event of Armed Conflict. Retrieved from: https://unesdoc.unesco.org/ark:/48223/pf0000187580. Last accessed: sept. 2024

181. Vavulin, M., Nevskaya, I., & Tybykova, L., 2019. Digital macro-photogrammetry in documentation of old Turkic runiform inscriptions in the Altai Mountains. Mediterranean Archaeology and Archaeometry, 19(2), 81-81.https://doi.org/10.5281/ZENODO.3239053

182. Verdiani, G., Formaglini, P., Giansanti, F., Giraudeau, S., 2018. Close-Up, Macro and Micro Photogrammetry and Image Perspective: A Comparative Studio on Different Lenses at Work with Small and Medium Size Objects 2, 235–248.

183. Wang, R., Law, A.C., Garcia, D., Yang, S., Kong, Z., 2021. Development of structured light 3D-scanner with high spatial resolution and its applications for additive manufacturing quality assurance. Int J Adv Manuf Technol 117, 845–862. https://doi.org/10.1007/s00170-021-07780-2

184. Wang X., Sun, L., Lei, P., Chen, J., He, J., Zhou, Y., 2021. High-resolution 3D range gated laser imaging for unmanned underwater vehicles. Presented at the Proc.SPIE, p. 1190207. https://doi.org/10.1117/12.2601579

185. Weise, T., Leibe, B., Van Gool, L., 2007. Fast 3D Scanning with Automatic Motion Compensation, in: 2007 IEEE Conference on Computer Vision and Pattern Recognition. Presented at the 2007 IEEE Conference on Computer Vision and

Pattern Recognition, IEEE, Minneapolis, MN, USA, pp. 1–8. https://doi.org/10.1109/CVPR.2007.383291

186. Westoby, M. J., Brasington, J., Glasser, N. F., Hambrey, M. J., & Reynolds, J. M. 2012. Structure-from-Motion photogrammetry: A low-cost, effective tool for geoscience applications. Geomorphology, 179, 300–314. https://doi.org/10.1016/j.geomorph.2012.08.021.

187. Willems, G., Verbiest, F., Moreau, W., Hameeuw, H., 2005. Easy and Cost-Effective Cuneiform Digitizing. In: proceedings of the 6th International Symposium on Virtual Reality, Archaeology and Cultural Heritage (VAST 2005), edited by Mark Mudge, Nick Ryan, and Roberto Scopigno, 73–80. Eurographics Association.

188. Wolf, P. R., Dewitt, B. A., Wilkinson, B.E., 2014. Elements of Photogrammetry with Applications in GIS. 4th ed. New York: McGraw-Hill Education. 9780071761123

189. Wycisk, P., Hubert, T., Gossel, W., Neumann, Ch., 2009. High-resolution 3D spatial modelling of complex geological structures for an environmental risk assessment of abundant mining and industrial megasites. Computers & Geosciences 35, 165–182. https://doi.org/10.1016/j.cageo.2007.09.001

190. Xiu-feng, Z., 2007. Edge detection for laser image of target-shape based on local maximum intensity. Opto-electronic Engineering.

191. Yanagi, H., & Chikatsu, H., 2010. 3D modelling of small objects using macrolens in digital very close range photogrammetry. Int. Arch. Photogramm. Remote Sens. Spatial Inf. Sci, 38, 617-622.

192. Yang, C., Liu, F., Song, Z., 2014. A unified probabilistic graphical model based approach for the robust decoding of color structured light pattern, in: 2014 4th IEEE International Conference on Information Science and Technology. Presented at the 2014 4th IEEE International Conference on Information Science and Technology (ICIST), IEEE, Shenzhen, China, pp. 627–630. https://doi.org/10.1109/ICIST.2014.6920556

193. Yang, Y.F., Aggarwal, J.K., 1988. An overview of geometric modeling using active sensing. IEEE Control Syst. Mag. 8, 5–13. https://doi.org/10.1109/37.471

194. Yogender, Raghavendra, S., Kushwaha, S.K.P., 2020. Role of Ground Control Points (GCPs) in Integration of Terrestrial Laser Scanner (TLS) and Close-range Photogrammetry (CRP), in: Ghosh, J.K., Da Silva, I. (Eds.), Applications of

Geomatics in Civil Engineering, Lecture Notes in Civil Engineering. Springer Singapore, Singapore, pp. 531–537. https://doi.org/10.1007/978-981-13-7067-0_42

195. Zanuttigh, P., Marin, G., Dal Mutto, C., Dominio, F., Minto, L., Cortelazzo, G.M., 2016. Time-of-Flight and Structured Light Depth Cameras. Springer International Publishing, Cham. https://doi.org/10.1007/978-3-319-30973-6

196. Zhan, D., Yu, L., Xiao, J., Chen, T., 2015. Multi-Camera and Structured-Light Vision System (MSVS) for Dynamic High-Accuracy 3D Measurements of Railway Tunnels. Sensors 15, 8664–8684. https://doi.org/10.3390/s150408664

197. Zhan, K., Fritsch, D., Wagner, J.F., 2021. Integration of photogrammetry, computed tomography and endoscopy for gyroscope 3D digitization. Int. Arch. Photogramm. Remote Sens. Spatial Inf. Sci. XLVI-M-1–2021, 925–931. https://doi.org/10.5194/isprs-archives-XLVI-M-1-2021-925-2021

198. Zhang, C., Chen, J., Li, P., Han, S., Xu, J., 2024. Integrated high-precision real scene 3D modelling of karst cave landscape based on laser scanning and photogrammetry. Sci Rep 14, 20485. https://doi.org/10.1038/s41598-024-71113-y

199. Zhang L., Curless, B., Seitz, S.M., 2002. Rapid shape acquisition using color structured light and multi-pass dynamic programming, in: Proceedings. First International Symposium on 3D Data Processing Visualization and Transmission. Presented at the First International Symposium on 3D Data Processing Visualization and Transmission, IEEE Comput. Soc, Padova, Italy, pp. 24–36. https://doi.org/10.1109/TDPVT.2002.1024035

200. Zhang, S., 2010. Recent progresses on real-time 3D shape measurement using digital fringe projection techniques. Optics and Lasers in Engineering 48, 149–158. https://doi.org/10.1016/j.optlaseng.2009.03.008

201. Zhang, S., Yau, S.-T., 2006. High-resolution, real-time 3D absolute coordinate measurement based on a phase-shifting method. Opt. Express 14, 2644. https://doi.org/10.1364/OE.14.002644

202. Zhang, T., Xing Niu, J., Liu, S., Tao Pan, T., B Gupta, B., 2021. Three-dimensional Measurement Using Structured Light Based on Deep Learning. Computer Systems Science and Engineering 36, 271–280. https://doi.org/10.32604/csse.2021.014181

203. Zhang, Y., Yilmaz, A., 2016. Structured light based 3D scanning for specular surface by the combination of gray code and phase shifting. Int. Arch.

Photogramm. Remote Sens. Spatial Inf. Sci. XLI-B3, 137–142. https://doi.org/10.5194/isprsarchives-XLI-B3-137-2016

204. Zhao, X., Yu, T., Liang, D., He, Z., 2024. A review on 3D measurement of highly reflective objects using structured light projection. Int J Adv Manuf Technol 132, 4205–4222. https://doi.org/10.1007/s00170-024-13566-z

205. Zhao, Y., Mohamed Supri, T.B., Yang, S., Qin, Y., 2020. A new static method of calibration for low-cost laser triangulation systems. Measurement 156, 107613. https://doi.org/10.1016/j.measurement.2020.107613

206. Zong, Y., Liang, J., Pai, W., Ye, M., Ren, M., Zhao, J., Tang, Z., Zhang, J., 2022. A high-efficiency and high-precision automatic 3D scanning system for industrial parts based on a scanning path planning algorithm. Optics and Lasers in Engineering 158, 107176. https://doi.org/10.1016/j.optlaseng.2022.107176

207. Zuo, C., Feng, S., Huang, L., Tao, T., Yin, W., Chen, Q., 2018. Phase shifting algorithms for fringe projection profilometry: A review. Optics and Lasers in Engineering 109, 23–59. https://doi.org/10.1016/j.optlaseng.2018.04.019

ACKNOWLEDGEMENTS

The completion of this doctoral thesis is the result of collaboration with a number of individuals who have guided and supported me throughout these three years. First and foremost, I would like to express my gratitude to my thesis supervisors, Prof. Gabriele Bitelli and Prof. Valentina Girelli. Your guidance and exemplary support have been invaluable to me.

I would also like to thank the other professors and researchers within the research group who have mentored, assisted, and supported me during these years, especially Prof. Maria Alessandra Tini and Prof. Luca Vittuari. My sincere thanks go as well to Prof. Jose Luis Lerma, who guided me during my time abroad at the Polytechnic University of Valencia.

Furthermore, I am deeply grateful to my fellow PhD colleagues who have provided both practical and emotional support, particularly Francesca Trevisiol, Enrica Vecchi, Giulia Fiorini, and Matteo Cappuccio, who also collaborated on the development of some of the experiments and studies conducted for this thesis.

I extend my heartfelt thanks to all the other professors and researchers in the Geomatics group at DICAM, and to Dr. Chiara Bonini, whose contribution has been fundamental over these years.

A special mention goes to the institutions that enabled the implementation of experiments on real case studies, specifically the University Museum System (SMA) and the University Library (BUB) of the University of Bologna, along with all their staff. I would also like to thank the Civic Archaeological Museum of Bologna and "Luigi Ghirotti" Riccione Territorial Museum.